Projet COROUSSO

ANR-10-SEGI-003

Tâche 1 :
Conception Optimale et Modelisation du Robot Porteur

Livrable 1.1 :

Modèles élastiques et élasto-dynamiques de robots porteurs

Projet ANR-2010-SEGI-003-COROUSSO

Partenaires :

	Rédigé par	Approuvé par	Validé par
Date	24/02/2012	24/02/2012	15/05/2013
Nom(s)	A. KLIMCHIK A. PASHKEVITCH	A. PASHKEVITCH	G. ABBA
Signature(s)			

Liste de diffusion		
Nom	Organisme	Fonction
	ANR	

Indice de révision	Modifié par	Description des principales évolutions	Date de mise en application	Pages concernées

SOMMAIRE

1 Introduction 5

2 Robot-based processing of high-performance materials 8
2.1 Modern trends in machining 8
2.2 Machining of high performance materials 10
2.3 Machining with robots versus traditional machining tools 14
2.4 References 22

3 Stiffness matrix of robotic manipulators with passive joints 25
3.1 Introduction 25
3.2 Motivation example 27
3.3 Passive joints in a serial chain 29
3.4 Passive joints in a parallel manipulator 31
3.5 Computational techniques 32
3.5.1 Recursive computations: single-joint decomposition 32
3.5.2 Analytical computations: chains with trivial passive joints 33
3.6 Application examples 37
3.7 Conclusion 40
3.8 Appendix A : Properties of stiffness matrix K_C 40
3.9 Appendix B: Recursive computation of the stiffness matrix K_C 42
3.10 References 43

4 Stiffness modeling of robotic-manipulators under auxiliary loadings 46
4.1 Introduction 46
4.2 Problem statement 47
4.3 Static equilibrium equations 48
4.4 Static equilibrium configuration 49
4.5 Stiffness matrix 50
4.6 Illustrative examples 53
4.6.1 Serial chain with torsional springs 53
4.6.2 Serial chains with torsional and translational springs 55
4.7 Conclusion 56
4.8 References 57

5 Stability of manipulator configuration under external loading 59
5.1 Introduction 59
5.2 Problem statement 60
5.2.1 Motivation 60
5.2.2 Basic assumptions and research problems 62
5.3 Stability of kinematic chain configuration under loading 62
5.3.1 Static equilibrium 62
5.3.2 Stability criterion 64

5.4 Stability of The end-platform location under external loading 65
5.4.1 Cartesian stiffness matrix of a serial kinematic chain 66
5.4.2 Cartesian stiffness matrix of parallel manipulator 66
5.5 Application examples 68
5.5.1 Stiffness analysis for serial chain with 1D-springs 68
5.5.2 Stability of serial chain under auxiliary loading 71
5.5.3 Kinetostatic singularity in the neighborhood of the flat configuration 73
5.6 Conclusions 75
5.7 References 75

6 Stiffness modeling of non-perfect parallel manipulators 77
6.1 Introduction 77
6.2 Stiffness modeling background 78
6.3 Stiffness models aggregation for small loading 79
6.3.1 Stiffness model aggregation for perfect chains 79
6.3.2 Stiffness model aggregation for non-perfect chains 80
6.4 Stiffness models aggregation for high loading 82
6.4.1 Stiffness model of parallel manipulator 82
6.4.2 Compliance model of parallel manipulator 85
6.5 Application examples 86
6.5.1 Aggregation non-perfect serial chains without loading 86
6.5.2 Aggregation non-perfect serial chains under loading 88
6.6 Conclusion 89
6.7 References 90

7 Compliance error compensation technique for parallel robots composed of non-perfect serial chains 92
7.1 Introduction 92
7.2 Problem of compliance error compensation 93
7.3 Stiffness modeling background 96
7.4 Nonlinear technique for compliance error compensation 97
7.5 Illustrative example: compliance error compensation for milling 100
7.6 Conclusions 104
7.7 References 105

8 Conclusions 107

1 INTRODUCTION

At present, aerospace and ship building industries progressively replace conventional materials by new ones that provide essential advantages from the point of view of mechanical properties of the final products, but at the same time introduce some complexity in the manufacturing process. In particular, machining of modern high-performance materials requires revision of some approaches in design and programming of manufacturing cells that must provide high accuracy and high productivity simultaneously.

In machining of such materials, currently there are two main trends. The first of these is based on conventional CNC-machines that are provided by dedicated cutting tools, which are able to achieve desired quality and productivity. However, this classical approach has essential limitations and can be hardly applied when a workpiece geometry is complicated and its dimensions are rather large. In this case, the second trend, which is based on industrial robotic manipulators, looks very attractive. This type of machining cells can be implemented using either serial or parallel manipulators. Both approaches have their advantages and disadvantages. In particular, serial robots provide large workspace but usually are quite heavy and the influence of gravity forces is significant. In contrast, in parallel manipulators the gravity influence is essentially smaller (but not negligible), while the work envelop is limited by particularities of this architecture. Aside these, in both cases the cutting forces produce essential compliance errors that influence the quality of the final product. For this reason, stiffness analysis of robotic manipulators under essential external forces becomes a critical issue in design of robotic-based manufacturing cells for machining of modern high-performance materials.

In literature, the main results in manipulator stiffness analysis are obtained assuming that the compliance errors are small enough and may be evaluated by linear models. However, for the considered application area this assumption should be revised, which requires development of relevant non-linear stiffness modeling techniques that are able to evaluate the compliance errors caused by different types of external and internal loadings (cutting and gravity forces, internal preloading in joints introduced in order to eliminate backlash, forces generated by gravity compensators, internal stresses caused by assembling of non-perfect over-constrained closed-loops in parallel manipulators, etc.). Another difficulty is related to taking into account the influence of passive joints that are numerous in parallel manipulators. Hence, the manipulator stiffness modeling for these industry-motivated conditions is a challenge in robotic science.

In this work, to develop the desired stiffness model and corresponding compliance error compensation technique, the Virtual Joint Modeling (VJM) concept is used. This choice is motivated by its essential advantages for the considered application areas, such as high computational efficiency and acceptable accuracy. Compared to other alternative approaches (Finite Element Analysis, Matrix Structural Analysis), the VJM technique is more suitable for both on-line and off-line modes, but it should be essentially enhanced to ensure stiffness modeling in the cases of significant external/internal forces for manipulators with passive joints. In addition, the models to be developed should be able to detect some certain non-linear effects in the stiffness behavior of the manipulator under high loading (buckling for instance). In addition, existing approaches implicitly assume that all robot components are perfect and there are no internal stresses caused by assembling of over-constrained structure. So, in spite of the fact that the problem of stiffness modeling of serial and parallel manipulators was in the focus of numerous researches, the main results are in the area of linear stiffness analysis and there are still a number of open theoretical questions, some of which will be considered in this report.

This report focuses on enhancement of stiffness modeling techniques for serial and parallel manipulators in order to increase the accuracy and efficiency of robotic-based machining of high performance materials by means of compensation of the compliance errors (in on-line or/and off-line mode). To achieve this goal, several problems have to be solved:

Problem 1:

> Enhancement of VJM-based stiffness modeling technique for serial and parallel manipulators with arbitrary location of passive joints in the case of small deflections (unloaded mode).

Problem 2:

> Extension of the proposed VJM-based technique for the case of large deflections caused by internal and external loadings, taking into account related changes in Jacobians and equilibrium coordinates.

To address the above defined problems, the thesis is organized as follows:

Chapter 2 is devoted to the state of art and literature review on the robotic based processing of high performance materials. It includes a review of robot applications for machining of high performance materials, determination of potential demands, limitations and advantages.

Chapter 3 focuses on stiffness matrix computation for manipulators with passive joints, compliant actuators and flexible links. It proposes both explicit analytical expressions and an efficient recursive procedure that are applicable in general case and allow obtaining the desired matrix either in analytical or numerical form. Advantages of the developed technique and its ability to produce both singular and non-singular stiffness matrices are illustrated by application examples that deal with stiffness modeling of two Stewart-Gough platforms.

Chapter 4 focuses on the extension of the virtual-joint-based stiffness modeling technique for the case of different types of loadings applied both to the robot end-effector and to manipulator intermediate points (auxiliary loading). It is assumed that the manipulator can be presented as a set of compliant links separated by passive or active joints. It proposes a computationally efficient procedure that is able to obtain a non-linear force-deflection relation taking into account the internal and external loadings. It also produces the Cartesian stiffness matrix. This allows to extend the classical stiffness mapping equation for the case of manipulators with auxiliary loading. The results are illustrated by numerical examples.

Chapter 5 is devoted to the analysis of robotic manipulator behavior under internal and external loadings. The main contributions are in the area of stability analysis of manipulator configurations corresponding to the loaded static equilibrium. In contrast to other works, in addition to usually studied the end-platform behavior with respect to the disturbance forces, the problem of configuration stability for each kinematic chain is considered. The proposed approach extends the classical notion of the stability for the static equilibrium configuration that is completely defined the properties of the Cartesian stiffness matrix only. The advantages and practical significance of the proposed approach are illustrated by several examples that deal with serial kinematic chains and parallel manipulators. It is shown that under the loading the manipulator workspace may include some specific points that are referred to as elastostatic singularities where the chain configurations become unstable.

Chapter 6 focuses on the stiffness modeling of parallel manipulators composed of non-perfect serial chains, whose geometrical parameters differ from the nominal ones. In these manipulators, there usually exist essential internal forces/torques that considerably affect the stiffness properties and also change end-effector location. These internal loadings are caused by elastic deformations of the manipulator elements during assembling, while the geometrical errors in the chains are compensated by applying appropriate forces. For this type of manipulators, a non-linear stiffness modeling technique is proposed that allows us to take into account inaccuracy in the chains and to aggregate their stiffness models for the case of both small and large deflections. Advantages of the developed technique and its ability to compute the compliance errors caused by different factors are illustrated by an example that deals with parallel manipulator of the Orthoglide family.

Chapter 7 presents the compliance errors compensation technique for over-constrained parallel manipulators under external and internal loadings. This technique is based on the non-linear stiffness modeling which is able to take into account influence of non-perfect geometry of serial chains caused by manufacturing errors. Within the developed technique, the deviation compensation reduces to a proper adjusting of a target trajectory that is modified in the off-line mode. The advantages and practical significance of the proposed technique are illustrated by an example that deals with groove milling with Orthoglide manipulator that considers different locations of the workpiece. It is also demonstrated that the impact of the compliance errors and the errors caused by inaccuracy in serial chains cannot be taken into account using the superposition principle.

Finally, Chapter 8 summarise the main contribution of this report

2 ROBOT-BASED PROCESSING OF HIGH-PERFORMANCE MATERIALS

2.1 Modern trends in machining

General trends in machining. Generally, modern trends in machining are aimed at improving machining efficiency while reducing the product price. These trends are contradictive, so all related research focus on a compromise that ensures high manufacturing accuracy and acceptable cost. In the frame of formal models used in this area, most of the design objectives are usually converted into the constrains that define acceptable (but obviously not strictly optimal) values of corresponding performance measures. This approach allows us to reduce complexity of the related optimization problem, but does not eliminate the need for development of specific mathematical models for assessing of each particular performance.

The most useful ways of reducing the price and improving the product quality are related to the enhancement of cutting technology and optimization of tool path. In particular, reducing the total amount of material removal and using optimal cutting parameters for the maximization of metal removal rate yield an essential reduction of the manufacturing time. While the first improvement can be achieved rather easily (by proper dimensioning of raw primary part), the second one requires optimization of the machining process by increasing of the depth of cut and feed rate as well as the spindle speed to the maximum allowed levels. The later is obviously accompanied by an increase of cutting forces that still are not very essential for the conventional CNC-machines with rather rigid mechanical structure. However, in robotic-based processing, these forces may cause essential deformations of the manipulator and consequent impact on the processing accuracy. Therefore, this issue needs detailed analysis which will be in the focus of this work.

The tool path optimization is aimed at the reduction of non-cutting time as well as the minimisation of efforts in actuator drives by proper selection of the tool moving direction. The first of them is also called 'airtime' [5]in order to distinguish from the machining time when the tool is actually cutting material. As it follows from related research [32][48], the airtime can be quite significant when multiple tools are used or a number of small regions are being machined. Mathematically, this problem is formulated as a specific version of the traveling salesman problem with rather hard precedence constraints [33]. The second issue, minimisation of actuator efforts, is equivalent to optimization of tool path in the manipulator workspace. It was previously studied mainly using kinematic criterion [27], but machining application (especially for hard materials) requires direct computing of forces/torques in actuated joints that are also considered in this work.

Other issues that are important for manufacturing but are beyond of the scope of this work are related to minimization of setup time, using multi-operation machine tools and quick-change systems for tooling, automation of loading/unloading operations, improving accuracy of traditional roughing process, reduction of manufacturing lead time, applying of just-in-time production strategy, minimization of inventory cost, etc. [22]. Besides, on the product development stage, the concurrent engineering methodology is also attractive. Integration of all these approaches yields maximal utilization of expensive equipment and significantly reduces the product price.

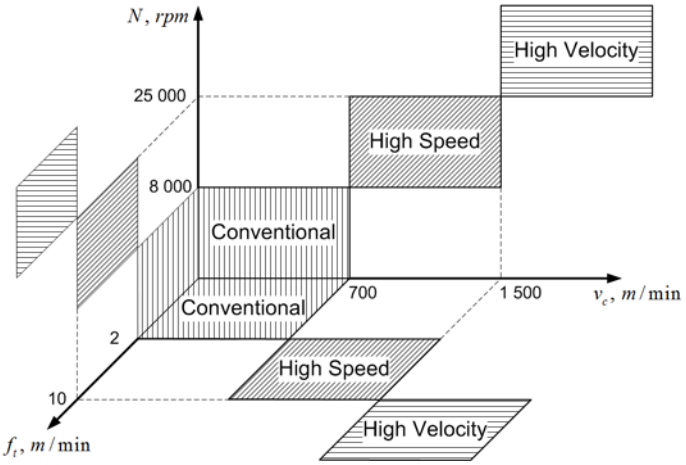

Figure 2.1 General limits for High Speed Machining [12]

It is worth mentioning that, in spite of obviously positive impact, some advances in modern machining technology adversely affect the processing accuracy. For instance, increasing depth of cut generates high forces/torques which may cause significant (and inadmissible) compliance deformations of the machining tool or robot. To reduce related machining errors there exist two main approaches. The first these is aimed at increasing of the machine tool or robot stiffness as well as optimal part placement in the workspace. However, increasing of the mechanism stiffness obviously leads to decreasing of the dynamic properties (due to higher mass and inertia of the links). The second approach is based on *compliance errors compensation* via proper off-line modification of control program describing desired tool trajectory or by using the force feedback in the online mode. To implement this approach, a suitable stiffness model of the CNC-machine or manipulator is required, which is proposed in the following chapters.

High Speed Machining (HSM). The most essential current trends in machining of high performance materials are integrated in HSM-concept, which has been already successfully implemented in several projects for the aerospace and ship building industries [43] that are known by their strong requirements for accuracy and high demands for efficiency. But simultaneously with obvious advantages, these applications demonstrated rather strong constrains on the specifications of the manufacturing equipment. This is caused by high spindle speed, high feed rate and by other factors. Typically, HSM-based manufacturing conditions are associated with the following parameters [12]:

- spindle speed N from 8000-10000 revolutions per minute (rpm) for widely used wares and up to 40000 rpm and higher for aerospace and medical industry, high accuracy wares and machining with small tools;
- cutting speed v_c from 700 m/min for milling with small tools;
- feed rate f_t has to be at least 2-2.5 m/min and amount up to 40 m/min and more for high velocity machining;
- spindle power P_{sp} from 10-15 kW for tools with low feed rate and traverse 50 kW for high velocity machining of stiff materials.

It should be stressed that all these specifications of the machining process are not strict and can vary, but they essentially differ from the conventional ones. Approximate manufacturing conditions limits for HSM

are summarized in Figure 2.1. Main advantages of HSM are summarized in Figure 2.2, which shows the influence of cutting speed on cutting forces, surface quality, time-cutting volume, thermal workpiece load and tool life travel [12].

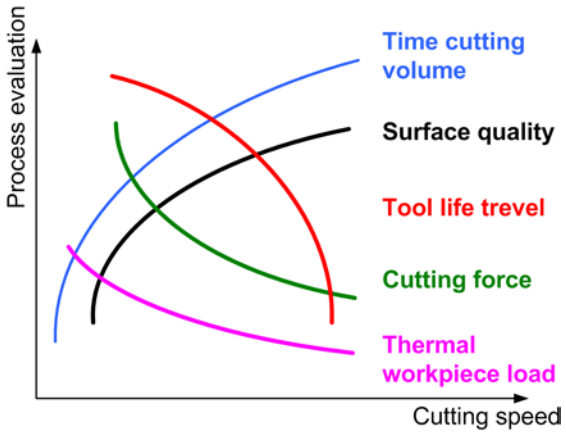

Figure 2.2 Influence of cutting speed on the process evaluation [12]

2.2 *Machining of high performance materials*

Machining of high performance materials generates significant loading on the processing mechanism caused by interaction of machining tool and workpiece (Figure 2.3). It is evident that, this loading is essentially higher compared to conventional materials and it leads to the compliance errors which can be significant and deteriorate surface property. Generally, the compliant errors depend on two independent factors: the loading value and the resistance of the machining mechanism to the loading. Let us concentrate first on the *computation of the force/torque* associated with the machining process, while the issue of the machining mechanism resistance to the loading will be considered further.

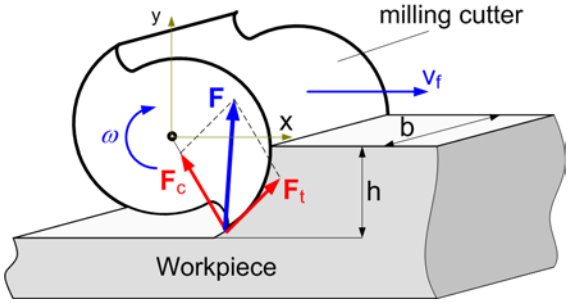

Figure 2.3 Cutting forces in machining process

In general, cutting forces depend on a number of factors. Among the most important ones are the materials of the machining tool and workpiece, the feed rate and the spindle rotation speed, the degree of tool wear, the tool temperature, the cutting geometry, the cutting width and thickness and other factors [47][20][55][49]. Moreover, the cutting forces are not constant and vary with the feed rate. Since in practice it is difficult to find the exact value of the cutting force, it is reasonable to estimate it for the worst case. For this reason, in engineering practice, usually simplified expressions are used where the impact of each factor is taken into account via a relevant correction coefficient [12][15][2]:

$$F = b \cdot h \cdot k_c \cdot K_{PRO} \cdot K_V \cdot K_\gamma \cdot K_{CM} \cdot K_{TW} \cdot K_{CL} \cdot K_{WS} \tag{2.1}$$

Here b, h are the chip width and thickness respectively, k_c is 'the specific cutting force', K_{PRO} is a correction factor for the manufacturing process, K_V is the cutting speed correction factor, K_γ is the rake angle correction factor, K_{CM} is the cutting material correction factor, K_{TW} is the tool wear correction factor, K_{CL} is the cutting fluid correction factors, K_{WS} is the workpiece shape correction factor. Typical values of the correction factors are presented in Table 2.1.

Table 2.1 Correction factors for the cutting force computing [15]

Correction factor	Notation	Value
Manufacturing process	K_{PRO}	$K_{PRO} = 1.2 - 1.4$ (the factor takes into account that the machining indices obtained from turning tests)
Cutting speed	K_V	$K_V = \frac{2.023}{v_c^{0.153}}$ for $v_c < 100\ m/\min$ $K_V = \frac{1.380}{v_c^{0.07}}$ for $v_c > 100\ m/\min$
Rake angle	K_γ	$K_\gamma = 1.09 - 0.012\angle^\circ$ (steel) $K_\gamma = 1.03 - 0.012\angle^\circ$ (cast iron)
Cutting material	K_{CM}	$K_{CM} = 1.05$ (HSS) $K_{CM} = 1.0$ (cemented carbide) $K_{CM} = 0.9 - 0.95$ (ceramic)
Tool wear	K_{TW}	$K_{TW} = 1.3 - 1.5$ $K_{TW} = 1.0$ for sharp cutting edge
Cutting fluid	K_{CL}	$K_{CL} = 1$ (dry) $K_{CL} = 0.85$ (non-water soluble coolant) $K_{CL} = 0.9$ (emulsion-type coolant)
Workpiece shape	K_{WS}	$K_{WS} = 1.0$ (outer diameter turning) $K_{WS} = 1.2$ (inner diameter turning)

Table 2.2 Mechanical properties of typical high performance materials [12]

Material	Main value of specific cutting power $k_{i1.1}$, $[\mathrm{N/mm^2}]$	Rise of the tangent m_c	Typical use
Monel 400 (NiCu30Fe)	2600	0.19	Aerospace material with favourable mechanical and chemical-corrosion properties, pressure tank construction, centrifuges, ship's valves
Inconell 718 (NiCr19NbMo)	2088	0.29	Aerospace material, excellent properties in the extremely low temperature range, very good corrosion resistance, rocket propulsion units, gas turbines, pumps
Ti Al 6 V 4	1370	0.21	Aircraft and spacecraft construction, fittings, mechanical engineering
Al Mg 4.5 Mn	780	0.23	Vehicle construction, shipbuilding, pressure tanks

The remaining coefficient k_c (so called 'the specific cutting force') that is not included in the above table, depends on the chip thickness h nonlinearly and is usually computed as [12]:

$$k_c = \frac{k_{c1.1}}{h^{m_c}} \tag{2.2}$$

where $k_{i1.1}$ is the main value of the specific cutting force (which depends on the material properties), m_c is its exponent. Table 2.2 contains typical values of $k_{c1.1}$ and m_c for several high performance materials.

There also exist nonlinear expressions for the cutting force which take into account some other specific factors. For instance, [34]has proposed the fractal model for cutting force

$$F = \frac{a_1 \cdot h + a_2 \cdot h^2}{1 + a_3 \cdot h} \tag{2.3}$$

where h is the cut depth and a_1, a_2, a_3 are the model coefficients that depend on material properties, specific chip thickness and cutting stiffness.

For the *worst-case analysis*, expressions (2.1) and (2.3) can be reduced to the linear relation

$$F_{max} = 2 \cdot k_c \cdot b \cdot h \tag{2.4}$$

which includes only factor k_c depending on the cutting tool and material properties as well as the cutting cross-section $b \times h$. Numerical values of the maximum cutting forces computed using this expression are presented in (2.4) which includes results for two high performance materials with different cutting settings. They allow us to compare F_{max} for two materials with essentially different cutting stiffness. In particular, for the same cutting depth $h = 0.2\ mm$, cutting width $b = 8\ mm$ and cutting speed from 1000 to 2000 m/min, the

cutting force is about 2 kN for the aluminum alloy (Al Mg 4.5 Mn) and close to 7 kN for Monel 400. It is evident that both of these values are high enough to cause significant deformations of the CNC-machine or robotic manipulator. For instance, for robot manipulator KUKA-240 [10]such loading may generate linear deflections 0.1..5.0 mm and angular deflections 0.1..0.2° depending on the cutting force direction.

It is worth mentioning that, for the constant feed rate, the cutting force reduces with increasing of the spindle speed. This effect is in good agreement with equation (2.4): increasing of the spindle speed for the same feed rate does not change the cutting speed, while the chip thickness h reduces. This effect is widely used in practice. But to save the processing time, usually the feed rate increases with the spindle speed. This does not allow us to reduce relevant compliance errors.

Another issue that should be taken into account while evaluating reactions associated with machining of high performance materials is related to the *spindle axial torque*. Usually this value is obtained from experiments [17], but it is also possible to estimate its range from nominal values of spindle power and rotation rate. For instance, the values 20 kW and 10000 rpm correspond to the torque of about 10 N·m (for the efficiency factor 50%). For typical industrial application based on robot KUKA-240, this torque may cause linear/angular deflections of 0.001..0.008 mm and 0.1..1.6° respectively (depending on the feed direction). Besides, the cutting forces may exert essential *lateral torque* with respect to the robot-mounting flange. For example, for the tool reference point offset of 100 mm, the cutting force 2-7 kN (see Table 2.3) produces the torque 20-140 N·m that makes non-negligible linear and angular deflections.

Table 2.3 Cutting forces for high performance materials

Material	Depth of cutting h, mm	Width of cutting b, mm	Cutting speed v_c m/min		
			1000	1500	2000
Monel 400 (NiCu30Fe)	0.2	8	6.97 kN	6.77 kN	6.64 kN
		16	13.94 kN	13.54 kN	13.28 kN
	1	8	25.65 kN	24.93 kN	24.44 kN
		16	51.30 kN	49.86 kN	48.88 kN
Al Mg 4.5 Mn	0.2	8	2.23 kN	2.17 kN	2.12 kN
		16	4.46 kN	4.34 kN	4.24 kN
	1	8	7.70 kN	7.48 kN	7.33 kN
		16	15.40 kN	14.96 kN	14.66 kN

Hence, the cutting forces and torques associated with milling of high performance materials are essentially higher compared to conventional ones. They may cause significant linear and angular deflections of the machining tool that lead to essential reduction of the accuracy and quality of the final product. This issue justifies the goal of this research work.

2.3 *Machining with robots versus traditional machining tools*

At present, there are two main approaches in designing of machining workcells: (i) utilization of classical CNC-machines with Cartesian architecture and (ii) using industrial robots of either serial or parallel architecture. Both of them have their own advantages and disadvantages that are briefly discussed below from the point of view of applicability to machining of high performance materials.

CNC-machines. Computer Numerical Control (CNC) machines refer to the automatic machine tools, which use abstractly programmed commands to specify the tool path and relative location of the workpiece while machining [23]. The earliest CNC equipment was based on existing traditional machine tools that were supplemented by motors that control the cutter feed rate. Further, all control execution functions were given to computers and the control program preparation was carried out in CAD/CAM environment [30][54][52]. The latter advances have essentially changed the machining process and provided fundamental benefits, which can be summarized as follows:

(i) full automation of the machining and programming processes, which requires the final dimensions of the product only; this reduces human errors to minimum;

(ii) ability to produce both simple trajectories and the surfaces of high complexity, which extend their application from conventional milling to drilling, lathing, laser cutting, etc.;

(iii) high accuracy and good surface quality that is insured by high rigidity of the tool manipulation mechanism and accurate control of the tool motions;

(iv) flexibility of machining which allows us to process different types of products and combine several operations (milling, drilling, grinding) by changing control program only; this essentially reduces the manufacturing time and the product cost;

There are also some other benefits that are offered by the CNC machines and promote their wide application in industry (advanced machine control, more precise production planning due to high reputability of the machining, etc.) [30]. However, relatively high cost and limited workspace are usually treated as their main disadvantages [19]. Typical examples of CNC-machines are presented in Figure 2.4.

(a) CNC milling machine (b) CNC grinding machine (c) CNC machining center

Figure 2.4 Examples of CNC-machines

Variety of existing CNC-machines is usually classified with respect to the type of motion control system, implemented control algorithm and the number of actuated axes. With respect to the *motion control system*, the CNC-machines may be classified as point-to-point and contouring ones. The first of them, also called a positioning system, moves the tool to the given location without control of the path and speed (they are not important for some applications, such as drilling). Continuous path systems ensure the path and speed control of the tool while machining, they implement simultaneous control of all driven axes. Typical application areas of continuous motion control are milling and turning.

Based on the *control algorithm,* the CNC-machines are divided into open-loop and closed-loop ones. In the open-loop systems, the actuator input is entirely defined by the programmed instructions and there is no feedback to check whether the desired goal (position, velocity) has been achieved. They are obviously rather sensitive to external disturbances, so their application area is limited by the cases where the accuracy requirements are not critical. In contrast, closed-loop systems have a feedback, which allows us to compensate any differences between the desired position/velocity and its actual value. This feedback may be implemented using both analogous and digital technique, the close-loop systems are usually considered to be very precise and attractive for accurate machining.

With respect to the third classification factor, the *number of axes,* the CNC-machines with 2, 3, 4 and 5 axes are distinguished. The first of these usually have only two translational driven axes that ensure control of the tool in the plane. The 3-axis machines are able to process more complex 3-dimentional surfaces, they usually employ three translational drives with mutually orthogonal axes. The more sophisticated are 4- and 5-axis CNC machines that are able to change the tool orientation, in addition to translational motions. This allows to produce more complex tool path movements and to process very complicated products. In general, increasing of the number of axes provides numerous advantages such as better surface quality, reduction of the machining time, improved access to under cuts and deep pockets, etc. It is worth also mentioning that the axes may be actuated either sequentially or simultaneously, but present systems usually implement the simultaneous control.

In modern CNC systems, the machining trajectory design is highly automated and is performed in a CAD/CAM environment. It is used for creating spatial representation of a part; planning and optimization of the tool paths and cutting parameters in creating CNC code; loading, initialization, and operating the CNC-machine; etc. So, CAD/CAM technologies introduce essential benefits to machining such as higher productivity, reduced design time, more accurate designs, less time required for modifications, repeatability.

Hence, the CNC-machines ensure a number of benefits for machining of high performance materials. However, for some aeronautic applications that are closely related to this research, they have rather limited workspace and are not applicable for machining of large dimensional parts. In this case, industrial robots are more attractive, so their suitability for the milling of high performance materials is considered below.

Industrial robots. For the considered application area, robots could gain all functionalities of the CNC-machines and are reasonable alternative for them. Also, they provide *larger workspace* and more *flexibility* [11][4][21]. Besides, emerging technologies allow robots to perform diverse manufacturing processes such as complex cutting and material removal, tapping and drilling, surface finishing and others. All these functions can be realized by the same robot, that makes it universal, while CNC-machines can execute only one or a group of similar operations. In addition, robot-based machining cells are applicable for secondary operations and have a relatively large working envelope, which is extremely important for large components. Such

machining cells are more flexible and allow us to produce different products at the same time, they can be also easily adopted to manufacturing of other products. They usually provide two alternative solutions to modify the tool path: (i) to change it in the CAD/CAM system, or (ii) to teach a robot in some key points. Robots are more intelligent and ensure more sophisticated motion control, and users can map their inaccuracies and compensate for them off-line using a dedicated model (the stiffness model for instance, as in this work) [40].

In machining applications, robots often use force and torque sensors that allow online estimation of the deflections in the tool locations with respect to the desired ones. The force and torque sensors are usually integrated into a robot's wrist, and the robot controller are able to compensate these deflections via relevant calculations. However, to achieve good quality of machining process and to eliminate robots errors caused by different factors, some additional research is required [42]. This is the main issue that resists to robot applications in some areas.

With respect to their architecture, all industrial robots can be classified into two groups. First group includes robots with strictly serial architecture, which are currently the most common industrial ones. The second group put together manipulators with strictly parallel architecture and cross-linkages [25][26]. Typical examples of robots from both groups are presented in Figure 2.5. In order to indicate advantages of both architectures let us focus on their principal features.

(a) serial industrial robot (b) parallel industrial robot

Figure 2.5 A serial Kuka robot (a) and an Adept parallel robots (b)

Serial robots. This type of robots is based on serial kinematic chains composed of rather rigid links connected by actuated joints. The joints may be either rotational or translational. The main advantage of serial robots is large workspace with respect to their own volume and occupied floor space. But, since serial manipulators have open kinematic structure, all errors are accumulated and amplified from link to link. Besides, it is impossible (or rather difficult) to get high stiffness and high dynamic properties simultaneously. For instance, robots with high stiffness usually are heavy and cannot provide high speed. Moreover, their own weight induces undesirable significant stresses in actuated joints that reduces allowed payload. On the other hand, serial robots with small link mass have low stiffness and cannot provide high payload because of significant compliance errors. These issues essentially decrease efficiency and application areas of such manipulators. However, some limitations related to manufacturing errors can be withdrawn by advanced control.

According to its kinematic architecture, serial manipulators can be classified into three main groups: (a) SCARA robots, (b) Articulated robots and (c) Cartesian/Gantry robots [57]. It is worth mentioning that

sometimes the robot classification includes some other types of manipulators (cylindrical, spherical, etc.) but here they are included in articulated ones.

The *SCARA* acronym stands for "Selective Compliant Assembly Robot", it is also often referred to as: "Selective Compliant Articulated Robot Arm". This type of robots is based on a 4-axis manipulator (Figure 2.6a) [9] that ensures motion to any point within its workspace (X-Y-Z translation) and the end-effector rotation around the vertical axis (theta-Z). For this architecture, the vertical Z-motion is independent and is provided by a dedicated linear actuator, while three remaining rotational joints (with parallel axes) ensure full range of translations and rotations in XY-plane. Because of this specific architecture (with three parallel rotational joints), SCARA is slightly compliant in the XY-plane but is rather rigid in the Z-direction (so called selective compliance). The selective compliant feature makes this robot highly suitable for many types of assembly operations. Due to low mass in moving parts, it provides very good dynamic properties. This promote SCARA to be ideal for pick-and-place, palletizing and de-palletizing, machine loading/unloading and packaging applications, which require fast, repeatable and articulate point-to-point movements.

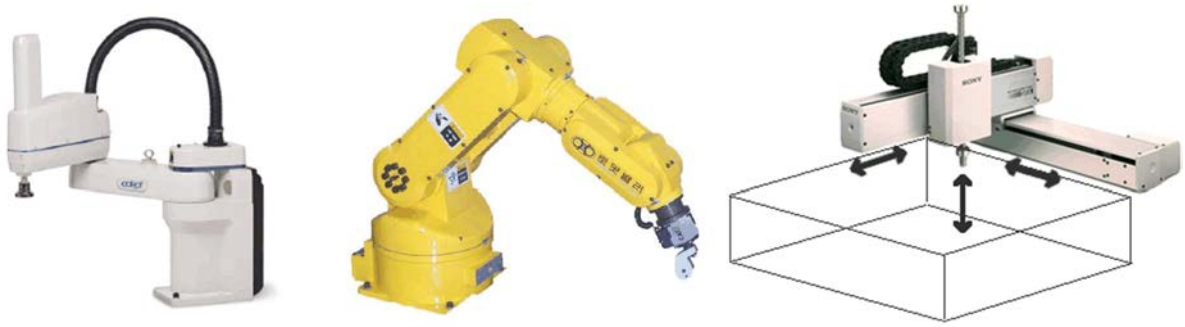

(a) SCARA robot (b) articulated robot (c) Cartesian/Gantry robot

Figure 2.6 Typical architectures of serial robots

The second group includes *articulated robots* (Figure 2.6b) [24][3], which are also called "anthropomorphic arms". Their mechanical structure is based on rotational joints and the links are arranged in a chain. Usually the articulated robots have five or six controlled axes, while robots with seven and more actuated joints also exist. This structure provides very good kinematic dexterity, so the robots have an ability to reach the target location over obstacles and ensure almost any position and orientation of the tool within the workspace. Essential advantage of the articulated robots is that they are very compact and provide the largest workspace relative to their size. However, because of complexity of direct/inverse kinematics, their control is not trivial: when driving an articulated robot in its natural coordinate system (joint space), it is difficult to obtain a straight-line-motion of the end-effector in Cartesian space. So, intensive computations are required to transform the Cartesian location into the actuated joint angles (and vice versa), but this problem is not already significant because of essential computing capacity of modern microprocessors. The capabilities of the articulated robots make them well suit for a wide variety of industrial application, including machining [31][1].

The third group includes *Cartesian robots* (Figure 2.6c) [8], which have almost the same kinematic architecture as conventional CNC-machines. The main differences are in the areas of control principle, programming language and mechanical design of the end-effector connector, which for the robots is rather universal. The mechanical structure of such robots is based on three translational actuated joints whose axes

are mutually orthogonal. Such arrangement ensures very simple control when any motion in X-Y-Z space is achieved by straightforward actuation of relevant joints. Cartesian robots have a rectangular workspace whose volume can be increased easily. Extremely large work envelope is ensured by Gantry robots (also belonging to the Cartesian family), where one of the horizontal translational axes is supported at both ends. Due to their mechanical structure, Cartesian robots provide high rigidity and good accuracy but their kinematic dexterity is rather limited; sometimes they cannot reach around objects. Besides, to satisfy the large workspace requirement, they need large volumes to operate and occupy essential floor space. Because of its rigidity, such robots are very attractive for machining applications, but only if the tool orientation may remain the same during processing.

(a) HexaM 5-axis milling machine

(b) Hexapod OKUMA machine

(c) Machine Verne

(d) Hexapod-Machine Mikromat 6X

(e) Urane SX

Figure 2.7 Examples of parallel robots integrated in the machining cells

Parallel robots. This type of robots, which are also often referred to as parallel kinematic machines (PKM), is a closed-loop mechanism whose end-effector is linked to the base by several independent kinematic chains [25]. The kinematic chains are composed of several links that are connected to each other by both passive joints and actuated joints (rotational or translational). Such kinematics claim to offer several essential *advantages*, like high structural rigidity, high dynamic capacities and high accuracy [44][50][51]. Another important advantage of parallel robots is better accuracy, because here the position and orientation errors of separate kinematic chains are averaged by the end-platform (instead of straightforward accumulation, as in serial robots). Besides, using special arrangement of kinematic chains, it is possible to ensure high stiffness and high dynamic properties simultaneously. These capabilities make the parallel robots well suitable for high-

speed machining and they are often used in the manufacturing cells (Figure 2.7), for instance in HexaM 5-axis milling machine, Hexapod OKUMA machine, the VERNE machine, Hexapod-Machine Mikromat 6X, Urane SX, and others [36][14][16][28][39][41].

However, parallel robots have very complex workspace and highly non-linear relation between natural coordinates (actuated joints) and Cartesian ones. Consequently, their performances (maximum speeds, accuracy and rigidity) essentially differ from point to point and also depend on the moving directions. Other *disadvantages* of parallel manipulators are their large footprint-to-workspace ratio (except the Tricept robot which requires less space) and small range of motion because of parallel configuration. These are the main obstacles for the machine application of parallel robots [18][38][50].

At present, there exists a large variety of parallel manipulators, several examples are presented in Figure 2.8. Depending on the architecture, they may be divided into two groups that differ by the type of connection between the base-platform and the serial chains [6].

The first group contains manipulators with fixed foot points and variable length struts. Most robots of this group implement the Stewart-Gough architecture, have 6 degrees of freedom and are called Hexapods (Figure 2.9) [25]. They provide high precision and accuracy, good stiffness and high load/weight ratio. Due to these essential advantages, Hexapods are often used in flight simulators, precision machining, surgical robots, and other areas. By variation of the link lengths, Hexapods may satisfy both small and large workspace, but increasing of the link length has a direct effects on the accuracy. The main technical problem of Hexapod is high friction in the ball joints. Typical examples of parallel manipulators belonging to the first group are presented in (Figure 2.8 a-g), they include VARIAX, HEXA, TRICEPT, TRIPOD, Delta and others [13][35][37][29][7][46][56].

The second group includes manipulators with foot points gliding on fixed linear joints. Robots of this group differ by the number of actuated translational axes and their location with respect to each other, as well as by the type of links connecting the base and moving platforms. Typically, they have 5 or 6 degrees of freedom (HEXAGLIDE, HexaM) but there are also 3 degrees of freedom translational manipulators of this family (Orthoglide) that employ parallelogram-based links similar to Delta robots [53][6][45]. The robots of the second group (see Figure 2.8 h-l) are attractive for machining application because of lower moving mass compared to the hexapods and tripods. However, to ensure large workspace, such robots require large volumes to operate and occupy essential floor space.

Hence, parallel robots provide essential benefits compared to the serial ones, which promote them to high speed and high precision machining applications considered in this work. For this reason, they have already been employed in commercial machining centers (see Figure 2.7) that progressively replace conventional CNC machines based on serial Cartesian architecture. A short summary of a dedicated comparison study is given below.

Figure 2.8 Typical architectures of parallel robots

(a) Fanuc F-200i Robot

(b) M-840 HexaLight 6-Axis Positioning System

(c) M-850K Ultra-High Load Hexapod

(d) M-850K Large-Aperture High-Load Hexapod

Figure 2.9 Examples of Hexapod parallel kinematic machines

Résumé. Integrated results of the above analysis are summarized in Table 2.4. They show that the CNC-machines are quite suitable for majority of machining operations provided that a large workspace and high dynamics are not required. However, for high speed machining of relatively large parts that are widely used in the aerospace and shipbuilding industries, conventional CNC-machines can be hardly used. In contrast, robotic manipulators are able to execute such tasks and simultaneously ensure higher flexibility of automated machining cells. The only problem with robots application is their rather low stiffness that leads to non-negligible position errors under the forces/torques of the technological process. Thus, the next section focuses on the robot accuracy issue.

Table 2.4 Comparison of CNC and robotic-based machining

Performance factor	Conventional XYZ CNC-machines	Robotic-based machining	
		Serial robots	Parallel robots
Workspace	Limited (by foot print)	Large (limited by link lengths)	Limited (by parallel architecture)
Flexibility	Limited number of operations	Any operation in the workspace	
Dynamics	Low	Limited	High
Accuracy	High	Depends on the stiffness, link weights and payload	
Stiffness	High	Moderate, compliance is accumulated along the chain	High, separate chain stiffness is aggregated

2.4 References

[1] E. Abele, M. Weigold, S. Rothenbücher, Modeling and Identification of an Industrial Robot for Machining Applications, Annals of the CIRP Vol. 56/1/2007, 387-390

[2] Dubbel handbook of mechanical engineering, Ed. W. Beitz and K.-H. Kuttner, Springer-Verlag London Limited, Great Britain 1994

[3] F. Benamar, P. Bidaud, F. Le Menn, Generic differential kinematic modeling of articulated mobile robots, Mechanism and Machine Theory, Volume 45, Issue 7, 2010, Pages 997-1012

[4] T. Brogardh, Present and future robot control development—An industrial perspective, Annual Reviews in Control 31 (2007) 69–79

[5] K. Castelino R. D'Souza and P.K. Wright, Tool-path Optimization for Minimizing Airtime during Machining, Journal of Manufacturing Systems Vol. 22/No, 3 2003, 173-180

[6] D. Chablat, P. Wenger, Architecture Optimization of a 3-DOF Parallel Mechanism for Machining Applications, the Orthoglide, IEEE Transactions On Robotics and Automation 19(3) (2003) 403-410.

[7] R. Clavel (1988). DELTA, a fast robot with parallel geometry, *Proceedings, of the 18th International Symposium of Robotic Manipulators*, IFR Publication, pp. 91–100.

[8] M. Dadfarnia, N. Jalili, Z. Liu, D.M. Dawson, An observer-based piezoelectric control of flexible Cartesian robot arms: theory and experiment, Control Engineering Practice, Vol. 12, Issue 8, 2004, pp. 1041-1053

[9] M. Taylan Das, L. Canan Dülger, Mathematical modelling, simulation and experimental verification of a scara robot, Simulation Modelling Practice and Theory, Volume 13, Issue 3, April 2005, Pages 257-271

[10] C. Dumas, S. Caro, M. Cherif, S. Garnier and B. Furet, A Methodology for Joint Stiffness Identification of Serial Robots, Intelligent Robots and Systems (IROS), 2010 IEEE/RSJ International Conference on, pp. 464 - 469

[11] Irene Fassi, Gloria J. Wiens,Multiaxis Machining: PKMs and Traditional Machining Centers, Journal of Manufacturing Processes, Volume 2, Issue 1, 2000, Pages 1-14

[12] Garant machining manual, http://www.hoffmann-group.com/download/en/ zerspanungshandbuch/en-zerspanungshandbuch.pdf

[13] M. Geldart, P. Webb, H. Larsson, M. Backstrom, N. Gindy, K. Rask, A direct comparison of the machining performance of a variax 5 axis parallel kinetic machining centre with conventional 3 and 5 axis machine tools, International Journal of Machine Tools and Manufacture, Vol. 43, Issue 11, 2003, pp. 1107-1116

[14] Goto, J, Okuma Krauss-Maffei Injection Moulding Machine--OSP KM-5000 With Computerized Numerical Control, Jpn. Plast. Age. Vol. 23, no. 205, pp. 35-38. Sept.-Oct. 1985

[15] Springer handbook of mechanical engineering, Ed. K-H Grote and E. Antonsson, Springer, New York 2009

[16] Daniel Kanaan, Philippe Wenger, Damien Chablat, Kinematic analysis of a serial–parallel machine tool: The VERNE machine, Mechanism and Machine Theory, Volume 44, Issue 2, 2009, Pages 487-498

[17] B. Kaya, C. Oysu, H.M. Ertunc, Force-torque based on-line tool wear estimation system for CNC milling of Inconel 718 using neural networks, Advances in Engineering Software 42 (2011) 76–84

[18] Kim, J., Park, C., Kim, J. and Park F.C., 1997, "Performance Analysis of Parallel Manipulator Architectures for CNC Machining Applications," Proc. IMECE Symp. On Machine Tools, Dallas.

[19] Krause, P.C., Analysis of Electrical Machinery, New Work, McGraw-Hill (1984)

[20] A. Lamikiz, L.N. Lorpez de Lacalle, J.A. Sarnchez, M.A. Salgado, Cutting force estimation in sculptured surface milling, International Journal of Machine Tools & Manufacture 44 (2004) 1511–1526

[21] Soren Larsson, J.A.P. Kjellander, Motion control and data capturing for laser scanning with an industrial robot, Robotics and Autonomous Systems 54 (2006) 453–460

[22] Shih-Wei Lin, Zne-Jung Lee, Kuo-Ching Ying, Chung-Cheng Lu, Minimization of maximum lateness on parallel machines with sequence-dependent setup times and job release dates, Computers & Operations Research 38(2011) 809–815

[23] Chih-Ching Lo, CNC machine tool surface interpolator for ball-end milling of free-form surfaces, International Journal of Machine Tools & Manufacture 40 (2000) 307–326

[24] Shin-ichi Matsuoka, Kazunori Shimizu, Nobuyuki Yamazaki, Yoshinari Oki, High-speed end milling of an articulated robot and its characteristics, Journal of Materials Processing Technology, Volume 95, Issues 1-3, 15 October 1999, Pages 83-89

[25] J.-P. Merlet, Parallel Robots, Kluwer Academic Publishers, Dordrecht, 2006.

[26] J.-P. Merlet, C. Gosselin, Parallel mechanisms and robots, In B. Siciliano, O. Khatib, (Eds.), Handbook of robotics, Springer, Berlin, 2008, pp. 269-285.

[27] A. Nektarios, N.A. Aspragathos, Optimal location of a general position and orientation end-effector's path relative to manipulator's base, considering velocity performance, Robotics and Computer-Integrated Manufacturing, Volume 26, Issue 2, April 2010, Pages 162-173

[28] Neugebauer, R., Wieland, F., Schwaar, M., Karczewski, Z., Hochmuth, C., Erfahrungen mit dem Mikromat Hexapod 6X (1998), Internationales Parallelkinematik-Kolloquium 1998. Zürich: IWF ETH-Zürich, 1998, pp. 65-79

[29] K.E. Neumann, 1988, “Robot,” United State Patent no. 4,732,625.

[30] S.T. Newmana, A. Nassehi, X.W. Xu, R.S.U. Rosso Jr, L. Wang, Y. Yusof, L. Ali, R. Liu, L.Y. Zheng, S. Kumar, P. Vichare, V. Dhokia, Strategic advantages of interoperability for global manufacturing using CNC technology, Robotics and Computer-Integrated Manufacturing 24 (2008) 699– 708

[31] Adel Olabi, Richard Béarée, Olivier Gibaru, Mohamed Damak, Feedrate planning for machining with industrial six-axis robots, Control Engineering Practice, Volume 18, Issue 5, May 2010, Pages 471-482

[32] Cuneyt Oysu, Zafer Bingu, Application of heuristic and hybrid-GAS Aalgorithms to tool-path optimizati on problem for minimizing airtime during machining, Engineering Applications of Artificial Intelligence 22 (2009) 389–396

[33] C. O. Ozgur, J. R. Brown, A two-stage traveling salesman procedure for the single machine sequence-dependent scheduling problem, Omega, Volume 23, Issue 2, April 1995, Pages 205-219

[34] H. Paris, D. Brissaud, A. Gouskov, A More Realistic Cutting Force Model at Uncut Chip Thickness Close to Zero, Annals of the CIRP, 56:415-418, 2007

[35] Pierrot, F., Dauchez, P., Fournier, A., HEXA: a fast six-DOF fully-parallel robot, Fifth International Conference on Advanced Robotics, 1991. 'Robots in Unstructured Environments', 91 ICAR., vol. 2 pp. 1158 - 1163

[36] F. Pierrot and T. Shibukawa, From Hexa to previous termHexaM.next term In: C.R. Boër, L. Molinari-Tosatti and K.S. Smith, Editors, Parallel kinematic previous termmachines:next term theoretical aspects and industrial requirements, Springer-Verlag (1999), pp. 357–364.

[37] Francois Pierrot, Vincent Nabat, Olivier Company, Sebastien Krut, Optimal Design of a 4-DOF Parallel Manipulator, From Academia to Industry, IEEE Transactions on Robotics, vol. 25, no. 2, 2009 pp 213-224

[38] Rehsteiner, F., Neugebauer, R., Spiewak, S. and Wieland, F., 1999, “Putting Parallel Kinematics Machines (PKM) to Productive Work,” Annals of the CIRP, Vol. 48:1, pp. 345–350.

[39] Renault Automation Magazine, n° 21, may 1999

[40] P. Rocco, G. Ferretti, G. Magnani, Implicit force control for industrial robots in contact with stiff surfaces, Automatica, Volume 33, Issue 11, November 1997, Pages 2041-2047

[41] Seungkil Son, Taejung Kim, Sanjay E. Sarma, Alexander Slocum, A hybrid 5-axis CNC milling machine, Precision Engineering, Volume 33, Issue 4, October 2009, Pages 430-446

[42] J. Sulzer, I. Kovač, Enhancement of positioning accuracy of industrial robots with a reconfigurable fine-positioning module, Precision Engineering, 34(2) 2010, pp. 201-217

[43] Myriam Terrier, Arnaud Dugas, Jean-Yves Hascoet, Qualification of parallel kinematics machines in high-speed milling on free form surfaces, International Journal of Machine Tools & Manufacture 44 (2004) 865–877.

[44] Tlusty, J., Ziegert, J, and Ridgeway, S., 1999, “Fundamental Comparison of the Use of Serial and Parallel Kinematics for Machine Tools,” Annals of the CIRP, Vol. 48:1, pp. 351–356.

[45] Toyama, T. et al, 1998, “Machine Tool Having Parallel Structure,” United State Patent no. 5,715,729.

[46] Tsai, L.W. and Joshi, S., 2000, “Kinematics and Optimization of a Spatial 3-UPU Parallel Manipulator,” ASME Journal of Mechanical Design, Vol. 122, pp. 439–446.

[47] C.-L. Tsai, Y.-S. Liao, Prediction of cutting forces in ball-end milling by means of geometric analysis, journal of materials processing technology 205 (2008) 24–33

[48] Veeramani,D.,Gau,Y.S.,1998.Model for tool-path plan optimization in patch-by-patch machining. International Journal of Production Research 36(6), 1633–1651.

[49] Min Wan, Wei-Hong Zhang, Systematic study on cutting force modelling methods for peripheral milling, International Journal of Machine Tools & Manufacture 49 (2009) 424–432

[50] Wenger, P., Gosselin, C. and Maille, B., 1999, “A Comparative Study of Serial and Parallel Mechanism Topologies for Machine Tools,” Proc. PKM’99, Milano, pp. 23–32.

[51] Wenger, P., Gosselin, C. and Chablat, D., 2001, “A Comparative Study of Parallel Kinematic Architectures for Machining Applications,” Proc. Workshop on Computational Kinematics, Seoul, Korea, pp. 249–258.

[52] A. Werner, Z. Lechniak, K. Skalski, K. Keĵdzior, Design and manufacture of anatomical hip joint end prostheses using CAD/CAM systems, Journal of Materials Processing Technology 107 (2000) 181±186

[53] Wiegand, A., Hebsacker, M., Honegger, M., Parallele Kanematik und Lineamotoren: Hexaglide - ein neues, hochdynamisches Werkzeugmaschinenkonzept, Technische Rundschau Transfer Nr. 25, 1996.

[54] X.W. Xu, S.T. Newman, Making CNC machine tools more open, interoperable and intelligent—a review of the technologies, Computers in Industry 57 (2006) 141–152

[55] Min Xu, R. B. Jerard and B. K. Fussell, Energy Based Cutting Force Model Calibration for Milling, Computer-Aided Design & Applications, Vol. 4, Nos. 1-4, 2007, pp 341-351

[56] Dan Zhang, Lihui Wang, Conceptual development of an enhanced tripod mechanism for machine tool, Robotics and Computer-Integrated Manufacturing, Volume 21, Issues 4-5, 2005, Pages 318-327

[57] http://www.robotmatrix.org/default.htm

3 STIFFNESS MATRIX OF ROBOTIC MANIPULATORS WITH PASSIVE JOINTS

3.1 Introduction

IN many applications, manipulator stiffness becomes one of the most important performance measures of a robotic system. In particular, for milling, drilling and other types of machining, the stiffness defines the positioning errors due to interaction between the workpiece and the technological tool. Similarly, in industrial pick-and-place automation, the manipulator stiffness defines admissible velocity/acceleration while approaching the target point, in order to avoid undesirable displacements due to inertia forces. Other examples include medical robots, where elastic deformations of mechanical components under the task load are the primary source of positioning errors.

Numerically, this property is usually described by the stiffness matrix $\mathbf{K}_C$, which defines a linear relation between the translational/rotational displacement in Cartesian space and the static forces/torques causing this transition (assuming that all of them are small enough). The inverse of $\mathbf{K}_C$ is usually called the compliance matrix and is denoted as $\mathbf{k}_C$. As it follows from related works, for conservative systems, $\mathbf{K}_C$ is 6×6 semi-definite non-negative symmetrical matrix but in general case its structure may be non-diagonal to represent the coupling between the translation and rotation.

The problem of stiffness matrix computing for different types of manipulators has been in the focus of robotic experts for several decades [1-18]. The existing approaches may be roughly divided into three main groups: (i) the Finite Element Analysis (FEA) [19-23], (ii) the Matrix Structural Analysis (SMA) [24-28], and (iii) the Virtual Joint Method (VJM) [1-2,8,14,29-30]. The most accurate of them is obviously the FEA-based technique but it requires rather high computational expenses. The SMA is less computationally hard due to fairly large structural elements employed (3D flexible beams instead of numerous tiny tetrahedrals and hexahedrals of FEA) but nevertheless it is not convenient for the parametric analysis. And finally, the VJM method is the most attractive in robotic domain since it operates with an extension of the traditional rigid model that is completed by a set of compliant virtual joints (localized springs), which describe elastic properties of the links, joints and actuators. This Chapter contributes to the VJM technique and focuses on some particularities of the manipulators with passive joints.

For conventional serial manipulators (without passive joints), the VJM approach yields rather simple analytical presentation of the desired stiffness matrix $\mathbf{K}_C$. Relevant expression $\mathbf{K}_C = \mathbf{J}_\theta^{-T}\mathbf{K}_\theta\mathbf{J}_\theta^{-1}$ can be found in the work of Salisbury [1] who assumed that the mechanical elasticity is concentrated in actuators and the deflections are small enough to apply linear approximation of the force-deflection relation. Here the matrix $\mathbf{K}_\theta$ aggregates the stiffness coefficients of all elastic joints, and $\mathbf{J}_\theta$ is the corresponding kinematic Jacobian. Further, this result was extended by Gosselin for case of parallel manipulators taking into account elasticity of other mechanical elements [2]. More recent publications present VJM-based stiffness analysis for particular case studies, such as various variants of the Stewart–Gough platform, manipulators with US/UPS legs, CaPAMan, Orthoglide, H4 etc. [27-34].

It should be noted that in the majority of related works, the presence of passive joints[1] does not cause any specific computational problems, since these joints are eliminated via geometrical constraints describing the assembling of the relevant parallel architecture [2]. Besides, in most of publications, it is implicitly assumed that the Jacobian $\mathbf{J}_\theta$ describing influence of the elastic joints on the end-location is non-singular[2], i.e. $rank\left(\mathbf{J}_\theta\right)=6$, to ensure inversion of the related matrix in the modified expression $\mathbf{K}_C=\left(\mathbf{J}_\theta\mathbf{K}_\theta^{-T}{}_\theta\mathbf{J}_\theta^T\right)^{-1}$ that always produce non-singular $\mathbf{K}_C$. It is obvious that the assumption concerning $\mathbf{J}_\theta$ is completely realistic if the VJM model includes at least a single 6-dimensional virtual spring of a general type (see [38] for details), while it is not realistic that the manipulator stiffness matrix is always non-singular. Hence, common stiffness modelling techniques must be revised with respect to influence of passive joints, which in certain cases can not be straightforwardly eliminated from the kinetostatic equations and, consequently, may cause singularity of $\mathbf{K}_C$[3].

In this Chapter, another approach is applied that originates from our publication [30] where the desired stiffness matrix $\mathbf{K}_C$ of size 6×6 is extracted from the inverse of a larger matrix, of size $\left(6+n_q\right)\times\left(6+n_q\right)$, which additionally includes the passive joint Jacobian $\mathbf{J}_q$ (n_q is the passive joint number). Advantages of this approach and its ability to produce singular stiffness matrices were confirmed by a number of examples, but explicit analytical solution was not presented. Hence, this work concentrates on analytical computations of the stiffness matrix and also on influence of the passive joints on particular elements of $\mathbf{K}_C$.

It is also worth mentioning that some previous works [30] propose (or at least discuss) a trivial solution of the considered problem, which deals with a straightforward modification of the matrix $\mathbf{K}_\theta$, in accordance with the passive joint type and geometry (corresponding rows and columns are set to zero). However, as it will be shown below, this straightforward approach gives true results if (and only if) the matrix $\mathbf{K}_\theta$ is diagonal, but it is not valid in general case where there is a coupling between different types of the elementary virtual springs presented by non-diagonal coefficients.

The remainder of this Chapter is organised as follows. Section 4.2 presents a simple motivation example that confirms the problem non-triviality. Then, Sections 4.3 and 4.4 propose relevant analytical solutions for a serial kinematic chain and a parallel manipulator respectively. Section 4.5 focuses on computational issues and proposes recursive procedure and a set of corresponding analytical rules. Section 4.6 contains application

[1] It should be mentioned that here passive joints have stiffness equal to zero and they should be distinguished from passive compliant joints studied by other authors, whose stiffness is nonzero.

[2] It is important to distinguish the conventional kinematic Jacobian $\mathbf{J}$, which is computed with respect to actuated coordinates and may be both singular and non-singular, and the Jacobian $\mathbf{J}_\theta$ that is computed with respect to the virtual springs coordinates and is always non-singular. Besides, they differ in sizes, which for a standard serial 6-d.o.f. manipulator are respectively 6x6 and 6×36.

[3] The main problem with straightforward application of the classical expression $\mathbf{K}_C=(\mathbf{J}_\theta\mathbf{K}_\theta^{-1}\mathbf{J}_\theta^T)^{-1}$ to the manipulators with passive joints is related to the invertibility of the matrix $\mathbf{K}_\theta$, which becomes singular if stiffness of some virtual springs is assign to zero (to describe the passive joint properties). In fact, there are two sequential inversions here applied to singular matrices that may be treated similarly to an indeterminate form "1/(1/0)" in calculus that finally produces 0, but cannot be obtained numerically. So, finally, double inversion of singular matrix should produce another singular matrix, but numerical computations obviously fails. To overcome this difficulty and to solve the problem in a rigorous way, our previous publication [30] proposes a dedicated technique that deals with inversion of non-singular matrices of higher dimension and extraction from them relevant 6x6 sub-matrix.

examples that demonstrate the developed technique advantages. And finally, Section 4.7 summarizes the main results and gives prospective for future work.

3.2 Motivation example

Let us present first a simple example that demonstrates non-trivial transformation of the stiffness matrix due to the presence of passive joints. For the purpose of simplicity, let us limit our study to 2D Cartesian space and consider a single manipulator link, which is assumed to be fixed at the one end. It is also assumed that the external loading (the forces F_x, F_y and the torque M_z) is applied to another end; either directly or through a passive joint.

Under these assumptions, the elastostatic properties of the link can be described by a symmetrical stiffness matrix $\mathbf{K} = \left[K_{ij} \right]$ of size 3×3 and its potential energy due to elastic deformations (linear deflections $\delta x, \delta y$ and angular deflection $\delta\varphi$) may be expressed as

$$E\left(\delta x, \delta y, \delta\varphi\right) = \frac{1}{2} \cdot \left[\delta x \ \delta y \ \delta\varphi\right] \cdot \begin{bmatrix} K_{11} & K_{12} & K_{13} \\ K_{21} & K_{22} & K_{23} \\ K_{31} & K_{32} & K_{33} \end{bmatrix} \cdot \begin{bmatrix} \delta x \\ \delta y \\ \delta\varphi \end{bmatrix} \tag{3.1}$$

If the link is equipped with a passive joint, the energy of this mechanical system (link with passive joint) must be minimized with respect to the joint variable[4]. For instance, in the case of the rotational passive joint R_z allowing free rotation around the z-axis at the reference point, the potential energy should be rewritten as

$$E_p\left(\delta x, \delta y\right) = \min_{\delta\varphi} E\left(\delta x, \delta y, \delta\varphi\right) \tag{3.2}$$

and the passive joint variable $\delta\varphi$ may be expressed via the remaining coordinates as $\delta\varphi = -(K_{13}\,\delta x + K_{23}\,\delta y) / K_{33}$. Then, after relevant transformations and computations of the second-order derivatives (i.e. the Hessian of E_p with respect to *x*, *y* and φ)

$$K_{11}^p = \partial^2 E_p / \partial x^2 , \ K_{12}^p = \partial^2 E_p / \partial x \partial y , \ldots K_{33}^p = \partial^2 E_p / \partial \varphi^2 \tag{3.3}$$

the desired stiffness matrix of links with passive joint may be expressed as

$$\mathbf{K}_p = \left[\begin{array}{cc:c} K_{11} - \dfrac{K_{13} \cdot K_{31}}{K_{33}} & K_{12} - \dfrac{K_{32} \cdot K_{13}}{K_{33}} & 0 \\ K_{21} - \dfrac{K_{23} \cdot K_{31}}{K_{33}} & K_{22} - \dfrac{K_{23} \cdot K_{32}}{K_{33}} & 0 \\ \hdashline 0 & 0 & 0 \end{array}\right] \tag{3.4}$$

This expression clearly shows that, if the matrix $\mathbf{K}$ is non-diagonal, a trivial transformation that was proposed in some previous works (i.e., simple setting to zero of the third row and column) does not produce a truthful result. Moreover, the elements of the upper-left 2×2 block must be modified taking into account the

[4] It is worth mentioning that in novel compliant robotics systems it may be required to maximise the potential energy storage in order to exploit/recycle it to improve energy efficiency [40] [41]

elements of $\mathbf{K}$ that are located outside of this block. Similar results corresponding to other types of passive joints are summarized in Table 3.1, where they are also applied to classical 2D beam (in this case, some elements of the $\mathbf{K}_p$ are four times lower compared to $\mathbf{K}$). This conclusion motivates development of a general methodology of the stiffness matrix transformation, which is presented below.

Table 3.1 Transformation of the link stiffness matrix due to passive joints (2D case)

Physical model	Stiffness matrix	Physical model	Stiffness matrix
Original link (no passive joint)			
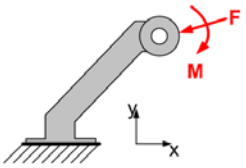	$\begin{bmatrix} K_{11} & K_{12} & K_{13} \\ K_{21} & K_{22} & K_{23} \\ K_{31} & K_{32} & K_{33} \end{bmatrix}$	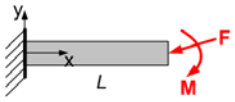	$E\begin{bmatrix} \frac{A}{L} & 0 & 0 \\ 0 & \frac{12I_z}{L^3} & -\frac{6I_z}{L^2} \\ 0 & -\frac{6I_z}{L^2} & \frac{4I_z}{L} \end{bmatrix}$
Link with translational passive joint along x-axis			
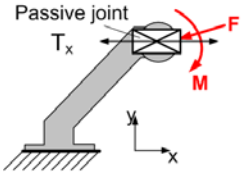	$\begin{bmatrix} 0 & 0 & 0 \\ 0 & K_{22}-\frac{K_{12}K_{21}}{K_{11}} & K_{23}-\frac{K_{13}K_{21}}{K_{11}} \\ 0 & K_{32}-\frac{K_{31}K_{12}}{K_{11}} & K_{33}-\frac{K_{13}K_{31}}{K_{11}} \end{bmatrix}$	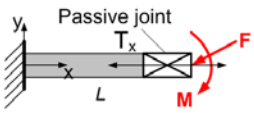	$E\begin{bmatrix} 0 & 0 & 0 \\ 0 & \frac{12I_z}{L^3} & -\frac{6I_z}{L^2} \\ 0 & -\frac{6I_z}{L^2} & \frac{4I_z}{L} \end{bmatrix}$
Link with translational passive joint along y-axis			
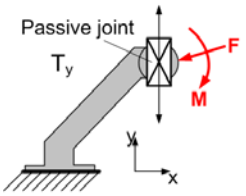	$\begin{bmatrix} K_{11}-\frac{K_{12}K_{21}}{K_{22}} & 0 & K_{13}-\frac{K_{12}K_{23}}{K_{22}} \\ 0 & 0 & 0 \\ K_{31}-\frac{K_{21}K_{32}}{K_{22}} & 0 & K_{33}-\frac{K_{23}K_{32}}{K_{22}} \end{bmatrix}$	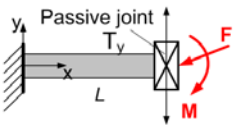	$E\begin{bmatrix} \frac{A}{L} & 0 & 0 \\ 0 & 0 & 0 \\ 0 & 0 & \frac{I_z}{L} \end{bmatrix}$
Link with rotational passive joint around z-axis			
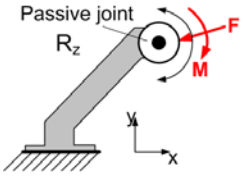	$\begin{bmatrix} K_{11}-\frac{K_{13}K_{31}}{K_{33}} & K_{12}-\frac{K_{13}K_{32}}{K_{33}} & 0 \\ K_{21}-\frac{K_{23}K_{31}}{K_{33}} & K_{22}-\frac{K_{23}K_{32}}{K_{33}} & 0 \\ 0 & 0 & 0 \end{bmatrix}$	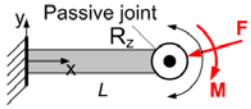	$E\begin{bmatrix} \frac{A}{L} & 0 & 0 \\ 0 & \frac{3I_z}{L^3} & 0 \\ 0 & 0 & 0 \end{bmatrix}$

E is Young's module — I_z is quadratic movement

L is length of link — A is link cross-section

3.3 *Passive joints in a serial chain*

In contrast to conventional serial manipulators, whose kinematics does not include passive joints and assures full controllability of the end-effector, parallel manipulators include a number of under-actuated serial chains that are mutually constrained by special connection to the base and to the end-platform. Let us derive an analytical expression for the stiffness matrix of such kinematic chain taking into account influence of the passive joints.

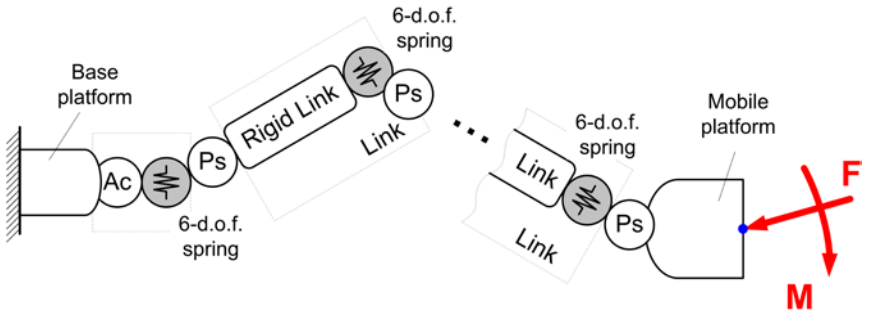

Figure 3.1 The VJM model of a general serial chain (Ps – passive joint, Ac – actuated joint)

The kinematic chain under study (Figure 3.1) consists of a fixed base, a series of flexible links, a moving platform, and a number of actuated or passive joints separating these elements. Following the methodology proposed in our previous publications [30], a relevant VJM model may be presented as a sequence of rigid links separated by passive joints and six-dimensional virtual springs describing elasticity of the links and actuators. For this VJM representation, the direct kinematics is defined by a product of homogeneous transformations that after extraction of end-platform position and orientation is transformed into the vector function

$$\mathbf{t} = \mathbf{g}(\mathbf{q}, \boldsymbol{\theta}) \tag{3.5}$$

where the vector $\mathbf{t} = (\mathbf{p}, \boldsymbol{\varphi})^T$ includes the position $\mathbf{p} = (x, y, z)^T$ and orientation $\boldsymbol{\varphi} = (\varphi_x, \varphi_y, \varphi_z)^T$ of the platform in Cartesian space (Euler angles), the vector $\mathbf{q} = \left(q_1, q_2, \ldots, q_{n_q}\right)^T$ contains passive joint coordinates, the vector $\boldsymbol{\theta} = \left(\theta_1, \theta_2, \ldots, \theta_{n_\theta}\right)^T$ collects coordinates of all virtual springs; n_q and n_θ are the sizes of $\mathbf{q}$ and $\boldsymbol{\theta}$ respectively.

It can be proven [30] that the static equilibrium equations of this mechanical system may be written as

$$\mathbf{J}_\theta{}^T \mathbf{F} = \mathbf{K}_\theta \boldsymbol{\theta}; \quad \mathbf{J}_\mathbf{q}{}^T \mathbf{F} = \mathbf{0} \tag{3.6}$$

where $\mathbf{J}_q = \partial \mathbf{g}(\mathbf{q}, \boldsymbol{\theta}) / \partial \mathbf{q}$, $\mathbf{J}_\theta = \partial \mathbf{g}(\mathbf{q}, \boldsymbol{\theta}) / \partial \boldsymbol{\theta}$ are kinematic Jacobians with respect to the passive and virtual joint coordinates respectively, $\mathbf{F}$ is the external loading (force and torque), and $\mathbf{K}_\theta$ the aggregated stiffness matrix of the virtual springs. Using these equations simultaneously with (3.5) and applying the first-order linear approximation under assumption that corresponding values of the external force $\mathbf{F}$ and the coordinate variations $\delta\mathbf{q}, \boldsymbol{\theta}, \delta\mathbf{t}$ are small enough, one can derive the matrix expression[5]

[5] Relevant technique is explained in details in [30] and is based on linearization of equation (5) and solving it together with expressions (6) with respect to external loading **F** and passive joint coordinates **q**.

$$\begin{bmatrix} \mathbf{F} \\ \delta\mathbf{q} \end{bmatrix} = \begin{bmatrix} \mathbf{J}_\theta \mathbf{K}_\theta^{-1} \mathbf{J}_\theta^T & \mathbf{J}_q \\ \mathbf{J}_q^T & \mathbf{0} \end{bmatrix}^{-1} \cdot \begin{bmatrix} \delta\mathbf{t} \\ \mathbf{0} \end{bmatrix} \tag{3.7}$$

that allows obtaining the desired Cartesian stiffness matrix $\mathbf{K}_C$ numerically [30]. Corresponding procedure includes inversion of $(6+n_q)\times(6+n_q)$ matrix in the right-hand side of (3.7) and extracting from it the upper-left sub-matrix of the size 6×6 that defines a liner force-deflection relation in Cartesian space:

$$\mathbf{F} = \mathbf{K}_C \delta\mathbf{t} \tag{3.8}$$

In spite of computational simplicity, the above procedure is not convenient for the parametric stiffness analysis that usually relies on analytical expressions. To derive such expression for the matrix $\mathbf{K}_C$, let us apply the blockwise inversion based on the Frobenius formula [42]

$$\begin{bmatrix} \left(\mathbf{K}_C^0\right)^{-1} & \mathbf{J}_q \\ \mathbf{J}_q^T & \mathbf{0} \end{bmatrix}^{-1} = \begin{bmatrix} \mathbf{K}_C^0 - \mathbf{K}_C^0 \mathbf{J}_q \left(\mathbf{J}_q^T \mathbf{K}_C^0 \mathbf{J}_q\right)^{-1} \mathbf{J}_q^T \mathbf{K}_C^0 & * \\ * & * \end{bmatrix} \tag{3.9}$$

where $\mathbf{K}_C^0 = \left(\mathbf{J}_\theta \mathbf{K}_\theta^{-1} \mathbf{J}_\theta^T\right)^{-1}$, that allows to present the desired stiffness matrix as (see Appendix B for details, Eq. B.6)

$$\mathbf{K}_C = \mathbf{K}_C^0 - \mathbf{K}_C^0 \mathbf{J}_q \left(\mathbf{J}_q^T \mathbf{K}_C^0 \mathbf{J}_q\right)^{-1} \mathbf{J}_q^T \mathbf{K}_C^0 \tag{3.10}$$

where the first term $\mathbf{K}_C^0$ is the stiffness matrix of the corresponding serial chain *without passive joints* and the second term defines the stiffness decrease *due to the passive joint*s. It worth mentioning that this result is in good agreement with other relevant works [14, 43, 44] where $\mathbf{K}_C$ was presented as the difference of two similar components but the second one was computed in a different way.

Analyzing the latter expression (see Appendix A : Properties of stiffness matrix $\mathbf{K}_C$), one can get to the following conclusion concerning computational singularities:

Remark 1. The first term of the expression (3.10) is non-singular if and only if $rank\left(\mathbf{J}_\theta\right) = 6$, i.e. if the VJM model of the chain includes at least 6 independent virtual springs.

Remark 2. The second term of the expression (3.10) is non-singular if and only if $rank\left(\mathbf{J}_q\right) = n_q$, i.e. if the VJM model of the chain does not include redundant passive joints (i.e. all passive joints are kinematically independent).

Remark 3. If both terms of (3.10) are non-singular, their difference produces a symmetrical stiffness matrix, which always singular and $rank\left(\mathbf{K}_C\right) = 6 - n_q$.

Remark 4. If the matrix $\mathbf{K}_C^0$ of the chain without passive joints is symmetrical and positive-definite, the stiffness matrix of the chain with passive joints $\mathbf{K}_C$ is also symmetrical but positive-semidefinite.

Hence, in practice, expression (10) does not cause any computational difficulties and always produce a singular stiffness matrix of rank $6-n_q$. In analytical computations, it can be also useful the following proposition (see Appendix B: Recursive computation of the stiffness matrix $\mathbf{K}_C$) that allows sequential modification of the original stiffness matrix $\mathbf{K}_C^0$ in accordance with the following proposition:

Proposition. If the chain does not include redundant passive joints, expression (10) allows recursive presentation

$$\mathbf{K}_C^{i+1} = \mathbf{K}_C^i - \mathbf{K}_C^i \mathbf{J}_q^i \left(\mathbf{J}_q^{i\,T} \mathbf{K}_C^i \mathbf{J}_q^i \right)^{-1} \mathbf{J}_q^{i\,T} \mathbf{K}_C^i; \qquad i = 0,1,2... \tag{3.11}$$

where $\mathbf{K}_C^0 = \left(\mathbf{J}_\theta \mathbf{K}_\theta^{-1} \mathbf{J}_\theta^T \right)^{-1}$ and the sub-Jacobians $\mathbf{J}_q^i \subset \mathbf{J}_q$ are extracted from $\mathbf{J}_q = \left[\mathbf{J}_q^1, \mathbf{J}_q^2, ... \right]$ in arbitrary order (column-by-column, or by groups of columns), the superscripts '*i*' and '*i+1*' define the iteration number.

Corollary. The desired stiffness matrix $\mathbf{K}_C$ can be computed in n_q steps, by sequential application of expression (11) for each column of the Jacobian $\mathbf{J}_q$ (i.e. for each passive joint separately). If for the i-th iteration, the second term in expression (11) is singular, this step should be skipped (this case corresponds to the so-called redundant passive joint whose influence on the stiffness matrix has been already taken into account at the previous steps).

These results give convenient analytical and numerical computational techniques that are presented in details in Section 4.6.

3.4 Passive joints in a parallel manipulator

Let us consider now a parallel manipulator, which may be presented as a strictly parallel system of the actuated serial legs connecting the base and the end-platform (Figure 3.2) [45]. Using the methodology described in previous section and applying it to each leg, there can be computed a set of *m* Cartesian stiffness matrices $\mathbf{K}_C^{(i)}$ expressed with respect to the same coordinate system but corresponding to different platform points (here, the superscript '(i)' denotes the kinematic chain number and it differs from the superscript 'i' in Section III which denotes the iteration number, *m* is the number of serial kinematic chains in the manipulator architecture). If initially the chain stiffness matrices were computed in local coordinate systems, their transformation is performed in standard way [46], as

$$\mathbf{K}_C^{glob} = \begin{bmatrix} \mathbf{R} & \mathbf{0} \\ \mathbf{0} & \mathbf{R} \end{bmatrix} \cdot \mathbf{K}_C^{loc} \cdot \begin{bmatrix} \mathbf{R}^T & \mathbf{0} \\ \mathbf{0} & \mathbf{R}^T \end{bmatrix} \tag{3.12}$$

where $\mathbf{R}$ is a 3×3 rotation matrix describing orientation of the local coordinate system with respect to the global one.

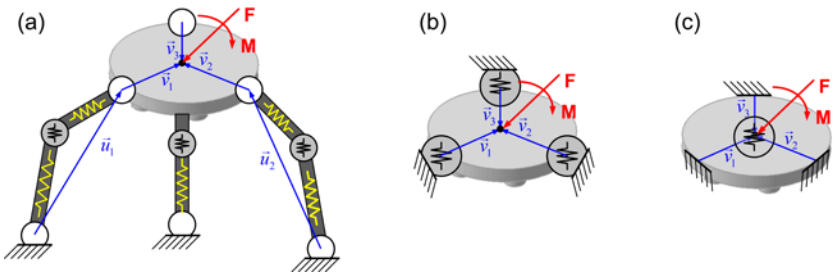

Figure 3.2 Typical parallel manipulator (a) and transformation of its VJM models (b, c)

To aggregate these matrices $\mathbf{K}_C^{(i)}$, they must be also re-computed with respect to same reference point of the platform. Assuming that the platform is rigid enough (compared to the legs), this conversion can be

performed by extending the legs by a virtual rigid link connecting the end-point of the leg and the reference point of the platform (see Fig. 2 where these extensions are defined by the vectors $\mathbf{v}_i$).

After such extension, an equivalent stiffness matrix of the leg may be expressed using relevant expression for a usual serial chain, i.e. as $\mathbf{J}_v^{(i)^{-T}}\mathbf{K}_C^{(i)}\mathbf{J}_v^{(i)^{-1}}$, where the Jacobian $\mathbf{J}_v^{(i)}$ defines differential relation between the coordinates of the *i*-th virtual spring and the reference frame of the end-platform. Hence, using the superposition principle, the final expression for the stiffness matrix of the considered parallel manipulator can be written as

$$\mathbf{K}_C^{(m)} = \sum_{i=1}^{m} \mathbf{J}_v^{(i)^{-T}}\mathbf{K}_C^{(i)}\mathbf{J}_v^{(i)^{-1}} \tag{3.13}$$

Besides, it is implicitly assumed here that all stiffness matrices (both for the legs and for the whole manipulator) are expressed in the same global coordinate system. Hence, the axes of all virtual springs are parallel to the axes *x*, *y*, *z* of this system and corresponding Jacobians and their inverses can be easily computed analytically as

$$\mathbf{J}_v^{(i)} = \begin{bmatrix} \mathbf{I}_3 & (\mathbf{v}_i\times) \\ \mathbf{0} & \mathbf{I}_3 \end{bmatrix}_{6\times 6}, \qquad \mathbf{J}_v^{(i)-1} = \begin{bmatrix} \mathbf{I}_3 & -(\mathbf{v}_i\times) \\ \mathbf{0} & \mathbf{I}_3 \end{bmatrix}_{6\times 6} \tag{3.14}$$

where $\mathbf{I}_3$ is a identity matrix of size 3×3, and $(\mathbf{v}\times)$ is a skew-symmetric matrix corresponding to the vector $\mathbf{v}$:

$$(\mathbf{v}\times) = \begin{bmatrix} 0 & -v_z & v_y \\ v_z & 0 & -v_x \\ -v_y & v_x & 0 \end{bmatrix} \tag{3.15}$$

Therefore, expression (3.13) allows explicit aggregation of the leg stiffness matrices with respect to any given reference point of the platform. It is worth mentioning that in practice, the matrices $\mathbf{K}_C^{(i)}$ are always singular while there aggregation usually produce non-singular singular matrix. Relevant examples are presented in following sections.

3.5 Computational techniques

Explicit expressions (3.10), (13) derived in previous sections allow obtaining the Cartesian stiffness matrix instantly, for any Jacobian $\mathbf{J}_q$ describing special location of the passive joints. However, recursive equation (3.11) allows essentially *simplify the computational procedure* by sequential modification of the original stiffness matrix $\mathbf{K}_C^0$ for each passive joint independently, using separate columns of $\mathbf{J}_q = [\mathbf{J}_{q1,}\ \mathbf{J}_{q2},\ldots]$. Moreover, for some typical cases, relevant computations may be easily performed analytically. This section presents some useful techniques related to this approach.

3.5.1 Recursive computations: single-joint decomposition

Let us assume that a current recursion deals with a single passive joint corresponding to the *i*-th column of the Jacobian $\mathbf{J}_q$, which is denoted as $\mathbf{J}_q^i$ and has size 6×1. In this case, the matrix expression $(\mathbf{J}_q^{i\,T}\mathbf{K}_C^i\mathbf{J}_q^i)^{-1}$ is reduced to the size of 1×1 and the matrix inversion is replaced by a simple scalar division. Besides, the term $\mathbf{K}_C^i\mathbf{J}_q^i$ has size 6×1, so the recursion (3.11) is simplified to

$$\mathbf{K}_C^{i+1} = \mathbf{K}_C^i - \frac{1}{\mu}\mathbf{u}_i \cdot \mathbf{u}_i^T \;\; or \;\; \left[K_{jk}^{(i+1)}\right] = \left[K_{jk}^{(i)}\right] - \frac{1}{\mu}\left[u_j^{(i)} u_k^{(i)}\right] \tag{3.16}$$

where $\mathbf{u}_i = \mathbf{K}_C^i \mathbf{J}_q^i$ is a 6×1 vector and $\mu = \mathbf{J}_q^{i\,T} \mathbf{K}_C^i \mathbf{J}_q^i$ is a scalar. Using methodology presented in Appendix A, it can be also proved that each recursions reduces the rank of the stiffness matrix by 1

$$rank\left(\mathbf{K}_C^{i+1}\right) = rank\left(\mathbf{K}_C^i\right) - 1 \tag{3.17}$$

provided that the current Jacobian $\mathbf{J}_q^i$ is independent of the previous ones $\mathbf{J}_q^1$, $\mathbf{J}_q^2$... (i.e. the *i*-th passive joints is not redundant relatively to the joints $1,\ldots,i-1$).

Since in practice any combination of passive joints can be decomposed into elementary translational and rotational ones, it is enough to consider only two types of the Jacobian columns $\mathbf{J}_{qi}$:

$$\mathbf{J}_{tran} = \left[e_1, e_2, e_3, 0, 0, 0\right]^T; \quad \mathbf{J}_{rot} = \left[d_1, d_2, d_3, e_1, e_2, e_3\right]^T \tag{3.18}$$

where the unit vector $\mathbf{e} = \left[e_1 \quad e_2 \quad e_3\right]$, $\mathbf{e}^T\mathbf{e} = 1$ defines orientation of the passive joint axis (both for translational and rotational ones) and the vector $\mathbf{d} = \left[d_1 \quad d_2 \quad d_3\right]$ defines influence of the rotational passive joints on the linear velocity at the reference point, i.e. $\mathbf{d} = \mathbf{e} \times \mathbf{r}$ where $\mathbf{r}$ is a vector from the joint centre point to the reference point. After relevant substitutions, one can obtain the following expression for the translational joint

$$\mu = \sum_{j=1}^{3}\sum_{k=1}^{3} K_{jk}^{(i)} e_j e_k; \qquad u_j = \sum_{k=1}^{3} K_{jk}^{(i)} e_k \tag{3.19}$$

and for the rotational one

$$\begin{gathered}\mu = \sum_{j=1}^{3}\sum_{k=1}^{3} K_{jk}^{(i)} d_j d_k + 2\sum_{j=1}^{3}\sum_{k=4}^{6} K_{jk}^{(i)} d_j e_{k-3} + \sum_{j=4}^{6}\sum_{k=4}^{6} K_{jk}^{(i)} e_{j-3} e_{k-3}; \\ u_j = \sum_{k=1}^{3} K_{jk}^{(i)} d_k + \sum_{k=4}^{6} K_{jk}^{(i)} e_{k-3}\end{gathered} \tag{3.20}$$

Hence, in general case, the recursion (3.11) involves rather intricate matrix transformation, different from simple setting to zero a row and/or a column. Let us consider now several specific (but rather typical) cases where the transformation rules are more simple and elegant.

3.5.2 Analytical computations: chains with trivial passive joints

In practice, many parallel robots include kinematic chains for which the passive joint axes are collinear to the axes x, *y* or *z* of the Cartesian coordinate system. For such architectures, the vector-columns of the Jacobian $\mathbf{J}_q$ include a number of zero elements, so the expressions (13) can be essentially simplified. Let us consider a set of trivial cases where $\mathbf{J}_q^i$ are created from the columns of the identity matrix $\mathbf{I}_{6\times 6}$:

$$\mathbf{J}_q^{(1)} = \begin{bmatrix} 1 \\ 0 \\ 0 \\ 0 \\ 0 \\ 0 \end{bmatrix}, \quad \mathbf{J}_q^{(2)} = \begin{bmatrix} 0 \\ 1 \\ 0 \\ 0 \\ 0 \\ 0 \end{bmatrix}, \quad \ldots, \quad \mathbf{J}_q^{(6)} = \begin{bmatrix} 0 \\ 0 \\ 0 \\ 0 \\ 0 \\ 1 \end{bmatrix} \tag{3.21}$$

Corresponding passive joints will be further referred to as the 'trivial' ones. It can be easily proved that they cover the following range of the joint geometry:

- translational passive joint with arbitrary spatial position (but with the joint axis directed along *x*, *y* or *z*);
- rotational passive joints positioned at the reference point (and with the joint axis directed along *x*, *y* or *z*).

Besides, it is worth to consider additional case-study corresponding to

- rotational passive joints shifted by a distance *L* with respect to the reference point in the direction either *x*, *y* or *z* (and with the joint axis directed along *x*, *y* or *z*),

which will be further referred to as the 'quasi-trivial' and gives the Jacobian columns of the following structure:

$$\mathbf{J}_q^{(4+)} = \begin{bmatrix} 0 \\ d_y \\ d_z \\ 1 \\ 0 \\ 0 \end{bmatrix}, \quad \mathbf{J}_q^{(5+)} = \begin{bmatrix} d_x \\ 0 \\ d_z \\ 0 \\ 1 \\ 0 \end{bmatrix}, \quad \mathbf{J}_q^{(6+)} = \begin{bmatrix} d_x \\ d_y \\ 0 \\ 0 \\ 0 \\ 1 \end{bmatrix} \tag{3.22}$$

where d_x, d_y, d_z denote the elements of the vector $\mathbf{d}$, which are equal here either $\pm L$ or 0.

For the trivial passive joints, assuming that $\mathbf{J}_q^{(p)}$ denotes the vector-column with a single non-zero element in the *p*-th position, a straightforward substitution yields $u_j = K_{jp}^{(i)}$; $\mu = K_{pp}^{(i)}$. So, the recursive expression (16) for the Cartesian stiffness matrix is simplified to

$$\left[K_{jk}^{(i+1)}\right] = \left[K_{jk}^{(i)}\right] - \left[\frac{K_{jp}^{(i)} K_{pk}^{(i)}}{K_{pp}^{(i)}}\right] \tag{3.23}$$

that is very similar to those presented in the motivation example (see Section II). Also, here the *p*–th row and column of the matrix $\mathbf{K}_C^{i+1}$ become equal to zero

$$K_{pk}^{(i+1)} = 0; \quad K_{kp}^{(i+1)} = 0; \quad \forall p = 1,\ldots 6 \tag{3.24}$$

and the recursive computations are easily performed analytically.

For practical convenience, the above considered case-studies are summarized in Table 3.2 where the original stiffness matrix

Table 3.2 Stiffness matrix transformations caused by trivial passive joints

Type of joint	Jacobian	Modified Stiffness matrix
Translational T_x 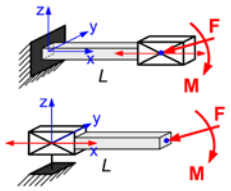	$\mathbf{J}_q^{(1)} = \begin{bmatrix} 1 \\ 0 \\ 0 \\ 0 \\ 0 \\ 0 \end{bmatrix}$	$\begin{bmatrix} 0 & 0 & 0 & 0 & 0 & 0 \\ 0 & K_{22} & 0 & 0 & 0 & K_{26} \\ 0 & 0 & K_{33} & 0 & K_{35} & 0 \\ 0 & 0 & 0 & K_{44} & 0 & 0 \\ 0 & 0 & K_{53} & 0 & K_{55} & 0 \\ 0 & K_{62} & 0 & 0 & 0 & K_{66} \end{bmatrix}$
Translational T_y 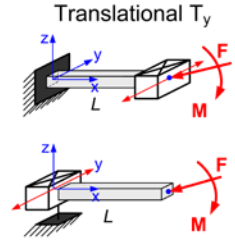	$\mathbf{J}_q^{(2)} = \begin{bmatrix} 0 \\ 1 \\ 0 \\ 0 \\ 0 \\ 0 \end{bmatrix}$	$\begin{bmatrix} K_{11} & 0 & 0 & 0 & 0 & 0 \\ 0 & 0 & 0 & 0 & 0 & 0 \\ 0 & 0 & K_{33} & 0 & K_{35} & 0 \\ 0 & 0 & 0 & K_{44} & 0 & 0 \\ 0 & 0 & K_{53} & 0 & K_{55} & 0 \\ 0 & 0 & 0 & 0 & 0 & \frac{K_{66}}{4} \end{bmatrix}$
Translational T_z 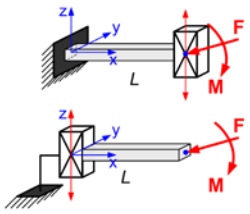	$\mathbf{J}_q^{(3)} = \begin{bmatrix} 0 \\ 0 \\ 1 \\ 0 \\ 0 \\ 0 \end{bmatrix}$	$\begin{bmatrix} K_{11} & 0 & 0 & 0 & 0 & 0 \\ 0 & K_{22} & 0 & 0 & 0 & K_{26} \\ 0 & 0 & 0 & 0 & 0 & 0 \\ 0 & 0 & 0 & K_{44} & 0 & 0 \\ 0 & 0 & 0 & 0 & \frac{K_{55}}{4} & 0 \\ 0 & K_{62} & 0 & 0 & 0 & K_{66} \end{bmatrix}$
Rotational R_x 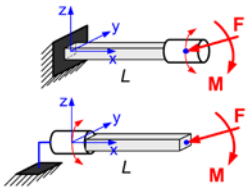	$\mathbf{J}_q^{(4+)} = \begin{bmatrix} 0 \\ 0 \\ 0 \\ 1 \\ 0 \\ 0 \end{bmatrix}$	$\begin{bmatrix} K_{11} & 0 & 0 & 0 & 0 & 0 \\ 0 & K_{22} & 0 & 0 & 0 & K_{26} \\ 0 & 0 & K_{33} & 0 & K_{35} & 0 \\ 0 & 0 & 0 & 0 & 0 & 0 \\ 0 & 0 & K_{53} & 0 & K_{55} & 0 \\ 0 & K_{62} & 0 & 0 & 0 & K_{66} \end{bmatrix}$
Rotational R_y 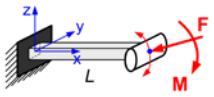	$\mathbf{J}_q^{(5+)} = \begin{bmatrix} 0 \\ 0 \\ 0 \\ 0 \\ 1 \\ 0 \end{bmatrix}$	$\begin{bmatrix} K_{11} & 0 & 0 & 0 & 0 & 0 \\ 0 & K_{22} & 0 & 0 & 0 & K_{26} \\ 0 & 0 & \frac{K_{33}}{4} & 0 & 0 & 0 \\ 0 & 0 & 0 & K_{44} & 0 & 0 \\ 0 & 0 & 0 & 0 & 0 & 0 \\ 0 & K_{62} & 0 & 0 & 0 & K_{66} \end{bmatrix}$
Rotational R_z 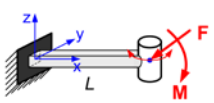	$\mathbf{J}_q^{(6+)} = \begin{bmatrix} 0 \\ 0 \\ 0 \\ 0 \\ 0 \\ 1 \end{bmatrix}$	$\begin{bmatrix} K_{11} & 0 & 0 & 0 & 0 & 0 \\ 0 & \frac{K_{22}}{4} & 0 & 0 & 0 & 0 \\ 0 & 0 & K_{33} & 0 & K_{35} & 0 \\ 0 & 0 & 0 & K_{44} & 0 & 0 \\ 0 & 0 & K_{53} & 0 & K_{55} & 0 \\ 0 & 0 & 0 & 0 & 0 & 0 \end{bmatrix}$

$$\mathbf{K}_C^0 = \left[\begin{array}{ccc|ccc} K_{11} & 0 & 0 & 0 & 0 & 0 \\ 0 & K_{22} & 0 & 0 & 0 & K_{26} \\ 0 & 0 & K_{33} & 0 & K_{35} & 0 \\ \hline 0 & 0 & 0 & K_{44} & 0 & 0 \\ 0 & 0 & K_{53} & 0 & K_{55} & 0 \\ 0 & K_{62} & 0 & 0 & 0 & K_{66} \end{array}\right] \tag{3.25}$$

is assumed to be sparse in accordance with the structure corresponding to a beam-type link whose cross-section are symmetrical with respect to y- and z-axis, and its elements are expressed via the physical parameters as

$$\begin{array}{l} K_{11} = EA/L; \quad K_{22} = 12EI_z / L^3; \quad K_{33} = 12EI_y / L^3; \\ K_{44} = GJ/L; \quad K_{55} = 4EI_z / L; \quad K_{66} = 4EI_Z / L; \\ K_{35} = K_{53} = 6EI_y / L^2; \quad K_{26} = K_{62} = -6EI_z / L^2 \end{array} \tag{3.26}$$

where L is the link length, A is its cross-section area, I_y, I_z, and J are the quadratic and polar moments of inertia of the cross-section, and E and G are the Young's and Coulomb's modules respectively.

As follows from these results, trivial passive joints can be easily taken into account by using simple analytical expressions (3.23) but relevant modifications of the stiffness matrix are more serious than simple zeroing of relevant rows and columns (in addition, some elements must be reduced in half or fourfold, see Table 3.2). Moreover, for the quasi-trivial passive joints, the stiffness matrix may be singular but does not include purely zero rows and columns (see Table 3.3). Hence, the developed technique is essential for VJM-based stiffness modeling of mechanisms with passive joints.

Table 3.3 Examples of stiffness matrix transformations for quasi-trivial passive joints

Type of joint	Jacobian	Modified Stiffness matrix
Rotational R_y 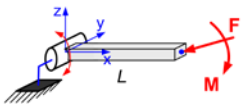	$\mathbf{J}_q^{(5+)} = \begin{bmatrix} 0 \\ 0 \\ -L \\ 0 \\ 1 \\ 0 \end{bmatrix}$	$\begin{bmatrix} K_{11} & 0 & 0 & 0 & 0 & 0 \\ 0 & K_{22} & 0 & 0 & 0 & K_{26} \\ 0 & 0 & \frac{K_{33}}{4} & 0 & \frac{K_{35}}{2} & 0 \\ 0 & 0 & 0 & K_{44} & 0 & 0 \\ 0 & 0 & \frac{K_{53}}{2} & 0 & \frac{3 \cdot K_{55}}{4} & 0 \\ 0 & K_{62} & 0 & 0 & 0 & K_{66} \end{bmatrix}$
Rotational R_z 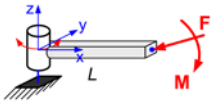	$\mathbf{J}_q^{(6+)} = \begin{bmatrix} 0 \\ L \\ 0 \\ 0 \\ 0 \\ 1 \end{bmatrix}$	$\begin{bmatrix} K_{11} & 0 & 0 & 0 & 0 & 0 \\ 0 & \frac{K_{22}}{4} & 0 & 0 & 0 & \frac{K_{26}}{2} \\ 0 & 0 & K_{33} & 0 & K_{35} & 0 \\ 0 & 0 & 0 & K_{44} & 0 & 0 \\ 0 & 0 & K_{53} & 0 & K_{55} & 0 \\ 0 & \frac{K_{62}}{2} & 0 & 0 & 0 & \frac{3 \cdot K_{66}}{4} \end{bmatrix}$

3.6 Application examples

Let apply now the developed technique to computing of the stiffness matrix for two versions of a general Stewart-Gough platform presented in Figure 3.3 [43, 47-49]. It is assumed that in both cases the manipulator base and the moving plate (platform) are connected by six similar extensible legs (Figure 3.4) but their spatial arrangements are different:

Case A: the legs are regularly connected to the base and platform, with the same angular distance 60° (it is obviously degenerate design, where the stiffness matrix should be singular)

Case B: the legs are connected to the base and platform in three pairs, with the angular distance of 120° between the mounting points (it is classical design of Stewart-Gough where the stiffness matrix should be non-singular).

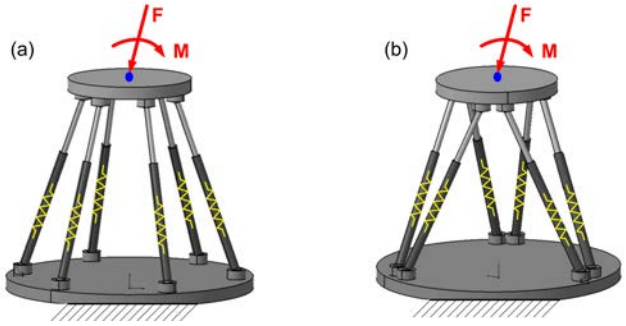

Figure 3.3 Geometry of the Stewart-Gough platforms under study

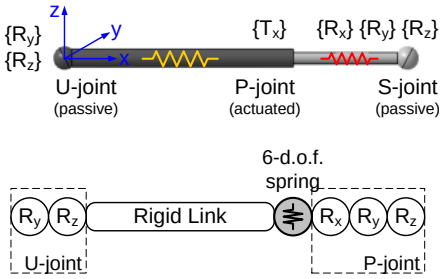

Figure 3.4 Geometry of the manipulator leg and its VJM model

For both designs, the original leg stiffness (i.e. without the passive joints) can be described by the sparse matrix (3.25) corresponding to the symmetric beam. Further, to take into account influence the passive joints, it should be recursively applied the procedure (3.11) with the elementary Jacobians

$$\mathbf{J}_{Rx}^{(1)}=\begin{bmatrix}0\\0\\0\\1\\0\\0\end{bmatrix};\ \mathbf{J}_{Ry}^{(2)}=\begin{bmatrix}0\\0\\0\\0\\1\\0\end{bmatrix};\ \mathbf{J}_{Rz}^{(3)}=\begin{bmatrix}0\\0\\0\\0\\0\\1\end{bmatrix};\ \mathbf{J}_{Ry+}^{(4)}=\begin{bmatrix}0\\0\\-L\\0\\1\\0\end{bmatrix};\ \mathbf{J}_{Rz+}^{(5)}=\begin{bmatrix}0\\L\\0\\0\\0\\1\end{bmatrix} \tag{3.27}$$

where *L* is the leg length. It is obvious that, due to trivial structure of $\mathbf{J}_q^i$, the recursive computations can be easily performed analytically (see subsection V.B.). They sequentially produce the following results:

$$\mathbf{K}_C^0 = \left[\begin{array}{ccc:ccc} K_{11} & 0 & 0 & 0 & 0 & 0 \\ 0 & K_{22} & 0 & 0 & 0 & K_{26} \\ 0 & 0 & K_{33} & 0 & K_{35} & 0 \\ \hdashline 0 & 0 & 0 & K_{44} & 0 & 0 \\ 0 & 0 & K_{53} & 0 & K_{55} & 0 \\ 0 & K_{62} & 0 & 0 & 0 & K_{66} \end{array}\right] \quad \mathbf{K}_C^1 = \left[\begin{array}{ccc:ccc} K_{11} & 0 & 0 & 0 & 0 & 0 \\ 0 & K_{22} & 0 & 0 & 0 & K_{26} \\ 0 & 0 & K_{33} & 0 & K_{35} & 0 \\ \hdashline 0 & 0 & 0 & 0 & 0 & 0 \\ 0 & 0 & K_{53} & 0 & K_{55} & 0 \\ 0 & K_{62} & 0 & 0 & 0 & K_{66} \end{array}\right]$$

$$\mathbf{K}_C^2 = \left[\begin{array}{ccc:ccc} K_{11} & 0 & 0 & 0 & 0 & 0 \\ 0 & K_{22} & 0 & 0 & 0 & K_{26} \\ 0 & 0 & K_{33}/4 & 0 & 0 & 0 \\ \hdashline 0 & 0 & 0 & 0 & 0 & 0 \\ 0 & 0 & 0 & 0 & 0 & 0 \\ 0 & K_{62} & 0 & 0 & 0 & K_{66} \end{array}\right] \quad \mathbf{K}_C^3 = \left[\begin{array}{ccc:ccc} K_{11} & 0 & 0 & 0 & 0 & 0 \\ 0 & K_{22}/4 & 0 & 0 & 0 & 0 \\ 0 & 0 & K_{33}/4 & 0 & 0 & 0 \\ \hdashline 0 & 0 & 0 & 0 & 0 & 0 \\ 0 & 0 & 0 & 0 & 0 & 0 \\ 0 & 0 & 0 & 0 & 0 & 0 \end{array}\right]$$

$$\mathbf{K}_C^4 = \left[\begin{array}{ccc:ccc} K_{11} & 0 & 0 & 0 & 0 & 0 \\ 0 & K_{22}/4 & 0 & 0 & 0 & 0 \\ 0 & 0 & 0 & 0 & 0 & 0 \\ \hdashline 0 & 0 & 0 & 0 & 0 & 0 \\ 0 & 0 & 0 & 0 & 0 & 0 \\ 0 & 0 & 0 & 0 & 0 & 0 \end{array}\right] \quad \mathbf{K}_C^5 = \left[\begin{array}{ccc:ccc} K_{11} & 0 & 0 & 0 & 0 & 0 \\ 0 & 0 & 0 & 0 & 0 & 0 \\ 0 & 0 & 0 & 0 & 0 & 0 \\ \hdashline 0 & 0 & 0 & 0 & 0 & 0 \\ 0 & 0 & 0 & 0 & 0 & 0 \\ 0 & 0 & 0 & 0 & 0 & 0 \end{array}\right]$$

Hence, in final form, the derived matrix includes only the traction/compression term (and not bending, torsion, etc.) what perfectly agrees with other results on Stewart-Gough platforms.

Further, to be applied to each leg, the obtained matrix must be transformed from the local to the global coordinate system. In this specific case, due to the special structure of $\mathbf{K}_C^5$, relevant transformation [24, 46]

$$\mathbf{K}_{C_i} = \begin{bmatrix} \mathbf{R}_i & \mathbf{0} \\ \mathbf{0} & \mathbf{R}_i \end{bmatrix} \cdot K_{11} \cdot \left[\begin{array}{ccc:c} 1 & & & \mathbf{0}_{3\times3} \\ & 0 & & \\ & & 0 & \\ \hdashline \multicolumn{3}{c:}{\mathbf{0}_{3\times3}} & \mathbf{0}_{3\times3} \end{array}\right] \cdot \begin{bmatrix} \mathbf{R}_i^T & \mathbf{0} \\ \mathbf{0} & \mathbf{R}_i^T \end{bmatrix} \tag{3.28}$$

expressed via the orthogonal rotation matrix $\mathbf{R}_i$ describing orientation of the *i*-th local coordinate system with respect to the global one, is easily reduced to

$$\mathbf{K}_{C_i} = K_{11} \cdot \left[\begin{array}{c:c} \mathbf{u}_i^0 \cdot \mathbf{u}_i^{0T} & \mathbf{0}_{3\times3} \\ \hdashline \mathbf{0}_{3\times3} & \mathbf{0}_{3\times3} \end{array}\right]. \tag{3.29}$$

where $\mathbf{u}_i^0$ is the unit vector directed along the leg axis $\mathbf{u}_i$ (see Figure 3.2). Besides, before aggregation, the stiffness matrices of separate legs $\mathbf{K}_{C_i}$ must be re-computed with respect to same reference point in accordance with expressions (3.13), (3.14) which yields

$$\mathbf{K}_C = K_{11} \cdot \sum_{i=1}^{6} \left[\begin{array}{c|c} \mathbf{I}_3 & \mathbf{0} \\ \hline (\mathbf{v}_i\times) & \mathbf{I}_3 \end{array} \right] \cdot \left[\begin{array}{c|c} \mathbf{u}_i^0 \cdot \mathbf{u}_i^{0T} & \mathbf{0}_{3\times3} \\ \hline \mathbf{0}_{3\times3} & \mathbf{0}_{3\times3} \end{array} \right] \cdot \left[\begin{array}{c|c} \mathbf{I}_3 & (\mathbf{v}_i\times)^T \\ \hline \mathbf{0} & \mathbf{I}_3 \end{array} \right] \tag{3.30}$$

where $\mathbf{v}_i$ is the vector from the leg end-point to the platform reference point (see Figure 3.2). So, after relevant transformations, one can get the final expression of the manipulator stiffness matrix

$$\mathbf{K}_C = K_{11} \cdot \sum_{i=1}^{6} \left[\begin{array}{c|c} (\mathbf{u}_i^0\mathbf{u}_i^{0T}) & (\mathbf{u}_i^0\mathbf{u}_i^{0T})\cdot(\mathbf{v}_i\times)^T \\ \hline (\mathbf{v}_i\times)\cdot(\mathbf{u}_i^0\mathbf{u}_i^{0T}) & (\mathbf{v}_i\times)\cdot(\mathbf{u}_i^0\mathbf{u}_i^{0T})\cdot(\mathbf{v}_i\times)^T \end{array} \right] \tag{3.31}$$

or

$$\mathbf{K}_C = K_{11} \cdot \sum_{i=1}^{6} \left[\begin{array}{c} \mathbf{u}_i^0 \\ \hline (\mathbf{v}_i\times\mathbf{u}_i^0) \end{array} \right] \cdot \left[\mathbf{u}_i^{0T} \;\vdots\; (\mathbf{v}_i\times\mathbf{u}_i^0)^T \right] \tag{3.32}$$

where the vector $\mathbf{u}_i$, $\mathbf{v}_i$ describing spatial locations of the legs and computed via the direct kinematics, and $\mathbf{v}_i\times\mathbf{u}_i^0$ denotes the vector product (in contrast to the above notation $(\mathbf{v}_i\times)$ which is referred to the corresponding skew-symmetric matrix).

The derived equation was applied to both case studies, assuming that the manipulators are in their "*home*" configurations when the platform is parallel to the base and it is symmetrical with respect to the vertical axis. Corresponding expressions for the leg vectors are

$$\mathbf{u}_i = \begin{bmatrix} r\cos(\psi_i) - R\cos(\phi_i) \\ r\sin(\psi_i) - R\sin(\phi_i) \\ h \end{bmatrix}, \qquad \mathbf{v}_i = \begin{bmatrix} -r\cos(\psi_i) \\ -r\sin(\psi_i) \\ 0 \end{bmatrix} \tag{3.33}$$

where R and r denote the circle radius which comprise the leg connection point at the base and moving platform respectively, $\phi_i = \psi_i \in \{0, 60°, 120°, 180°, 240°, 300°\}$ for the case A, and $\phi_i \in \{0, 120°, 120°, 240°, 240°, 360°\}$; $\psi_i \in \{60, 60, 180°, 180°, 300°, 300°\}$ for the case B. Substitution of these vectors to the expression (3.32) leads to the following stiffness matrices

$$\mathbf{K}_C^{(A)} = \frac{3K_{11}}{L^2} \left[\begin{array}{ccc|ccc} d_a^2 & 0 & 0 & 0 & rhd_a & 0 \\ 0 & d_a^2 & 0 & -rhd_a & 0 & 0 \\ 0 & 0 & 2h^2 & 0 & 0 & 0 \\ \hline 0 & -rhd_a & 0 & r^2h^2 & 0 & 0 \\ rhd_a & 0 & 0 & 0 & r^2h^2 & 0 \\ 0 & 0 & 0 & 0 & 0 & 0 \end{array} \right] \tag{3.34}$$

and

$$\mathbf{K}_C^{(B)} = \frac{3K_{11}}{L^2} \left[\begin{array}{ccc|ccc} d_a^2 + Rr & 0 & 0 & 0 & rhd_b & 0 \\ 0 & d_a^2 + Rr & 0 & -rhd_b & 0 & 0 \\ 0 & 0 & 2h^2 & 0 & 0 & 0 \\ \hline 0 & -rhd_b & 0 & r^2h^2 & 0 & 0 \\ rhd_b & 0 & 0 & 0 & r^2h^2 & 0 \\ 0 & 0 & 0 & 0 & 0 & 1.5\,r^2R^2 \end{array} \right] \tag{3.35}$$

where $d_a = R - r$; $d_b = R/2 - r$; L is the leg length, h is the vertical distance between the base and the platform, and the superscripts 'A' and 'B' define the relevant case study. As follows from these expressions, in 'zero' location the matrix $\mathbf{K}_C^{(A)}$ is singular and allows "free" rotation of the end-platform around the vertical axis. In contrast, for the same location the matrix $\mathbf{K}_C^{(B)}$ is non-singular and the manipulator resists to all external forces/torques applied to the platform. These results are in good agreement with previous research on the Stewart-Gough platforms and confirm efficiency of the developed computational technique for manipulator stiffness modeling [9, 47].

3.7 Conclusion

For robotic manipulators with passive joints, the stiffness matrices of separate kinematic chains are *singular*. So, the most of existing stiffness analysis methods can not be applied directly and this problem is usually overcome by elimination the passive joint coordinates via geometrical constraints describing the manipulator assembly. However, such techniques degenerate if the number of passive joints is redundant and/or the resulting matrix is inherently singular.

To deal with such architectures in more efficient way, this Chapter proposes an analytical approach that allows obtaining both *singular and non-singular* stiffness matrices and which is appropriate for a general case, independent of the type and spatial location of the passive joints. The developed approach is based on the extension of the virtual-joint modelling technique and includes two basic steps which sequentially produce stiffness matrices of separate chains and then aggregate them in a common matrix.

In contrast to previous works, the desired stiffness matrix is presented in an explicit *analytical form*, as a sum of *two terms.* The first of them has traditional structure and describes manipulator elasticity due to the link/joint flexibility, while the second one directly takes into account influence of the passive joints. It is proved that, for each chain, the rank-deficiency of the resulting matrix is equal to the number of independent passive joints. To simplify analytical computations, it is proposed a *recursive procedure* that sequentially modifies the original matrix in accordance with the geometry of each passive joint. For the trivial cases, for which the passive joint axes are collinear to the axes of the base coordinate system, this modification is presented in the form of simple analytical rules.

Advantages of the developed technique are illustrated by application examples that deal with stiffness modeling of two Stewart-Gough platforms. They demonstrate its ability to produce both singular and non-singular stiffness matrices, and also show its feasibility for analytical computations. These examples give also some prospective for future work that include development of the dedicated techniques for the stiffness matrix aggregation in the case of non-rigid platform and an extension of these results for the case of manipulators with external loading.

3.8 Appendix A : Properties of stiffness matrix K_C

Let us analyze in details expression (3.10) that allows computing the stiffness matrix of a serial chain with passive joints $\mathbf{K}_C$ from corresponding matrix of the chain without passive joints $\mathbf{K}_C^0$. Assuming that $rank(\mathbf{K}_C^0) = 6$, this matrix can be factorised into the product of two non-singular square matrices $\mathbf{K}_C^0 = \mathbf{S}^T\mathbf{S}$. This yields a compact presentation of the desired matrix in the form

$$\mathbf{K}_C = \mathbf{S}^T \cdot \mathbf{M} \cdot \mathbf{S} \qquad \text{A1}$$

where

$$\mathbf{M} = \mathbf{I} - (\mathbf{S}\,\mathbf{J}_q)\cdot\left(\mathbf{J}_q^T\mathbf{S}^T\mathbf{S}\,\mathbf{J}_q\right)^{-1}\cdot(\mathbf{J}_q^T\mathbf{S}^T) \qquad \text{A2}$$

and the inverse $(\mathbf{J}_q^T\mathbf{S}^T\mathbf{S}\,\mathbf{J}_q)^{-1}$ exists due to the assumption $rank(\mathbf{J}_q) = n_q$. Further, the product $\mathbf{S}\mathbf{J}_q$ can be also factorised using the SVD-technique [50] as

$$\mathbf{S}\mathbf{J}_q = \mathbf{U}\,\boldsymbol{\Sigma}\,\mathbf{V}^T = \left[u_{ij}\right]_{6\times 6}\cdot\left[\frac{\boldsymbol{\Sigma}_q}{\mathbf{0}}\right]_{6\times n_q}\cdot\left[v_{ij}\right]_{n_q\times n_q} \qquad \text{A3}$$

where $\mathbf{U}$, $\mathbf{V}$ are the orthogonal matrices and the matrix $\boldsymbol{\Sigma}_q = diag(\sigma_1, \sigma_2, \ldots)$ is composed of n_q non-zero singular values σ_i (provided that $rank(\mathbf{J}_q) = n_q$). The latter gives the following presentation of $\mathbf{M}$

$$\mathbf{M} = \mathbf{U}\cdot\left(\mathbf{I} - \boldsymbol{\Sigma}\left(\boldsymbol{\Sigma}^T\boldsymbol{\Sigma}\right)^{-1}\boldsymbol{\Sigma}^T\right)\cdot\mathbf{U}^T. \qquad \text{A4}$$

where the product $\boldsymbol{\Sigma}\left(\boldsymbol{\Sigma}^T\boldsymbol{\Sigma}\right)^{-1}\boldsymbol{\Sigma}^T$ may be computed in a straightforward way:

$$\boldsymbol{\Sigma}\left(\boldsymbol{\Sigma}^T\boldsymbol{\Sigma}\right)^{-1}\boldsymbol{\Sigma}^T = \left[\frac{\boldsymbol{\Sigma}_q}{\mathbf{0}}\right]\cdot\left(\left[\boldsymbol{\Sigma}_q \quad \mathbf{0}\right]\cdot\left[\frac{\boldsymbol{\Sigma}_q}{\mathbf{0}}\right]\right)^{-1}\cdot\left[\boldsymbol{\Sigma}_q \quad \mathbf{0}\right] = \begin{bmatrix}\mathbf{I}_{n_q} & \mathbf{0}\\ \mathbf{0} & \mathbf{0}\end{bmatrix}_{6\times 6}. \qquad \text{A5}$$

So, the inner part of $\mathbf{M}$ may be presented as

$$\mathbf{M}' = \mathbf{I} - \boldsymbol{\Sigma}\left(\boldsymbol{\Sigma}^T\boldsymbol{\Sigma}\right)^{-1}\boldsymbol{\Sigma}^T = \left[\begin{array}{c|c}\mathbf{0}_{n_q} & \mathbf{0}\\ \hline \mathbf{0} & \mathbf{I}_{6-n_q}\end{array}\right]_{6\times 6} \qquad \text{A6}$$

This leads to the final expression

$$\mathbf{K}_C = \mathbf{S}^T\cdot\mathbf{U}\,\mathbf{M}'\,\mathbf{U}^T\cdot\mathbf{S} \qquad \text{A7}$$

that allows to evaluate the rank of the stiffness matrix $\mathbf{K}_C$

$$rank(\mathbf{K}_C) = rank(\mathbf{M}') = 6 - n_q \qquad \text{A8}$$

and to justify Remarks presented in Section III.

For computational convenience, the orthogonal matrix $\mathbf{U}$ may be split into six vector columns $\left[\mathbf{u}_1, \ldots, \mathbf{u}_6\right]$ and the matrix product $\mathbf{U}\,\mathbf{M}'\,\mathbf{U}^T$ is expressed as a subsume of $\mathbf{u}_i\mathbf{u}_i^T$ corresponding to the non-zero elements of $\mathbf{M}'$. This gives another presentation of the desired Cartesian stiffness matrix

$$\mathbf{K}_C = \mathbf{S}^T\cdot\left(\sum_{i=n_q+1}^{6}\mathbf{u}_i\mathbf{u}_i^T\right)\cdot\mathbf{S} \qquad \text{A9}$$

where the middle term includes only those unit vectors $\mathbf{u}_i$ that are not "compensated" by the passive joints (for this notation, the directions $\mathbf{u}_1, \ldots \mathbf{u}_{n_q}$ correspond to the end-effector motion due to the passive joints, which do not produce elastostatic reactions). It should be noted that in the case of $n_q = 0$, i.e. without passive joints, the total sum of $\mathbf{u}_i\mathbf{u}_i^T$ produces a unit matrix $\mathbf{I}_6$ and the latter expression is reduced to $\mathbf{K}_C^0 = \mathbf{S}^T\mathbf{S}$.

3.9 Appendix B: Recursive computation of the stiffness matrix K_C

Let us assume that the Jacobian $\mathbf{J}_q$ of size $6\times n_q$ is decomposed into two sub-matrices $[\mathbf{J}_{q1},\mathbf{J}_{q2}]$ of sizes $6\times n_{q1}$ and $6\times n_{q2}$ corresponding to non-intersected subsets of passive joints and the derived expression for the stiffness matrix is applied recursively, using sequentially the Jacobians $\mathbf{J}_{q1},\mathbf{J}_{q2}$:

$$\begin{aligned}\mathbf{K}_C^1 &= \mathbf{K}_C^0 - \mathbf{K}_C^0\mathbf{J}_{q1}\left(\mathbf{J}_{q1}^T\mathbf{K}_C^0\mathbf{J}_{q1}\right)^{-1}\mathbf{J}_{q1}^T\mathbf{K}_C^0\\ \mathbf{K}_C^2 &= \mathbf{K}_C^1 - \mathbf{K}_C^1\mathbf{J}_{q2}\left(\mathbf{J}_{q2}^T\mathbf{K}_C^1\mathbf{J}_{q2}\right)^{-1}\mathbf{J}_{q2}^T\mathbf{K}_C^1\end{aligned} \qquad \text{B1}$$

To evaluate the obtained matrix, let us substitute the first expression to the second one and perform some equivalent transformations using notations

$$\begin{aligned}&\mathbf{A}=\mathbf{J}_{q1}^T\mathbf{K}_C^0\mathbf{J}_{q1};\quad \mathbf{B}=\mathbf{J}_{q1}^T\mathbf{K}_C^0\mathbf{J}_{q2};\quad \mathbf{C}=\mathbf{J}_{q2}^T\mathbf{K}_C^0\mathbf{J}_{q1};\quad \mathbf{D}=\mathbf{J}_{q2}^T\mathbf{K}_C^0\mathbf{J}_{q2}\\ &\mathbf{H}=\mathbf{D}-\mathbf{C}\mathbf{A}^{-1}\mathbf{B}=\mathbf{J}_{q2}^T\mathbf{K}_C^0\mathbf{J}_{q2}-\mathbf{J}_{q2}^T\mathbf{K}_C^0\mathbf{J}_{q1}\cdot\left(\mathbf{J}_{q1}^T\mathbf{K}_C^0\mathbf{J}_{q1}\right)^{-1}\cdot\mathbf{J}_{q1}^T\mathbf{K}_C^0\mathbf{J}_{q2}\end{aligned} \qquad \text{B2}$$

This allows converting the original bulky expression

$$\begin{aligned}\mathbf{K}_C^2 &= \left\{\mathbf{K}_C^0 - \mathbf{K}_C^0\mathbf{J}_{q1}\left(\mathbf{J}_{q1}^T\mathbf{K}_C^0\mathbf{J}_{q1}\right)^{-1}\mathbf{J}_{q1}^T\mathbf{K}_C^0\right\} - \left\{\mathbf{K}_C^0 - \mathbf{K}_C^0\mathbf{J}_{q1}\left(\mathbf{J}_{q1}^T\mathbf{K}_C^0\mathbf{J}_{q1}\right)^{-1}\mathbf{J}_{q1}^T\mathbf{K}_C^0\right\}\times\\ &\times\mathbf{J}_{q2}\left(\mathbf{J}_{q2}^T\left\{\mathbf{K}_C^0 - \mathbf{K}_C^0\mathbf{J}_{q1}\left(\mathbf{J}_{q1}^T\mathbf{K}_C^0\mathbf{J}_{q1}\right)^{-1}\mathbf{J}_{q1}^T\mathbf{K}_C^0\right\}\mathbf{J}_{q2}\right)^{-1}\mathbf{J}_{q2}^T\left\{\mathbf{K}_C^0 - \mathbf{K}_C^0\mathbf{J}_{q1}\left(\mathbf{J}_{q1}^T\mathbf{K}_C^0\mathbf{J}_{q1}\right)^{-1}\mathbf{J}_{q1}^T\mathbf{K}_C^0\right\}\end{aligned} \qquad \text{B3}$$

into a more compact form

$$\mathbf{K}_C^2 = \mathbf{K}_C^0 - \mathbf{K}_C^0\cdot(\mathbf{J}_{q1}\mathbf{A}^{-1}\mathbf{J}_{q1}^T + \mathbf{J}_{q2}\mathbf{H}^{-1}\mathbf{J}_{q2}^T + \mathbf{J}_{q2}\mathbf{H}^{-1}\mathbf{C}\mathbf{A}^{-1}\mathbf{J}_{q1}^T - \mathbf{J}_{q1}\mathbf{A}^{-1}\mathbf{B}\,\mathbf{H}^{-1}\mathbf{J}_{q2}^T + \mathbf{J}_{q1}\mathbf{A}^{-1}\mathbf{B}\,\mathbf{H}^{-1}\mathbf{C}\mathbf{A}^{-1}\mathbf{J}_{q1}^T)\cdot\mathbf{K}_C^0 \qquad \text{B4}$$

that allows a matrix presentation

$$\mathbf{K}_C^2 = \mathbf{K}_C^0 - \mathbf{K}_C^0\cdot\begin{bmatrix}\mathbf{J}_{q1} & \mathbf{J}_{q2}\end{bmatrix}\left[\begin{array}{c|c}\mathbf{A}^{-1}+\mathbf{A}^{-1}\mathbf{B}\,\mathbf{H}^{-1}\mathbf{C}\mathbf{A}^{-1} & -\mathbf{A}^{-1}\mathbf{B}\,\mathbf{H}^{-1}\\ \hline -\mathbf{H}^{-1}\mathbf{C}\mathbf{A}^{-1} & \mathbf{H}^{-1}\end{array}\right]\cdot\begin{bmatrix}\mathbf{J}_{q1}^T\\ \mathbf{J}_{q2}^T\end{bmatrix}\cdot\mathbf{K}_C^0 \qquad \text{B5}$$

Further, using Frobenius formula for the blockwise matrix inverse

$$\begin{aligned}&\begin{bmatrix}\mathbf{A} & \mathbf{B}\\ \mathbf{C} & \mathbf{D}\end{bmatrix}^{-1} = \left[\begin{array}{c:c}\mathbf{A}^{-1}+\mathbf{A}^{-1}\mathbf{B}\mathbf{H}^{-1}\mathbf{C}\mathbf{A}^{-1} & -\mathbf{A}^{-1}\mathbf{B}\mathbf{H}^{-1}\\ \hdashline -\mathbf{H}^{-1}\mathbf{C}\mathbf{A}^{-1} & \mathbf{H}^{-1}\end{array}\right];\\ &\mathbf{H}=\mathbf{D}-\mathbf{C}\mathbf{A}^{-1}\mathbf{B}\end{aligned} \qquad \text{B6}$$

the derived expression can be presented in the form

$$\mathbf{K}_C^2 = \mathbf{K}_C^0 - \mathbf{K}_C^0\begin{bmatrix}\mathbf{J}_{q1} & \mathbf{J}_{q2}\end{bmatrix}\left[\begin{array}{c|c}\mathbf{J}_{q1}^T\mathbf{K}_C^0\mathbf{J}_{q1} & \mathbf{J}_{q1}^T\mathbf{K}_C^0\mathbf{J}_{q2}\\ \hline \mathbf{J}_{q2}^T\mathbf{K}_C^0\mathbf{J}_{q1} & \mathbf{J}_{q2}^T\mathbf{K}_C^0\mathbf{J}_{q2}\end{array}\right]^{-1}\begin{bmatrix}\mathbf{J}_{q1}^T\\ \mathbf{J}_{q2}^T\end{bmatrix}\mathbf{K}_C^0, \qquad \text{B7}$$

or

$$\mathbf{K}_C^2 = \mathbf{K}_C^0 - \mathbf{K}_C^0 \begin{bmatrix} \mathbf{J}_{q1} & \mathbf{J}_{q2} \end{bmatrix} \left(\begin{bmatrix} \mathbf{J}_{q1}^T \\ \mathbf{J}_{q2}^T \end{bmatrix} \mathbf{K}_C^0 \begin{bmatrix} \mathbf{J}_{q1} & \mathbf{J}_{q2} \end{bmatrix} \right)^{-1} \begin{bmatrix} \mathbf{J}_{q1}^T \\ \mathbf{J}_{q2}^T \end{bmatrix} \mathbf{K}_C^0 \qquad \text{B8}$$

that exactly coincide with the expression for the stiffness matrix $\mathbf{K}_C$ corresponding to the aggregated Jacobian $\mathbf{J}_q = [\mathbf{J}_{q1}, \mathbf{J}_{q2}]$. Hence, the desired stiffness matrix of the kinematic chain with passive joints can be computed recursively, using arbitrary partitioning of the Jacobian $\mathbf{J}_q$. Obviously, it is more convenient to apply column-wise petitioning that allow sequential modification of the matrix $\mathbf{K}_C^0$ taking into account geometry of each passive joint separately (and sequentially reducing the rang of the Cartesian stiffness matrix).

3.10 References

[1] J. Salisbury, Active Stiffness Control of a Manipulator in Cartesian Coordinates, in: 19th IEEE Conference on Decision and Control, 1980, pp. 87–97.

[2] C. Gosselin, Stiffness mapping for parallel manipulators, IEEE Transactions on Robotics and Automation 6(3) (1990) 377–382.

[3] B.-J. Yi, R.A. Freeman, Geometric analysis antagonistic stiffness redundantly actuated parallel mechanism, Journal of Robotic Systems 10(5) (1993) 581-603.

[4] Griffis, M., Duffy, J.: Global stiffness modeling of a class of simple compliant couplings. Mechanism and Machine Theory **28**(2), 207–224 (1993)

[5] Ciblak, N., Lipkin, H.: Asymmetric Cartesian stiffness for the modeling of compliant robotic systems. In: Proc. 23rd Biennial ASME Mechanisms Conference, Minneapolis, MN (1994)

[6] T. Pigoski, M. Griffis, J. Duffy, Stiffness mappings employing different frames of reference. Mechanism and Machine Theory 33(6) (1998) 825–838.

[7] Howard, S., Zefran, M., Kumar, V.: On the 6 x 6 Cartesian stiffness matrix for three-dimensional motions. Mechanism and Machine Theory **33**(4), 389–408 (1998)

[8] S. Chen, I. Kao, Conservative Congruence Transformation for Joint and Cartesian Stiffness Matrices of Robotic Hands and Fingers, The International Journal of Robotics Research 19(9) (2000) 835–847

[9] M.M. Svinin, S. Nosoe, M. Uchiyama, On the stiffness and stability of Gough-Stewart platforms, in: Proceedings of IEEE International Conference on Robotics and Automation (ICRA), 2001, pp. 3268–3273

[10] C.M. Gosselin, D. Zhang, Stiffness analysis of parallel mechanisms using a lumped model, International Jornal of Robotics and Automation 17 (2002) 17-27.

[11] O. Company, F. Pierrot, J.-C. Fauroux, A Method for Modeling Analytical Stiffness of a Lower Mobility Parallel Manipulator, in: Proceedings of IEEE International Conference on Robotics and Automation (ICRA), 2005, pp. 3232 - 3237

[12] G. Alici, B. Shirinzadeh, Enhanced stiffness modeling, identification and characterization for robot manipulators, Proceedings of IEEE Transactions on Robotics 21(4) (2005) 554–564.

[13] J. Kövecses, J. Angeles, The stiffness matrix in elastically articulated rigid-body systems, Multibody System Dynamics 18(2) (2007) 169–184.

[14] C. Quennouelle, C. M. Gosselin, Stiffness Matrix of Compliant Parallel Mechanisms, In: Springer Advances in Robot Kinematics: Analysis and Design, 2008, pp. 331-341.

[15] J.-P. Merlet, C. Gosselin, Parallel mechanisms and robots, In B. Siciliano, O. Khatib, (Eds.), Handbook of robotics, Springer, Berlin, 2008, pp. 269-285.

[16] J.-P. Merlet, Analysis of Wire Elasticity for Wire-driven Parallel Robots, In: Proceedings of the Second European Conference on Mechanism Science (EUCOMES 08), Springer, 2008, pp. 471-478

[17] T. Bonnemains, H. Chanel, C. Bouzgarrou and P. Ray, Definition of a new static model of parallel kinematic machines: highlighting of overconstraint influence, in: Proceedings of IEEE/ RSJ International Conference on Intelligent Robots and Systems (IROS), 2008, pp. 2416–2421.

[18] I. Tyapin, G. Hovland, Kinematic and elastostatic design optimization of the 3-DOF Gantry-Tau parallel kinamatic manipulator,Modelling, Identification and Control, 30(2) (2009) 39-56

[19] G. Piras, W.L. Cleghorn, J.K. Mills, Dynamic finite-element analysis of a planar high-speed, high-precision parallel manipulator with flexible links, Mechanism and Machine Theory 40 (7) (2005) 849–862.

[20] X. Hu, R. Wang, F. Wu, D. Jin, X. Jia, J. Zhang, F. Cai, Sh. Zheng, Finite Element Analysis of a Six-Component Force Sensor for the Trans-Femoral Prosthesis, In: V.G. Duffy (Ed.), Digital Human Modeling, Springer-Verlag, Berlin Heidelberg, 2007, pp. 633–639.

[21] K. Nagai, Zh. Liu, A Systematic Approach to Stiffness Analysis of Parallel Mechanisms and its Comparison with FEM, In: Proceeding of SICE Annual Conference, Kagawa University, Japan, 2007, pp 1087-1094.

[22] B.C. Bouzgarrou, J.C. Fauroux, G. Gogu, Y. Heerah, Rigidity analysis of T3R1 parallel robot with uncoupled kinematics, In: Proceedings Of the35th International Symposium on Robotics, Paris, France, 2004.

[23] R. Rizk, J.C. Fauroux, M. Mumteanu, G. Gogu, A comparative stiffness analysis of a reconfigurable parallel machine with three or four degrees of mobility, Journal of Machine Engineering 6 (2) (2006) 45–55.

[24] D. Deblaise, X. Hernot, P.Maurine, A systematic analytical method for PKM stiffness matrix calculation, In: Proceedings of the IEEE International Conference on Robotics and Automation (ICRA), Orlando, Florida, 2006, pp. 4213-4219.

[25] H. C. Martin, Introduction to matrix methods of structural analysis, McGraw-Hill Education, 1966

[26] X. Ding and J. S. Dai, Compliance Analysis of Mechanisms with Spatial Continuous Compliance in the Context of Screw Theory and Lie Groups, Journal of Mechanical Engineering Science, 2010 ,224 (8), pp. 2493-2504.

[27] Dai, J. S. and X. Ding, Compliance Analysis of a Three-legged Rigidly-connected Compliant Platform Device, the ASME Transaction, Journal of Mechanical Design, 2006, 128(4):755-764.

[28] Selig, J. M. and X., Ding, Structure of The Spatial Stiffness Matrix, International Journal of Robotics & Automation, 2002, Vol.17, Issue 1, pp. 1-16.

[29] Sh.-F. Chen, I. Kao, Geometrical Approach to The Conservative Congruence Transformation (CCT) for Robotic Stiffness Control, In: Proceedings of the 2002 IEEE Intemational Conference on Robotics and Automation (ICRA) Washington, DC, 2002, pp 544-549.

[30] A. Pashkevich, D. Chablat, P. Wenger, Stiffness analysis of overconstrained parallel manipulators, Mechanism and Machine Theory 44 (2009) 966-982.

[31] M. Ceccarelli, G. Carbone, A stiffness analysis for CaPaMan (Cassino Parallel Manipulator), Mechanism and Machine Theory 37 (5) (2002) 427–439.

[32] O. Company, S. Krut, F. Pierrot, Modelling and preliminary design issues of a 4-axis parallel machine for heavy parts handling, Journal of Multibody Dynamics 216 (2002) 1–11.

[33] D. Zhang, F. Xi, C.M. Mechefske, S.Y.T. Lang, Analysis of parallel kinematic machine with kinetostatic modeling method, Robotics and Computer-Integrated Manufacturing 20 (2) (2004) 151–165.

[34] R. Vertechy, V. Parenti-Castelli, Static and stiffness analyses of a class of over-constrained parallel manipulators with legs of type US and UPS, in: Proceedings of IEEE International Conference on Robotics and Automation (ICRA), 2007, pp. 561–567.

[35] Y. Li, Q. Xu, Stiffness analysis for a 3-PUU parallel kinematic machine, Mechanism and Machine Theory 43(2) (2008) 186-200.

[36] F. Majou, C. Gosselin, P. Wenger, D. Chablat, Parametric stiffness analysis of the Orthoglide, Mechanism and Machine Theory 42 (2007) 296-311.

[37] O. Company, S. Krut, F. Pierrot, Modelling and preliminary design issues of a 4-axis parallel machine for heavy parts handling, Journal of Multibody Dynamics 216 (2002) 1–11.

[38] A. Pashkevich, A. Klimchik, D. Chablat, Ph. Wenger, Accuracy Improvement for Stiffness Modeling of Parallel Manipulators, In: Proceedings of 42nd CIRP Conference on Manufacturing Systems, Grenoble, France, 2009.

[39] A. Taghaeipour, J. Angeles, L. Lessard, Online computation of the stiffness matrix in robotic structures using finite element analysis, report TR-CIM-10-05, Department of Mechanical engineering and centre for intelligent machines, McGill university, 2010

[40] S. Wolf, G. Hirzinger, A new variable stiffness design: Matching requirements of the next robot generation, 2008 IEEE International Conference on Robotics and Automation (2008), Pages: 1741-1746

[41] B. Vanderborght, B. Verrelst, R. Van Ham, M. Van Damme, P. Beyl and D. Lefeber, Development of a compliance controller to reduce energy consumption for bipedal robots, Volume 24, Number 4, 419-434, DOI: 10.1007/s10514-008-9088-5

[42] F. Gantmacher, Theory of matrices, AMS Chelsea publishing, 1959

[43] J. Chen, F. Lan, Instantaneous stiffness analysis and simulation for hexapod machines, Simulation Modelling Practice and Theory 16 (2008) 419–428

[44] C. Quennouelle, C. M.Gosselin, Instantaneous Kinemato-Static Model of Planar Compliant Parallel Mechanisms, In: Proceedings of ASME International Design Engineering Technical Conferences, Brooklyn, NY, USA, 2008.

[45] J.-P. Merlet, Parallel Robots, Kluwer Academic Publishers, Dordrecht, 2006.

[46] J. Angeles, Fundamentals of Robotic Mechanical Systems: Theory, Methods, and Algorithms, Springer, New York, 2007.

[47] Y.W. Li, J.S. Wang, L.P. Wang (2002). Stiffness analysis of a Stewart platform-based parallel kinematic machine, In: Proceedings of IEEE International Conference on Robotics and Automation (ICRA), Washington, US, 2002(4), pp. 3672–3677.

[48] B.S. El-Khasawneh, P.M. Ferreira, Computation of stiffness and stiffness bounds for parallel link manipulators, International Journal of Machine Tools and Manufacture 39 (2) (1999) 321–342.

[49] H.K. Arumugam, R.M. Voyles, S. Bapat, Stiffness analysis of a class of parallel mechanisms for micro-positioning applications, in: Proceedings of IEEE/ RSJ International Conference on Intelligent Robots and Systems (IROS), 2004, vol. 2, pp. 1826–1831.

[50] G. Strang, Introduction to Linear Algebra, Wellesley, MA, Wellesley Cambridge Press, 1998.

4 STIFFNESS MODELING OF ROBOTIC-MANIPULATORS UNDER AUXILIARY LOADINGS

4.1 Introduction

Manipulator stiffness modeling under internal and external loading is a relatively new research area that is important both for serial and parallel robots. In general case, these loadings may be of different nature and applied to different points/surfaces. For the stiffness modeling of robotic manipulator, it is reasonable to distinguish three main types of loading such as external loading applied to end-point, preloading in the joints and auxiliary loading applied to the intermediate points.

The *external loading* is caused mainly by an interaction between the robot end-effector and the workpiece, which is processed or transported in the considered technological process [1]. In most of robotic research works this loading is considered as a unique one [2] [3], however existence and effect of other types have not been discussed yet.

The *internal loading* in some joints may be introduced by the designer. For instance, to eliminate backlash, the joints may include preloaded springs, which generate the force or torque even in standard "mechanical zero" configuration [4]. Though the internal forces/torques do not influence on the global equilibrium equations, they may change the equilibrium configuration and also influence on the manipulator stiffness properties. For this reason, internal preloading is used sometimes for the purpose of improving the manipulator elasto-static properties, especially in the vicinity of kinematic singularities. Another case where the internal loading exists by default, is related over-constrained manipulators that are subject of the so-called antagonistic actuating [5]. Here, redundant actuators generate internal forces and torques that are equilibrated in the frame of closed loops.

The term *auxiliary loading*, in this Chapter, is used to denote external loading applied to any intermediate point (surface, etc.) of the manipulator different from the end-effector. Typical example of such type of loading is the gravity that is non-negligible for heavy manipulators employed in machining applications [6]. Besides, to compensate in certain degree the gravity influence, some manipulators include special mechanisms generating external forces/torques in the opposite direction (gravity compensators). In addition, some additional forces/torques may be generated by other sources (geometrical constrains, for instance). It should be noted that the external loading caused by gravity have obvious distributed nature, but usually it can be approximated by lumped forces that applied to one or several intermediate points.

From point of view of stiffness analysis, the external and internal forces/torques directly influence on the manipulator equilibrium configuration and, accordingly, may modify the stiffness properties. So, they must be undoubtedly be taken into account while developing the stiffness model. However, in most of the related works the Cartesian stiffness matrix has been computed for the nominal configuration, which does not take into account influence of external/internal loading. Such approach is suitable for the case of small deflections only. For the opposite case, the most important results have been obtained in [7-10], which deal with the stiffness analysis of serial and parallel manipulators under the end-point loading. Besides, some types of the internal preloading have been in the focus of [11], [12]. However, influence of the auxiliary loading has not been studied in details yet.

To our knowledge, the most advanced stiffness model for robotic manipulator has been proposed in [6], where numerous factors have been taken into account (conventional external loading, gravity forces, antagonistic redundant actuation, etc.). However, proposed approach is rather hard from computational point of view. Besides, in this work the Jacobians and all their derivatives were computed not in a "true" equilibrium configuration. For this reason, since the equilibrium obviously depends on the loading magnitude, some essential issues have been omitted.

The goal of this work is to generalize the non-linear stiffness modeling technique for the case of three types of loadings: (i) the external loading applied to the end-effector, (ii) preloading in the joints and (iii) auxiliary loading applied to the intermediate node-points. The developed model is based on the VJM-technique proposed in [13], which is able to obtain the force-deflection relation and the manipulator Cartesian stiffness matrix assuming that the external loading is applied to the end-effector only.

4.2 Problem statement

For stiffness modeling of serial kinematic chain with the loading applied to end-point, preloading in the joints and auxiliary loading applied to intermediate points let us use the VJM model that is presented in Figure 4.1. The serial chain under study consists of flexible links separated by passive and/or actuated joints. Its geometry (end-point location) is described by the vector function

$$\mathbf{t} = \mathbf{g}(\mathbf{q}, \boldsymbol{\theta}) \tag{4.1}$$

where the vector $\mathbf{t}$ defines the end-point location (position and orientation (Euler angles)); the vectors $\mathbf{q} = (q_1, q_2, ..., q_{n_q})^T$ and $\boldsymbol{\theta} = (\theta_1, \theta_2, ..., \theta_{n_\theta})^T$ collect all passive and virtual joints coordinates respectively; n_q, n_θ are the sizes of $\mathbf{q}$ and $\boldsymbol{\theta}$, respectively.

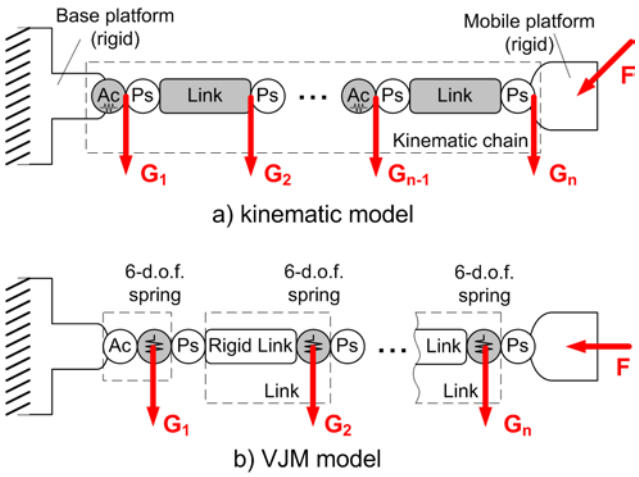

Figure 4.1 General structure of kinematic chain with auxiliary loading and its VJM model

Stiffness modeling for the manipulators with end-point loading and preloading in the joints have been already published in [13], However other types of loadings (here they are aggregated in the auxiliary loading) applied to intermediate points did not receive adequate attention in robotics. In practice, these loadings can be caused by gravity forces (generally they are distributed, but in practice they can be approximated by

localized ones) and/or gravity compensators. These forces will be denoted as $\mathbf{G}_j$, where $j=1,...,n$ is the node number in the serial chain starting from the fix base (here, $j=n$ corresponds to the end-point). It should be noted that for computational convenience, it is assumed that the end point loading consists of two components $\mathbf{G}_n$ and $\mathbf{F}$ of different nature.

It is evident that in general the auxiliary forces $\mathbf{G}_i$ depend on the manipulator configuration. So, let us assume that they are described by the functions

$$\mathbf{G}_j = \mathbf{G}_j(\mathbf{q},\boldsymbol{\theta}), \tag{4.2}$$

In contrast, for the external force $\mathbf{F}$, it is assumed that there is no direct relation with manipulator configuration.

For the serial chains with auxiliary loadings it is also required to extend the geometrical model. In particular, in addition to equation (4.1) defining the end-point location, it is necessary to introduce additional functions

$$\mathbf{t}_j = \mathbf{g}_j(\mathbf{q},\boldsymbol{\theta}), \quad j=1,...,n \tag{4.3}$$

defining locations of the nodes. It worth mentioning that for the serial chain, the position $\mathbf{t}_j$ depends on a sub-set of the joint coordinates (corresponding to the passive and virtual joints located between the base and the j-th node), but for the purpose of analytical simplicity let us use the whole set of the joint coordinates $(\mathbf{q},\boldsymbol{\theta})$ as the arguments of the functions $\mathbf{g}_i(...)$.

Using these assumptions and using results from our previous works [13][14], the problem of the manipulator stiffness modeling with auxiliary loadings can be split into several steps that are sequentially considered in the following sections.

4.3 Static equilibrium equations

To obtain a desired stiffness model, it is required to derive the static equilibrium equations that differ from the one used for the end-point loaded manipulator only due to influence of auxiliary loadings $\mathbf{G}_j$. Let us apply the principle of the virtual work and assume that the kinematic chain under external loadings $\mathbf{F}$ and $\mathbf{G}=[\mathbf{G}_1...\mathbf{G}_n]$ has the configuration $(\mathbf{q},\boldsymbol{\theta})$ and the locations of the end-point and the nodes are $\mathbf{t}=\mathbf{g}(\mathbf{q},\boldsymbol{\theta})$ and $\mathbf{t}_j=\mathbf{g}_j(\mathbf{q},\boldsymbol{\theta})$, $j=\overline{1,n}$ respectively.

Following the principle of virtual work, the work of external forces $\mathbf{G},\mathbf{F}$ is equal to the work of internal forces $\boldsymbol{\tau}_\theta$ caused by displacement of the virtual springs $\delta\boldsymbol{\theta}$

$$\sum_{j=1}^{n}\left(\mathbf{G}_j^{\mathrm{T}}\cdot\delta\mathbf{t}_j\right)+\mathbf{F}^{\mathrm{T}}\cdot\delta\mathbf{t}=\boldsymbol{\tau}_\theta^{\mathrm{T}}\cdot\delta\boldsymbol{\theta} \tag{4.4}$$

where the virtual displacements $\delta\mathbf{t}_j$ can be computed from the linearized geometrical model derived from (4.3)

$$\delta\mathbf{t}_j=\mathbf{J}_\theta^{(j)}\cdot\delta\boldsymbol{\theta}+\mathbf{J}_q^{(j)}\cdot\delta\mathbf{q}, \quad j=1..n, \tag{4.5}$$

which includes the Jacobian matrices

$$\mathbf{J}_{\theta}^{(j)} = \frac{\partial}{\partial \boldsymbol{\theta}} \mathbf{g}_j(\mathbf{q}, \boldsymbol{\theta}); \qquad \mathbf{J}_{\mathrm{q}}^{(j)} = \frac{\partial}{\partial \mathbf{q}} \mathbf{g}_j(\mathbf{q}, \boldsymbol{\theta}) \tag{4.6}$$

with respect to the virtual and passive joint coordinates respectively.

Substituting (4.5) to (4.4) we can get the equation

$$\sum_{j=1}^{n} \left(\mathbf{G}_j^{\mathrm{T}} \cdot \mathbf{J}_{\theta}^{(j)} \cdot \delta\boldsymbol{\theta} + \mathbf{G}_j^{\mathrm{T}} \cdot \mathbf{J}_{\mathrm{q}}^{(j)} \cdot \delta\mathbf{q} \right) + \left(\mathbf{F}^{\mathrm{T}} \cdot \mathbf{J}_{\theta}^{(n)} \cdot \delta\boldsymbol{\theta} + \mathbf{F}^{\mathrm{T}} \cdot \mathbf{J}_{\mathrm{q}}^{(n)} \cdot \delta\mathbf{q} \right) = \boldsymbol{\tau}_{\theta}^{\mathrm{T}} \cdot \delta\boldsymbol{\theta} \tag{4.7}$$

which has to be satisfied for any variation of $\delta\boldsymbol{\theta}, \delta\mathbf{q}$. It means that the terms regrouping the variables $\delta\boldsymbol{\theta}, \delta\mathbf{q}$ have the coefficients equal to zero, hence the force-balance equations can be written as

$$\boldsymbol{\tau}_{\theta} = \sum_{j=1}^{n} \mathbf{J}_{\theta}^{(j)\mathrm{T}} \cdot \mathbf{G}_j + \mathbf{J}_{\theta}^{(n)\mathrm{T}} \cdot \mathbf{F}; \quad \mathbf{0} = \sum_{j=1}^{n} \mathbf{J}_{\mathrm{q}}^{(j)\mathrm{T}} \cdot \mathbf{G}_j + \mathbf{J}_{\mathrm{q}}^{(n)\mathrm{T}} \cdot \mathbf{F} \tag{4.8}$$

These equations can be re-written in block-matrix form as

$$\boldsymbol{\tau}_{\theta} = \mathbf{J}_{\theta}^{(\mathrm{G})\mathrm{T}} \cdot \mathbf{G} + \mathbf{J}_{\theta}^{(\mathrm{F})\mathrm{T}} \cdot \mathbf{F}; \qquad \mathbf{0} = \mathbf{J}_{\mathrm{q}}^{(\mathrm{G})\mathrm{T}} \cdot \mathbf{G} + \mathbf{J}_{\mathrm{q}}^{(\mathrm{F})\mathrm{T}} \cdot \mathbf{F} \tag{4.9}$$

where

$$\begin{aligned} &\mathbf{J}_{\theta}^{(\mathrm{F})} = \mathbf{J}_{\theta}^{(n)}; \quad \mathbf{J}_{\mathrm{q}}^{(F)} = \mathbf{J}_{\mathrm{q}}^{(n)}; \quad \mathbf{J}_{\theta}^{(\mathrm{G})} = \left[\mathbf{J}_{\theta}^{(1)\mathrm{T}} \ldots \mathbf{J}_{\theta}^{(n)\mathrm{T}} \right]^{\mathrm{T}}; \\ &\mathbf{J}_{\mathrm{q}}^{(\mathrm{G})} = \left[\mathbf{J}_{\mathrm{q}}^{(1)\mathrm{T}} \ldots \mathbf{J}_{\mathrm{q}}^{(n)\mathrm{T}} \right]^{\mathrm{T}}; \qquad \mathbf{G} = \left[\mathbf{G}_1^{\mathrm{T}} \ldots \mathbf{G}_n^{\mathrm{T}} \right]^{\mathrm{T}} \end{aligned} \tag{4.10}$$

Finally, taking into account the virtual spring reaction $\boldsymbol{\tau}_{\theta} = \mathbf{K}_{\theta} \cdot \left(\boldsymbol{\theta} - \boldsymbol{\theta}^0 \right)$, where $\mathbf{K}_{\theta} = diag\left(\mathbf{K}_{\theta_1}, \ldots, \mathbf{K}_{\theta_n} \right)$, the desired static equilibrium equations can be presented as

$$\begin{aligned} &\mathbf{J}_{\theta}^{(\mathrm{G})\mathrm{T}} \cdot \mathbf{G} + \mathbf{J}_{\theta}^{(\mathrm{F})\mathrm{T}} \cdot \mathbf{F} = \mathbf{K}_{\theta} \cdot \left(\boldsymbol{\theta} - \boldsymbol{\theta}^0 \right) \\ &\mathbf{J}_{\mathrm{q}}^{(\mathrm{G})\mathrm{T}} \cdot \mathbf{G} + \mathbf{J}_{\mathrm{q}}^{(\mathrm{F})\mathrm{T}} \cdot \mathbf{F} = \mathbf{0} \end{aligned} \tag{4.11}$$

Further, these equations will be used for computing the static equilibrium configuration and corresponding Cartesian stiffness matrix.

4.4 Static equilibrium configuration

To obtain a relation between the external loading $\mathbf{F}$ and internal coordinates of the kinematic chain $(\mathbf{q}, \boldsymbol{\theta})$ corresponding to the static equilibrium, equations (4.11) should be solved either for different given values of $\mathbf{F}$ or for different given values of $\mathbf{t}$. In [13] these problems were referred to as the original and the dual ones respectively, but the dual problem was discovered to be the most convenient from computational point of view. Hence, let us solve static equilibrium equations with respect to manipulator configuration $(\mathbf{q}, \boldsymbol{\theta})$ and external loading $\mathbf{F}$ for given end-effector position $\mathbf{t} = \mathbf{g}(\mathbf{q}, \boldsymbol{\theta})$ and function of auxiliary-loadings $\mathbf{G}(\mathbf{q}, \boldsymbol{\theta})$

$$\begin{aligned}
&\mathbf{K}_\theta \cdot \left(\boldsymbol{\theta} - \boldsymbol{\theta}^0\right) = \mathbf{J}_\theta^{(G)T} \cdot \mathbf{G} + \mathbf{J}_\theta^{(F)T} \cdot \mathbf{F};\\
&\mathbf{J}_q^{(G)T} \cdot \mathbf{G} + \mathbf{J}_q^{(F)T} \cdot \mathbf{F} = \mathbf{0}\\
&\mathbf{t} = \mathbf{g}(\mathbf{q}, \boldsymbol{\theta});\\
&\mathbf{G} = \mathbf{G}(\mathbf{q}, \boldsymbol{\theta})
\end{aligned} \qquad (4.12)$$

where the unknown variables are $(\mathbf{q}, \boldsymbol{\theta}, \mathbf{F})$.

Since usually this system has no analytical solution, iterative numerical technique can be applied. So, the kinematic equations may be linearized in the neighborhood of the current configuration $(\mathbf{q}_i, \boldsymbol{\theta}_i)$

$$\mathbf{t}_{i+1} = \mathbf{g}(\mathbf{q}_i, \boldsymbol{\theta}_i) + \mathbf{J}_\theta^{(F)}(\mathbf{q}_i, \boldsymbol{\theta}_i) \cdot (\boldsymbol{\theta}_{i+1} - \boldsymbol{\theta}_i) + \mathbf{J}_q^{(F)}(\mathbf{q}_i, \boldsymbol{\theta}_i) \cdot (\mathbf{q}_{i+1} - \mathbf{q}_i); \qquad (4.13)$$

where the subscript 'i' indicates the iteration number and the changes in Jacobians $\mathbf{J}_\theta^{(G)}$, $\mathbf{J}_\theta^{(F)}$, $\mathbf{J}_q^{(G)}$, $\mathbf{J}_q^{(F)}$ and the auxiliary loadings $\mathbf{G}(\mathbf{q}, \boldsymbol{\theta})$ are assumed to be negligible from one iteration to another. Correspondingly, the static equilibrium equations in the neighborhood of $(\mathbf{q}_i, \boldsymbol{\theta}_i)$ may be rewritten as

$$\begin{aligned}
&\mathbf{J}_\theta^{(G)T} \cdot \mathbf{G} + \mathbf{J}_\theta^{(F)T} \cdot \mathbf{F}_{i+1} = \mathbf{K}_\theta \cdot \left(\boldsymbol{\theta}_{i+1} - \boldsymbol{\theta}^0\right)\\
&\mathbf{J}_q^{(G)T} \cdot \mathbf{G} + \mathbf{J}_q^{(F)T} \cdot \mathbf{F}_{i+1} = \mathbf{0}
\end{aligned}. \qquad (4.14)$$

Thus, combining (4.13) and (4.14), the iterative algorithm for computing of static equilibrium configuration for given end-effector location can be presented as

$$\begin{bmatrix} \mathbf{F}_{i+1} \\ \mathbf{q}_{i+1} \\ \boldsymbol{\theta}_{i+1} \end{bmatrix} = \begin{bmatrix} \mathbf{0} & \mathbf{J}_q^{(F)} & \mathbf{J}_\theta^{(F)} \\ \mathbf{J}_q^{(F)T} & \mathbf{0} & \mathbf{0} \\ \mathbf{J}_\theta^{(F)T} & \mathbf{0} & -\mathbf{K}_\theta \end{bmatrix}^{-1} \cdot \begin{bmatrix} \mathbf{t}_{i+1} - \mathbf{g}(\mathbf{q}_i, \boldsymbol{\theta}_i) + \mathbf{J}_\theta^{(F)} \cdot \boldsymbol{\theta}_i + \mathbf{J}_q^{(F)} \cdot \mathbf{q}_i \\ -\mathbf{J}_q^{(G)T} \cdot \mathbf{G}_i \\ -\mathbf{J}_\theta^{(G)T} \cdot \mathbf{G}_i - \mathbf{K}_\theta \cdot \boldsymbol{\theta}^0 \end{bmatrix} \qquad (4.15)$$

where $\mathbf{G}_{i+1} = \mathbf{G}(\mathbf{q}_{i+1}, \boldsymbol{\theta}_{i+1})$.

To reduce the size of a matrix to be inverted, the above system can be slightly simplified. In particular, based on analytical expression for $\boldsymbol{\theta} = \mathbf{K}_\theta^{-1}(\mathbf{J}_\theta^{(G)T} \cdot \mathbf{G} + \mathbf{J}_\theta^{(F)T} \cdot \mathbf{F}) + \boldsymbol{\theta}^0$, the unknown variables can be separated in two groups $(\mathbf{F}, \mathbf{q})$ and $\boldsymbol{\theta}$. This yields the iterative scheme

$$\begin{aligned}
&\begin{bmatrix} \mathbf{F}_{i+1} \\ \mathbf{q}_{i+1} \end{bmatrix} = \begin{bmatrix} \mathbf{J}_\theta^{(F)} \cdot \mathbf{K}_\theta^{-1} \cdot \mathbf{J}_\theta^{(F)T} & \mathbf{J}_q^{(F)} \\ \mathbf{J}_q^{(F)T} & \mathbf{0} \end{bmatrix}^{-1} \cdot \begin{bmatrix} \mathbf{t}_{i+1} - \mathbf{g}(\mathbf{q}_i, \boldsymbol{\theta}_i) + \mathbf{J}_\theta^{(F)} \boldsymbol{\theta}_i + \mathbf{J}_q^{(F)} \mathbf{q}_i - \mathbf{J}_\theta^{(F)} \mathbf{K}_\theta^{-1} \mathbf{J}_\theta^{(G)T} \mathbf{G}_i \\ -\mathbf{J}_q^{(G)T} \cdot \mathbf{G}_i \end{bmatrix}\\
&\boldsymbol{\theta}_{i+1} = \mathbf{K}_\theta^{-1} \left(\mathbf{J}_\theta^{(G)T} \cdot \mathbf{G}_i + \mathbf{J}_\theta^{(F)T} \cdot \mathbf{F}_{i+1}\right) + \boldsymbol{\theta}^0
\end{aligned} \qquad (4.16)$$

that requires matrix inversion of essentially lower order (for example, for 3-link manipulator with two passive joints and two actuated joints, the size of matrix inversion reduces from 34 to 14). It should be mentioned that $\mathbf{K}_\theta^{-1}$ is computed only once, outside of the iterative loop. The proposed algorithm allows us to compute static equilibrium configuration for the serial chains with passive joints and all types of loadings (internal preloading, external loadings applied to any point of the manipulator and loading from the technological process).

4.5 Stiffness matrix

Previous Section allows us to obtain the non-linear relation between elastic deflections $\Delta\mathbf{t}$ and external loading $\mathbf{F}$. In order to obtain the Cartesian stiffness matrix, let us linearize the force-deflection relation in the

neighborhood of the equilibrium. Following this approach, two equilibriums that correspond to the manipulator state variables $(\mathbf{F}, \mathbf{q}, \boldsymbol{\theta}, \mathbf{t})$ and $(\mathbf{F}+\delta\mathbf{F}, \mathbf{q}+\delta\mathbf{q}, \boldsymbol{\theta}+\delta\boldsymbol{\theta}, \mathbf{t}+\delta\mathbf{t})$ should be considered simultaneously. Here $\delta\mathbf{F}$, $\delta\mathbf{t}$ define small increments in the external loading and relevant displacement of the-end-point. Using this notation, the static equilibrium equations may be written as

$$\begin{aligned}&\mathbf{t}=\mathbf{g}(\mathbf{q},\boldsymbol{\theta})\\&\mathbf{K}_\theta\cdot(\boldsymbol{\theta}-\boldsymbol{\theta}^0)=\mathbf{J}_\theta^{(G)\mathrm{T}}\cdot\mathbf{G}+\mathbf{J}_\theta^{(F)\mathrm{T}}\cdot\mathbf{F}\\&\mathbf{J}_q^{(G)\mathrm{T}}\cdot\mathbf{G}+\mathbf{J}_q^{(F)\mathrm{T}}\cdot\mathbf{F}=\mathbf{0}\end{aligned}\qquad(4.17)$$

and

$$\begin{aligned}&\mathbf{t}+\delta\mathbf{t}=\mathbf{g}(\mathbf{q}+\delta\mathbf{q},\boldsymbol{\theta}+\delta\boldsymbol{\theta})\\&\mathbf{K}_\theta\cdot(\boldsymbol{\theta}+\delta\boldsymbol{\theta}-\boldsymbol{\theta}^0)=(\mathbf{J}_\theta^{(G)}+\delta\mathbf{J}_\theta^{(G)})^{\mathrm{T}}\cdot(\mathbf{G}+\delta\mathbf{G})+(\mathbf{J}_\theta^{(F)}+\delta\mathbf{J}_\theta^{(F)})^{\mathrm{T}}\cdot(\mathbf{F}+\delta\mathbf{F})\\&(\mathbf{J}_q^{(G)}+\delta\mathbf{J}_q^{(G)})^{\mathrm{T}}\cdot(\mathbf{G}+\delta\mathbf{G})+(\mathbf{J}_q^{(F)}+\delta\mathbf{J}_q^{(F)})^{\mathrm{T}}\cdot(\mathbf{F}+\delta\mathbf{F})=\mathbf{0}\end{aligned}\qquad(4.18)$$

where $\mathbf{t}$, $\mathbf{F}$, $\mathbf{G}$, $\mathbf{K}_\theta$, $\mathbf{q}$, $\boldsymbol{\theta}$, $\boldsymbol{\theta}^0$ are assumed to be known.

After linearization of the function $\mathbf{g}(\mathbf{q},\boldsymbol{\theta})$ in the neighborhood of loaded equilibrium, the system (4.17), (4.18) is reduced to three equations

$$\begin{aligned}&\delta\mathbf{t}=\mathbf{J}_\theta^{(F)}\cdot\delta\boldsymbol{\theta}+\mathbf{J}_q^{(F)}\cdot\delta\mathbf{q}\\&\mathbf{K}_\theta\cdot\delta\boldsymbol{\theta}=\delta\mathbf{J}_\theta^{(G)}\cdot\mathbf{G}+\mathbf{J}_\theta^{(G)}\cdot\delta\mathbf{G}+\delta\mathbf{J}_\theta^{(F)}\cdot\mathbf{F}+\mathbf{J}_\theta^{(F)}\cdot\delta\mathbf{F}\\&\delta\mathbf{J}_q^{(G)}\cdot\mathbf{G}+\mathbf{J}_q^{(G)}\cdot\delta\mathbf{G}+\delta\mathbf{J}_q^{(F)}\cdot\mathbf{F}+\mathbf{J}_q^{(F)}\cdot\delta\mathbf{F}=\mathbf{0}\end{aligned}\qquad(4.19)$$

which define the desired linear relations between $\delta\mathbf{t}$ and $\delta\mathbf{F}$, $\delta\mathbf{q}$, $\delta\boldsymbol{\theta}$ that are expressed via the stiffness matrices $\mathbf{K}_C$, $\mathbf{K}_{Cq}$, $\mathbf{K}_{C\theta}$. In this system, small variations of Jacobians may be expressed via the second order derivatives

$$\begin{aligned}&\delta\mathbf{J}_q^{(F)}=\mathbf{H}_{q\theta}^{(F)}\cdot\delta\boldsymbol{\theta}+\mathbf{H}_{qq}^{(F)}\cdot\delta\mathbf{q};\quad \delta\mathbf{J}_\theta^{(F)}=\mathbf{H}_{\theta\theta}^{(F)}\cdot\delta\boldsymbol{\theta}+\mathbf{H}_{\theta q}^{(F)}\cdot\delta\mathbf{q};\\&\delta\mathbf{J}_q^{(G)}=\mathbf{H}_{q\theta}^{(G)}\cdot\delta\boldsymbol{\theta}+\mathbf{H}_{qq}^{(G)}\cdot\delta\mathbf{q};\quad \delta\mathbf{J}_\theta^{(G)}=\mathbf{H}_{\theta\theta}^{(G)}\cdot\delta\boldsymbol{\theta}+\mathbf{H}_{\theta q}^{(G)}\cdot\delta\mathbf{q};\end{aligned}\qquad(4.20)$$

where

$$\begin{aligned}&\mathbf{H}_{\theta\theta}^{(G)}=\sum_{j=1}^{n}\frac{\partial^2}{\partial\boldsymbol{\theta}^2}\left(\mathbf{g}_j^{\,T}(\mathbf{q},\boldsymbol{\theta})\mathbf{G}_j\right);\quad \mathbf{H}_{\theta\theta}^{(F)}=\frac{\partial^2}{\partial\boldsymbol{\theta}^2}\left(\mathbf{g}^T(\mathbf{q},\boldsymbol{\theta})\mathbf{F}\right);\quad \mathbf{H}_{qq}^{(G)}=\sum_{j=1}^{n}\frac{\partial^2}{\partial\mathbf{q}^2}\left(\mathbf{g}_j^{\,T}(\mathbf{q},\boldsymbol{\theta})\mathbf{G}_j\right);\\&\mathbf{H}_{qq}^{(F)}=\frac{\partial^2}{\partial\mathbf{q}^2}\left(\mathbf{g}^T(\mathbf{q},\boldsymbol{\theta})\mathbf{F}\right);\quad \mathbf{H}_{\theta q}^{(G)}=\sum_{j=1}^{n}\frac{\partial^2}{\partial\boldsymbol{\theta}\,\partial\mathbf{q}}\left(\mathbf{g}_j^{\,T}(\mathbf{q},\boldsymbol{\theta})\mathbf{G}_j\right);\quad \mathbf{H}_{\theta q}^{(F)}=\frac{\partial^2}{\partial\boldsymbol{\theta}\,\partial\mathbf{q}}\left(\mathbf{g}^T(\mathbf{q},\boldsymbol{\theta})\mathbf{F}\right);\\&\mathbf{H}_{q\theta}^{(G)}=\sum_{j=1}^{n}\frac{\partial^2}{\partial\mathbf{q}\,\partial\boldsymbol{\theta}}\left(\mathbf{g}_j^{\,T}(\mathbf{q},\boldsymbol{\theta})\mathbf{G}_j\right);\quad \mathbf{H}_{q\theta}^{(F)}=\frac{\partial^2}{\partial\mathbf{q}\,\partial\boldsymbol{\theta}}\left(\mathbf{g}^T(\mathbf{q},\boldsymbol{\theta})\mathbf{F}\right)\end{aligned}\qquad(4.21)$$

Also, the auxiliary loading $\mathbf{G}$ may be computed via the first order derivatives as

$$\delta\mathbf{G}=\partial\mathbf{G}/\partial\boldsymbol{\theta}\cdot\delta\boldsymbol{\theta}+\partial\mathbf{G}/\partial\mathbf{q}\cdot\delta\mathbf{q}\qquad(4.22)$$

Further, let us introduce additional notations

$$\mathbf{H}_{\theta\theta}=\mathbf{H}_{\theta\theta}^{(\mathrm{F})}+\mathbf{H}_{\theta\theta}^{(\mathrm{G})}+\mathbf{J}_{\theta}^{(\mathrm{G})\mathrm{T}}\cdot\frac{\partial}{\partial\boldsymbol{\theta}}\mathbf{G};\qquad \mathbf{H}_{\theta\mathrm{q}}=\mathbf{H}_{\theta\mathrm{q}}^{(\mathrm{G})}+\mathbf{H}_{\theta\mathrm{q}}^{(\mathrm{F})}+\mathbf{J}_{\theta}^{(\mathrm{G})\mathrm{T}}\cdot\frac{\partial}{\partial\mathbf{q}}\mathbf{G};$$
$$\mathbf{H}_{\mathrm{q}\theta}=\mathbf{H}_{\mathrm{q}\theta}^{(\mathrm{G})}+\mathbf{H}_{\mathrm{q}\theta}^{(\mathrm{F})}+\mathbf{J}_{\mathrm{q}}^{(\mathrm{G})\mathrm{T}}\cdot\frac{\partial}{\partial\boldsymbol{\theta}}\mathbf{G};\qquad \mathbf{H}_{\mathrm{qq}}=\mathbf{H}_{\mathrm{qq}}^{(\mathrm{G})}+\mathbf{H}_{\mathrm{qq}}^{(\mathrm{F})}+\mathbf{J}_{\mathrm{q}}^{(\mathrm{G})\mathrm{T}}\cdot\frac{\partial}{\partial\mathbf{q}}\mathbf{G}\quad,\tag{4.23}$$

which allows us to present system (4.19) in the form

$$\begin{bmatrix}\delta\mathbf{t}\\ \mathbf{0}\\ \mathbf{0}\end{bmatrix}=\begin{bmatrix}\mathbf{0} & \mathbf{J}_{\mathrm{q}}^{(\mathrm{F})} & \mathbf{J}_{\theta}^{(\mathrm{F})}\\ \mathbf{J}_{\mathrm{q}}^{(\mathrm{F})\mathrm{T}} & \mathbf{H}_{\mathrm{qq}} & \mathbf{H}_{\mathrm{q}\theta}\\ \mathbf{J}_{\theta}^{(\mathrm{F})\mathrm{T}} & \mathbf{H}_{\theta\mathrm{q}} & -\mathbf{K}_{\theta}+\mathbf{H}_{\theta\theta}\end{bmatrix}\cdot\begin{bmatrix}\delta\mathbf{F}\\ \delta\mathbf{q}\\ \delta\boldsymbol{\theta}\end{bmatrix}\tag{4.24}$$

that has the same structure as for end-point loaded manipulator [13]. Hence, similarly the desired Cartesian stiffness matrices $\mathbf{K}_{\mathrm{C}}$ and stiffness matrices $\mathbf{K}_{\mathrm{C}\theta}$ and $\mathbf{K}_{\mathrm{Cq}}$ defining linear mappings of end-point displacement $\delta\mathbf{t}$ to internal coordinates deflections $\delta\boldsymbol{\theta}$ and $\delta\mathbf{q}$:

$$\delta\boldsymbol{\theta}=\mathbf{K}_{\mathrm{C}\theta}\cdot\delta\mathbf{t};\qquad \delta\mathbf{q}=\mathbf{K}_{\mathrm{Cq}}\cdot\delta\mathbf{t}\tag{4.25}$$

can be computed via either high order matrix inversion

$$\left[\begin{array}{c|c|c}\mathbf{K}_{\mathrm{C}} & * & *\\ \hline \mathbf{K}_{\mathrm{Cq}} & * & *\\ \hline \mathbf{K}_{\mathrm{C}\theta} & * & *\end{array}\right]=\begin{bmatrix}\mathbf{0} & \mathbf{J}_{\mathrm{q}}^{(\mathrm{F})} & \mathbf{J}_{\theta}^{(\mathrm{F})}\\ \mathbf{J}_{\mathrm{q}}^{(\mathrm{F})\mathrm{T}} & \mathbf{H}_{\mathrm{qq}} & \mathbf{H}_{\mathrm{q}\theta}\\ \mathbf{J}_{\theta}^{(\mathrm{F})\mathrm{T}} & \mathbf{H}_{\theta\mathrm{q}} & -\mathbf{K}_{\theta}+\mathbf{H}_{\theta\theta}\end{bmatrix}^{-1}\tag{4.26}$$

or lower order inversion

$$\left[\begin{array}{c|c}\mathbf{K}_{\mathrm{C}} & *\\ \hline \mathbf{K}_{\mathrm{Cq}} & *\end{array}\right]=\begin{bmatrix}\mathbf{J}_{\theta}^{(\mathrm{F})}\mathbf{k}_{\theta}^{\mathrm{F}}\mathbf{J}_{\theta}^{(\mathrm{F})\mathrm{T}} & \mathbf{J}_{\mathrm{q}}^{(\mathrm{F})}+\mathbf{J}_{\theta}^{(\mathrm{F})}\mathbf{k}_{\theta}^{\mathrm{F}}\mathbf{H}_{\theta\mathrm{q}}\\ \mathbf{J}_{\mathrm{q}}^{(\mathrm{F})\mathrm{T}}+\mathbf{H}_{\mathrm{q}\theta}\mathbf{k}_{\theta}^{\mathrm{F}}\mathbf{J}_{\theta}^{(\mathrm{F})\mathrm{T}} & \mathbf{H}_{\mathrm{qq}}+\mathbf{H}_{\mathrm{q}\theta}\mathbf{k}_{\theta}^{\mathrm{F}}\mathbf{H}_{\theta\mathrm{q}}\end{bmatrix}^{-1}\tag{4.27}$$

where $\mathbf{k}_{\theta}^{\mathrm{F}}=(\mathbf{K}_{\theta}-\mathbf{H}_{\theta\theta})^{-1}$ denotes the modified joint compliance matrix. It is obvious that, using these notations, the matrices $\mathbf{K}_{\mathrm{C}}$, $\mathbf{K}_{\mathrm{Cq}}$, $\mathbf{K}_{\mathrm{C}\theta}$ can be also computed analytically using the block matrix inversion [14]

$$\mathbf{K}_{\mathrm{C}}=\mathbf{K}_{C}^{0(F)}-\mathbf{K}_{C}^{0(F)}\cdot\left(\mathbf{J}_{\mathrm{q}}+\mathbf{J}_{\theta}\cdot\mathbf{k}_{\theta}^{\mathrm{F}}\cdot\mathbf{H}_{\theta\mathrm{q}}^{\mathrm{F}}\right)\cdot\mathbf{K}_{\mathrm{Cq}}\tag{4.28}$$

where $\mathbf{K}_{\mathrm{C}}^{0(\mathrm{F})}=(\mathbf{J}_{\theta}\cdot\mathbf{k}_{\theta}^{\mathrm{F}}\cdot\mathbf{J}_{\theta}^{\mathrm{T}})^{-1}$ defines stiffness of the kinematic chain without passive joints [2], [3] and

$$\mathbf{K}_{\mathrm{Cq}}=-\left(\mathbf{H}_{\mathrm{qq}}+\mathbf{H}_{\mathrm{q}\theta}\cdot\mathbf{k}_{\theta}^{\mathrm{F}}\cdot\mathbf{H}_{\theta\mathrm{q}}-\left(\mathbf{J}_{\mathrm{q}}^{\mathrm{T}}+\mathbf{H}_{\mathrm{q}\theta}\cdot\mathbf{k}_{\theta}^{\mathrm{F}}\cdot\mathbf{J}_{\theta}^{\mathrm{T}}\right)\mathbf{K}_{\mathrm{C}}^{0(\mathrm{F})}\cdot\left(\mathbf{J}_{\mathrm{q}}+\mathbf{J}_{\theta}\cdot\mathbf{k}_{\theta}^{\mathrm{F}}\cdot\mathbf{H}_{\theta\mathrm{q}}\right)\right)^{-1}\cdot\left(\mathbf{J}_{\mathrm{q}}^{\mathrm{T}}+\mathbf{H}_{\mathrm{q}\theta}\cdot\mathbf{k}_{\theta}^{\mathrm{F}}\cdot\mathbf{J}_{\theta}^{\mathrm{T}}\right)\cdot\mathbf{K}_{\mathrm{C}}^{0(\mathrm{F})}\tag{4.29}$$

Similarly, the matrix $\mathbf{K}_{\mathrm{C}\theta}$ can be expressed analytically as

$$\mathbf{K}_{\mathrm{C}\theta}=\mathbf{k}_{\theta}^{\mathrm{F}}\cdot\mathbf{J}_{\theta}^{\mathrm{T}}\cdot\mathbf{K}_{\mathrm{C}}+\mathbf{k}_{\theta}^{\mathrm{F}}\cdot\mathbf{H}_{\theta\mathrm{q}}\cdot\mathbf{K}_{\mathrm{Cq}}\tag{4.30}$$

Hence, the technique presented in this Section allows us to compute Cartesian stiffness matrix $\mathbf{K}_{\mathrm{C}}$ and stiffness matrices $\mathbf{K}_{\mathrm{C}\theta}$ and $\mathbf{K}_{\mathrm{Cq}}$ defining linear mappings of end-point displacement $\delta\mathbf{t}$ to internal coordinates deflections $\delta\boldsymbol{\theta}$ and $\delta\mathbf{q}$ for manipulators with external and internal loading applied to the intermediate nod-points (auxiliary loading). Presented approach deals with serial chains, however obtained results can be easily transferred to a parallel manipulators using aggregation technique from [13].

4.6 *Illustrative examples*

Let us now focus on the non-linear stiffness analysis of a serial chains under auxiliary loadings applied to an intermediate node. It is assumed that the considered chain consists of two links (either rigid or flexible) separated by a flexible joint. Relevant analysis includes evaluating stiffness variation due to the loading, detecting of buckling and computing corresponding critical forces, as well as analysis of the auxiliary spring influence on the chain stiffness.

4.6.1 Serial chain with torsional springs

Let us consider first a 2-link manipulator with a compliant actuator between the links and two passive joints at both ends. It is assumed that the left passive joint is fixed, while the right one can be moved along *x* direction (Figure 4.2a). Besides, here both rigid links have the same length L and the actuator stiffness is K_θ.

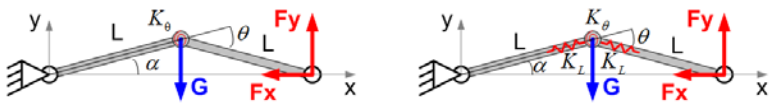

(a) serial chain with rigid links (b) serial chain with compliant links

Figure 4.2 Kinematic chains with compliant actuator between two rigid links (a) and compliant actuator between two compliant links (b)

Let us assume that the initial configuration (i.e. for $M_\theta = 0$) of the manipulator corresponds to $\theta_0 = -\pi/6$, where $\theta = -2\cdot\alpha$ is the coordinate of the actuated joint. It is also assumed that the external loading G is applied to the intermediate node (Figure 4.2a) and it is required to apply the external loading (F_x, F_y) at the end-point to compensate the auxiliary loading G. Since this example is quite simple, it is possible to obtain the force-deflection relation and the stiffness coefficient both analytically and numerically.

For this manipulator the force-displacement relation can be expressed in a parametric form as

$$F_x = -\frac{G}{2}\cdot\frac{\cos\alpha}{\sin\alpha} - 2\cdot\frac{K_\theta}{L}\cdot\frac{\alpha-\alpha_0}{\sin\alpha}; \qquad F_y = -\frac{G}{2}; \tag{4.31}$$

and stiffness of the manipulator can be presented as

$$K_x = -\frac{G}{4L}\cdot\frac{1}{\sin^3\alpha} - \frac{K_\theta}{L^2}\cdot\frac{(\alpha-\alpha_0)\cdot\cos\alpha - \sin\alpha}{\sin^3\alpha} \tag{4.32}$$

where $\alpha \in (-\pi/2;\ \pi/2)$ is treated as a parameter and $K_y = 0$.

As follows from expression (4.32), the stiffness coefficient K_x essentially depends on the auxiliary loading G. In particular, for the initial configuration, the coefficient K_x can be both positive and negative or even equal to zero when the auxiliary loading is equal to its critical value $G^* = 4K_\theta / L\cdot\sin\alpha_0$. It is evident that the case $G > G^*$ is very dangerous from practical point of view, since the chain configuration is unstable.

Summarized results for this case study are presented in Figure 4.3 that contain the force-deflection relations and values of translational stiffness K_x respectively. They show that the auxiliary loading G significantly reduces the stiffness of the serial chain. For example, in initial configuration ($\Delta x = 0$), for $G = 0$ the stiffness is $14.9\cdot K_\theta / L^2$, while for $G = 0.5\cdot G^*$ it reduces down to $8.67\cdot K_\theta / L^2$. Further increasing of the

auxiliary loading up to $G = 1.5 \cdot G^*$ leads to the unstable configuration with negative stiffness $-7.46 \cdot K_\theta / L^2$. Moreover, in the neighborhood of the critical value of $G \approx G^*$, the force-deflection curves have extremum points which may provoke buckling.

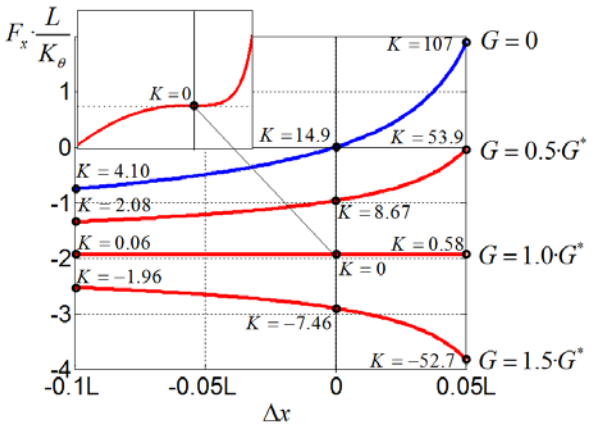

Figure 4.3 Force-deflections relations for different values of auxiliary loading G: chain with torsional spring ($G^* = 4K_\theta / L \cdot \sin\alpha_0$, $K_x = K \cdot K_\theta / L^2$)

Table 4.1 Functions and matrices used in numerical stiffness analysis of two-link manipulator with auxiliary loading (case of rigid links and compliant intermediate joint)

Intermediate point p_a	End-effector p_e
$\mathbf{g}_a = \begin{bmatrix} L_1 \cos q_1 \\ L_1 \sin q_1 \\ q_1 \end{bmatrix}$	$\begin{bmatrix} x_e \\ y_e \\ \varphi_e \end{bmatrix} = \begin{bmatrix} L_1 \cos q_1 + L_2 \cos(q_1 + \theta) \\ L_1 \sin q_1 + L_2 \sin(q_1 + \theta) \\ q_1 + \theta + q_2 \end{bmatrix}$
$\mathbf{J}_\theta^{(G)} = \begin{pmatrix} 0 \\ 0 \\ 1 \end{pmatrix}$	$\mathbf{J}_\theta^{(F)} = \begin{pmatrix} -L_2 \sin(q_1 + \theta) \\ -L_2 \cos(q_1 + \theta) \\ 1 \end{pmatrix}$
$\mathbf{J}_q^{(G)} = \begin{pmatrix} -L_1 \sin q_1 & 0 \\ L_1 \cos q_1 & 0 \\ 1 & 1 \end{pmatrix}$	$\mathbf{J}_q^{(F)} = \begin{pmatrix} -L_1 \sin q_1 - L_2 \sin(q_1 + \theta) & 0 \\ L_1 \cos q_1 + L_2 \cos(q_1 + \theta) & 0 \\ 1 & 1 \end{pmatrix}$
$\mathbf{H}_{\theta\theta}^{(G)} = [0]$ $\mathbf{H}_{\theta q}^{(G)} = [0 \quad 0]$ $\mathbf{H}_{q\theta}^{(G)} = [0 \quad 0]^T$ $\mathbf{H}_{qq}^{(G)} = \begin{bmatrix} h_1 & 0 \\ 0 & 0 \end{bmatrix}$	$\mathbf{H}_{\theta\theta}^{(F)} = [h_2]$ $\mathbf{H}_{\theta q}^{(F)} = [h_2 \quad 0]$ $\mathbf{H}_{q\theta}^{(F)} = [h_2 \quad 0]^T$ $\mathbf{H}_{qq}^{(F)} = \begin{bmatrix} h_3 & 0 \\ 0 & 0 \end{bmatrix}$
$h_1 = -L_1 \sin q_1 G_y$, $h_2 = -L_2 \cos(q_1 + \theta) F_x - L_2 \sin(q_1 + \theta) F_y$,	$h_3 = -(L_1 \cos q_1 + L_2 \cos(q_1 + \theta)) F_x - -(L_1 \sin q_1 + L_2 \sin(q_1 + \theta)) F_y$

For this case study, similar analysis has been also performed using the developed numerical technique presented in section IV and V. It worth mentioning that the numerical technique yielded the same results as the analytical one, which confirms validity of the developed approach. Some details concerning functions and matrices used in relevant expressions are presented in Table 4.1, where L_1 and L_2 denote the manipulator link lengths, q_1 and q_2 are the passive joint coordinates, θ is the virtual spring coordinate and θ_0 is the actuator coordinate. It is worth mentioning that the numerical technique yielded the same results as the analytical one, which confirms validity of the developed approach.

Hence, the presented case study demonstrates rather interesting features of stiffness behavior for kinematic chains under auxiliary loading that where not studied before (negative stiffness, non-monotonic force-deflection curves, etc.). This motivates considering more sophisticated examples, with more complicated compliant elements.

4.6.2 Serial chains with torsional and translational springs

In the second example, it is assumed that there are three compliant elements: an actuated joint with torsional stiffness parameter K_θ and two non-rigid links with translational stiffness K_L (Fig.2b). Intuitively, it is expected that such system should demonstrate more complicated stiffness behavior under the loadings compared to the previous one.

The force-deflection relations corresponding to serial chain with compliant links are presented in Fig.4. These curves have been obtained using functions and matrices presented in Table 4.2. Compared to the previous case, here for $G = 0...G^*$ there is only quantitative difference (i.e. the shape of the examined curves remains almost the same). However, for $G > G^*$ the chain may be not only unstable with respect to end-effector loading F_x, but also the chain configuration may become unstable. Geometrically, the latter qualitative difference is observed similar to buckling in vertically loaded arch. Summary of different chain configurations and their stiffness behavior is presented in Figure 4.5.

Summarizing Section 5.6, it should be concluded that auxiliary loading essentially influences on the stiffness behavior of robotic manipulators, may reduce the stiffness coefficient and also provoke undesirable phenomena (such as buckling) that must be taken into account by designers. This justifies results of this Chapter and gives perspectives for practical applications.

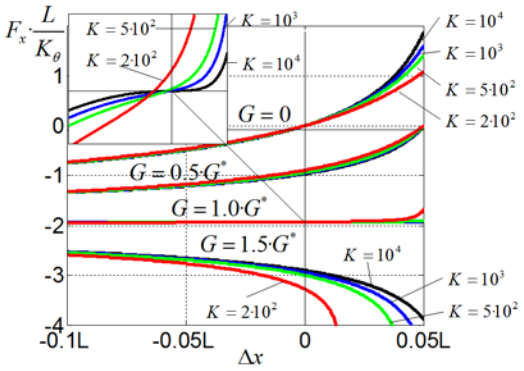

Figure 4.4 Force-deflections relations for different values of auxiliary loading G: chain with torsional and translational springs ($G^* = 4K_\theta / L \cdot \sin\alpha_0$, $K_L = K \cdot K_\theta / L^2$)

Table 4.2 Functions and matrices used in numerical stiffness analysis of two-link manipulator with auxiliary loading (case of rigid links and compliant intermediate joint)

Intermediate point p_a	End-effector p_e
$\mathbf{g}_a = \begin{bmatrix} (L_1+\theta_1)\cos q \\ (L_1+\theta_1)\sin q_1 \\ q_1 \end{bmatrix}$	$\begin{bmatrix} (L_1+\theta_1)\cos q_1 + (L_2+\theta_3)\cos(q_1+\theta_2) \\ (L_1+\theta_1)\sin q_1 + (L_2+\theta_3)\sin(q_1+\theta_2) \\ q_1+\theta_2+q_2 \end{bmatrix}$
$\mathbf{J}_\theta^{(G)} = \begin{pmatrix} j_1 & 0 & 0 \\ j_2 & 0 & 0 \\ 0 & 0 & 0 \end{pmatrix}$	$\mathbf{J}_\theta^{(F)} = \begin{pmatrix} j_1 & j_5 & j_7 \\ j_2 & j_6 & j_8 \\ 0 & 1 & 0 \end{pmatrix}$
$\mathbf{J}_q^{(G)} = \begin{pmatrix} j_3 & 0 \\ j_4 & 0 \\ 1 & 1 \end{pmatrix}$	$\mathbf{J}_q^{(F)} = \begin{pmatrix} j_3+j_5 & 0 \\ j_4+j_6 & 0 \\ 1 & 1 \end{pmatrix}$
$\mathbf{H}_{\theta\theta}^{(G)} = \begin{bmatrix} 0 & 0 & 0 \\ 0 & 0 & 0 \\ 0 & 0 & 0 \end{bmatrix}$	$\mathbf{H}_{\theta\theta}^{(F)} = \begin{bmatrix} 0 & 0 & 0 \\ 0 & h_3 & h_4 \\ 0 & h_4 & 0 \end{bmatrix}$
$\mathbf{H}_{\theta q}^{(G)} = \begin{bmatrix} h_1 & 0 \\ 0 & 0 \\ 0 & 0 \end{bmatrix}$	$\mathbf{H}_{\theta q}^{(F)} = \begin{bmatrix} h_5 & 0 \\ h_3 & 0 \\ h_4 & 0 \end{bmatrix}$
$\mathbf{H}_{q\theta}^{(G)} = \begin{bmatrix} h_1 & 0 & 0 \\ 0 & 0 & 0 \end{bmatrix}$	$\mathbf{H}_{q\theta}^{(F)} = \begin{bmatrix} h_5 & h_3 & h_4 \\ 0 & 0 & 0 \end{bmatrix}$
$\mathbf{H}_{qq}^{(G)} = \begin{bmatrix} h_2 & 0 \\ 0 & 0 \end{bmatrix}$	$\mathbf{H}_{qq}^{(F)} = \begin{bmatrix} h_6 & 0 \\ 0 & 0 \end{bmatrix}$
$j_1 = \cos q_1,\ j_2 = \sin q_1,\ j_3 = -(L_1+\theta_1)\sin q_1,\ j_4 = (L_1+\theta_1)\cos q_1,\ j_5 = -(L_2+\theta_3)\sin(q_1+\theta_2),$ $j_6 = (L_2+\theta_3)\cos(q_1+\theta_2),\ j_7 = \cos(q_1+\theta_2),\ j_8 = \sin(q_1+\theta_2)\ \ h_1 = -G_x \sin q_1 + G_y \cos q_1,$ $h_2 = -G_x(L_1+\theta_1)\cos q_1 - G_y(L_1+\theta_1)\sin q_1,\ h_3 = -F_x(L_2+\theta_3)\cos(q_1+\theta_2) - F_y(L_2+\theta_3)\sin(q_1+\theta),$ $h_4 = -F_x \sin(q_1+\theta_2) + F_y \cos(q_1+\theta),\ h_5 = -F_x \sin q_1 + F_y \cos q_1,\ h_6 = h_3 - F_x(L_1+\theta_1)\cos q_1 - F_y(L_1+\theta_1)\sin q_1$	

4.7 Conclusion

The Chapter presents generalization of the non-linear stiffness modeling technique for manipulators under internal and external loadings. The developed technique includes computing of the static equilibrium configuration corresponding to the loadings. It is able to obtain the non-linear force-deflection relation, the Cartesian stiffness matrix for the loaded mode as well as the matrices defining linear mappings from the end-point displacement into the deflections in passive and virtual joints. The obtained results allow us to extend the classical notion of "conservative congruence transformation" for the case of manipulators with auxiliary loading.

The advantages and use of the developed technique are illustrated by numerical examples that deal with a stiffness analysis of serial chains with different assumptions on the link flexibility. For the considered cases, functions and matrices that are used in numerical stiffness analyses are given. The presented results

also illustrate the ability of this technique to detect some nonlinear effects in the manipulator stiffness behavior (such as buckling).

In future, it is reasonable to develop an extension of the proposed technique that can be applied to the parallel manipulators with internal loops. Besides, it is useful to consider the manipulators with several end-points (or end-effectors). The main difficulty for both cases is related to the introducing of additional geometrical constraints that are defined by another compliant mechanism.

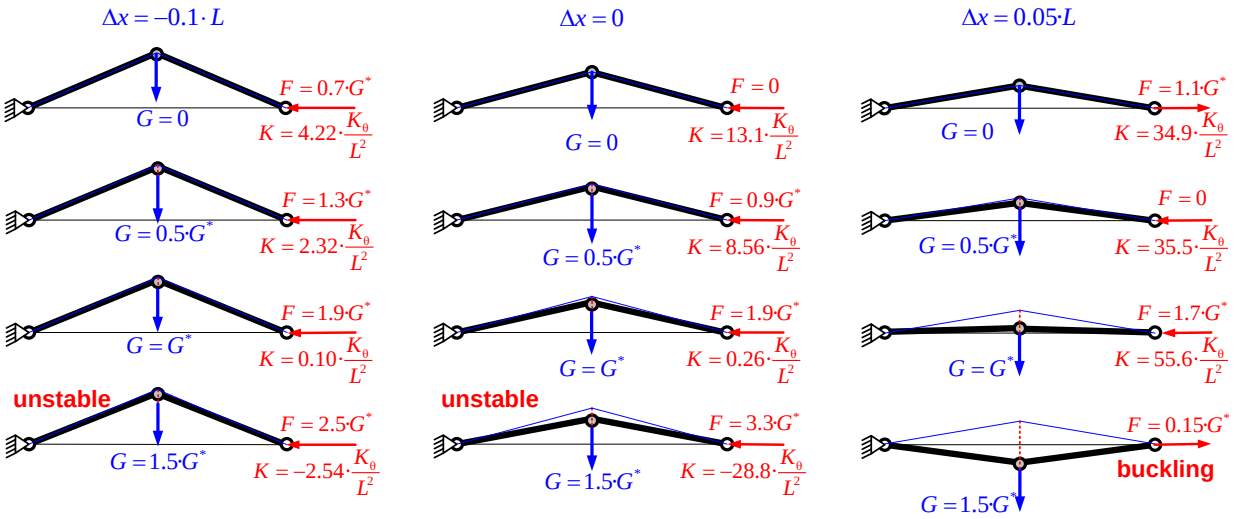

Figure 4.5 Configuration of kinematic chain with auxiliary loading: case of torsional and translational springs ($G^* = 4K_\theta / L \cdot \sin\alpha_0$, $K_L = 2 \cdot 10^2 \cdot K_\theta / L^2$)

4.8 References

[1] "Springer handbook of mechanical engineering", Ed. K-H Grote and E. Antonsson, Springer, New York 2009

[2] G. Alici, B. Shirinzadeh, "Enhanced stiffness modeling, identification and characterization for robot manipulators", Proceedings of IEEE Transactions on Robotics vol. 21(4). pp. 554–564, 2005.

[3] S. Chen, I. Kao, "Conservative Congruence Transformation for Joint and Cartesian Stiffness Matrices of Robotic Hands and Fingers", The International Journal of Robotics Research, vol. 19(9), pp. 835–847, 2000.

[4] M. Griffis, "Preloading compliant couplings and the applicability of superposition", Mechanism and Machine Theory, Vol. 41, Issue 7, pp. 845-862, 2006

[5] N. Vitiello, T. Lenzi, S. M. M. De Rossi, S. Roccella, M. C. Carrozza "A sensorless torque control for Antagonistic Driven Compliant Joints," Mechatronics, Vol. 20, Issue 3, pp. 355-367, 2010

[6] B.-J. Yi, R.A. Freeman, "Geometric analysis antagonistic stiffness redundantly actuated parallel mechanism", Journal of Robotic Systems vol. 10(5), pp. 581-603, 1993.

[7] Y. Li 1, Sh.-F. Chen, I. Kao, "Stiffness control and transformation for robotic systems with coordinate and non-coordinate bases", In: Proceedings of ICRA 2002, pp 550-555, 2002.

[8] C.Quennouelle, C. M. Gosselin, "Stiffness Matrix of Compliant Parallel Mechanisms", In Springer Advances in Robot Kinematics: Analysis and Design, pp. 331-341, 2008.

[9] I. Tyapin, G. Hovland, Kinematic and elastostatic design optimization of the 3-DOF Gantry-Tau parallel kinamatic manipulator, Modelling, Identification and Control, 30(2) (2009) 39-56

[10] J. Kövecses, J. Angeles, "The stiffness matrix in elastically articulated rigid-body systems," Multibody System Dynamics (2007) pp. 169–184, 2007.

[11] W. Wei, N. Simaan, "Design of planar parallel robots with preloaded flexures for guaranteed backlash prevention", Journal of Mechanisms and Robotics vol. 2(1), 10 pages, 2010.

[12] D. Chakarov, "Study of antagonistic stiffness of parallel manipulators with actuation redundancy", Mechanism and Machine Theory, vol. 39, pp. 583–601, 2004.

[13] A. Pashkevich, A. Klimchik, D. Chablat, "Enhanced stiffness modeling of manipulators with passive joints", Mechanism and Machine Theory, vol. 46(5), pp. 662-679, 2011.

[14] A.Pashkevich, D. Chablat, P.Wenger, "Stiffness analysis of overconstrained parallel manipulators", Mechanism and Machine Theory, vol. 44, pp. 966-982, 2008.

[15] G.H. Golub, C.F. van Loan, "Matrix computations", JHU Press, 1996

5 STABILITY OF MANIPULATOR CONFIGURATION UNDER EXTERNAL LOADING

5.1 Introduction

Manipulator stiffness modeling under loading is a relatively new research area that is important both for serial and parallel robots. In general case, loadings may be of different nature and applied to different points/surfaces. To evaluate stiffness properties, several methods can be applied such as Finite Element Analysis, Matrix Structural Analysis and Virtual Joint Modeling (VJM) [1-16], where the last one is the most attractive in robotic domain since it operates with an extension of the traditional rigid model that is completed by a set of virtual joints (localized springs), which describe elastic properties of the links, joints and actuators.

For *serial manipulators* the VJM approach has been used in the number of works [1-8]. The obtained results allows us to compute stiffness matrices both for serial manipulators without passive joints [1-5] and for serial chains of parallel manipulators with passive joints [8]. However, most of them addressed to the case of small deflections (unloaded mode) [5-6], only limited number of authors consider the case of large deflections (loaded mode) [2-3,7-8].

For *parallel manipulators*, the stiffness modeling is usually performed for all kinematic chains simultaneously [6][11], using the aggregated elastostatic equilibrium equations [12][13]. In contrast to these works, our approach is based on two-step procedure, which includes stiffness modeling of all kinematic chains *separately* and then *aggregates* them in a unique model. This approach has been already used by several authors [8][14], but related aggregation technique was reduced to simple summations of the Cartesian stiffness matrices for the kinematic chains and the external loadings applied to their end-points. This corresponds to “pure” parallel architectures where the end-point location of all kinematic chains are aligned and matched at the end-platform reference point. However, in practice, the parallel manipulator architecture is usually quite complex. In particular, the kinematic chains may be attached to different points of the end-platform.

It is obvious that the both external and internal loadings influence on the manipulator equilibrium configuration and, consequently, may modify the stiffness properties. So, they must be undoubtedly taken into account while developing the stiffness model. However, in most of related works the stiffness is evaluated in a quasi-static configuration without external or internal loading. There are very limited number of publications that directly address the case of “large deflections”, where in addition to the conventional “*elastic stiffness*” in the joints it is necessary to take into account the “*geometrical stiffness*” arising due to the change in the manipulator configuration under the load. The most essential results in this area were obtained in [7-10,14] where there are presented both some theoretical issues and several case studies for serial and parallel manipulators under end-point loading. Several authors [9,13] addressed the problem of stiffness analysis for the manipulators with internal preloading or antagonistic actuating, but in relevant equations some of the second order kinematic derivates were neglected. However, no one of them considered auxiliary loading.

This Chapter contributes to the VJM-based technique and focuses on the stability analysis of serial and parallel manipulators under external loading. It addressed both stability of end-platform location and stability of serial chain configuration. To address these issues, it is proposed a revision of the existing VJM-based stiffness modeling technique that includes development a non-linear stiffness model of the robotic

manipulator under essential loading that takes into account the external loading applied to end-effector, preloading in the joints and auxiliary loading applied to intermediate node-points.

5.2 Problem statement

5.2.1 Motivation

Traditionally, the stability of compliant mechanical systems (including manipulators) is defined as *resistance of the end-point location* $\mathbf{t}$ with respect to the "disturbing" effects of an external force $\mathbf{F}$ applied at this point. In such formulation, the stability is completely defined by the stiffness matrix $\mathbf{K}_C$ that describes the linear relations between the force and deflection deviations $\delta\mathbf{F}, \delta\mathbf{t}$ with respect to the values $\mathbf{F}$, $\mathbf{t}$.

$$\delta\mathbf{F} = \mathbf{K}_C \cdot \delta\mathbf{t} \tag{5.1}$$

It is obvious that for the stable location $\mathbf{t}$ the matrix $\mathbf{K}_C$ should be positive definite.

However, in the compliant manipulators with the passive joints, the equilibrium configuration $(\mathbf{q},\boldsymbol{\theta})$ corresponding to the same end-point location $\mathbf{t}$ cannot be unique (here the vector $\mathbf{q}$ contains passive joint coordinates; the vector $\boldsymbol{\theta}$ collects coordinates of all virtual joints). Moreover, these configurations may be both "stable" and "unstable" and may correspond to different values of potential energy stored in the virtual springs. From this point of view, it is worth to distinguish stability of the end-point location $\mathbf{t}$ and stability of the corresponding equilibrium configuration of the kinematic chain $(\mathbf{q},\boldsymbol{\theta})$, which may be defined as a *resistance of the chain shape* with respect to disturbances in redundant kinematic variables. This issue becomes extremely important for the loaded mode, when due to the kinematic redundancy caused by the passive joints and excessive number of virtual springs, small disturbances in $(\mathbf{q},\boldsymbol{\theta})$ may provoke essential change of current equilibrium configuration leading to the reduction of the potential energy and transition to another equilibrium state, while keeping the same end-point location. Hence, it is necessary to evaluate internal properties of the kinematic chain in the state of the loaded equilibrium that may correspond either to minimum or maximum of the potential energy for a fixed value of $\mathbf{t}$.

Let us illustrate this notion by the example of three-link chain (Figure 5.1a), which includes passive joints at both ends and two virtual torsional springs between the links, which insure the "straight" configuration for the unloaded mode. It is assumed that both ends of the chain are fixed by the external geometrical constrains while the internal configuration may change without shifting of the end-points, in accordance with redundant parameter value. It is evident that this chain is loaded, but corresponding value of the force **F** depends on particular configuration. Besides, among variety of possible configurations (corresponding to given end-point locations), only equilibrium ones are in the focus of interest.

For this case study, it is convenient to give an energy-based interpretation. The considered kinematic chain has one redundant parameter (rotation angle of any passive joint) and under geometrical constrains may occupy configurations with the different shapes. Relevant relation between the energy stored in the virtual springs and the redundant parameter value is presented in Figure 5.1b. Due to the physical nature of this chain, for each given end-point displacement Δ, the examined plot presents a continuous closed criss-cross curve that has exactly two minimum and maximum points, that correspond to the stable and unstable equilibriums respectively. Hence, numerical solution of static equilibrium equations may yield both stable and

unstable configurations, while in practice only stable ones should be considered. Thus, the criterion that allows to distinguish stable and unstable configurations of the kinematic chain is required.

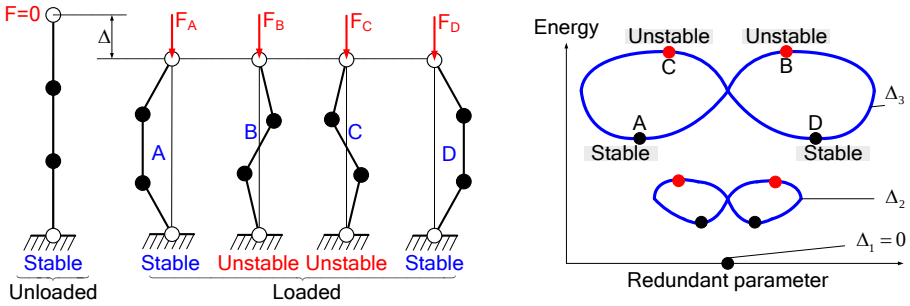

(a) equilibrium configurations (b) energy diagram

Figure 5.1 Stable and non-stable configurations of 3-link serial chain and their energy-based interpretation

Physical meaning of this stability notion (related to the kinematic chain shape) is illustrated in Figure 5.2, which contains several postures of the same parallel manipulator with exactly the same end-platform location. These postures differ in the shapes of serial kinematic chains that may be treated as internal configuration of the parallel manipulator, which is not "visible" from the end-platform side whose static stability is completely defined by the Cartesian stiffness matrix. In particular, Figure 5.2a,b present parallel manipulators that include at least one kinematic chain in unstable configuration that cannot be observed in practice but satisfy the general static equilibrium equation. In contrast, Figure 5.2c shows physically realizable posture of the same manipulator (with exactly the same location of the chain end-points) where for all kinematic chains the shapes are stable.

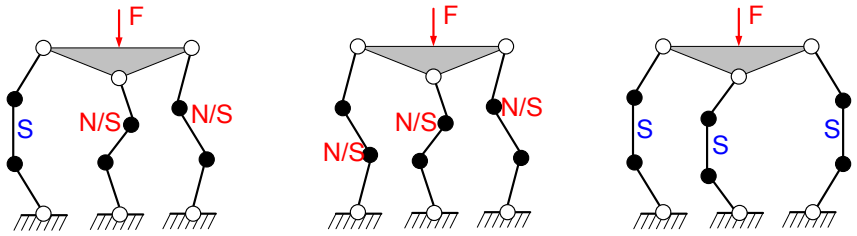

(a) PM with stable and unstable configurations (b) PM with unstable configurations (c) PM with stable configurations

Figure 5.2 2D parallel manipulators with serial chains in stable and unstable configurations

Hence, full-scale investigation of the stiffness properties of the loaded parallel manipulator must include the stability analysis of the internal kinematic chain configurations that is presented in this Chapter.

5.2.2 Basic assumptions and research problems

In order to address the stability of both end-point location and kinematic chain configuration, it is assumed that parallel manipulator has a strictly parallel structure. In this case, first, it is required to address to the stiffness modeling of serial kinematic chain and then, applying stiffness model aggregation technique, to obtain the stiffness matrix of the parallel manipulator.

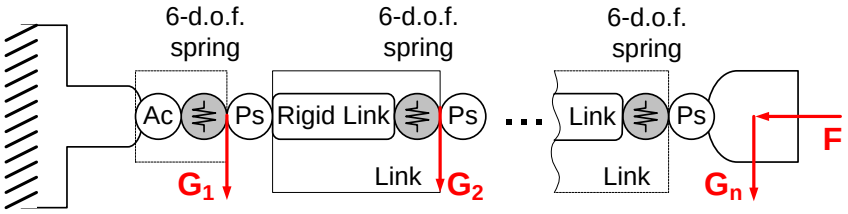

Figure 5.3 VJM model of kinematic chain with end-point and auxiliary loading

For stiffness modeling of serial kinematic chain let us use VJM model that is presented in Figure 5.3. It is assumed that, in addition to the end-point loading $\mathbf{F}$ the serial chain has an additional external loadings applied to the internal node points (auxiliary loading). These forces will be denoted as $\mathbf{G}_j$, where $j=1,...,n$ is the node number in the serial chain starting from the fix base. For such kinematic chains it is necessary to introduce the functions defining locations of the nodes

$$\mathbf{t}_j = \mathbf{g}_j(\mathbf{q},\boldsymbol{\theta}), \quad j=1,...,n \tag{5.2}$$

where the vector $\mathbf{t}_j$ includes the position and orientation of the i^{th} node; the vector $\mathbf{q}$ contains passive joint coordinates; the vector $\boldsymbol{\theta}$ collects coordinates of all virtual joints.

Using these assumptions and the methodology of VJM method proposed in [8][13], the problem of stability analysis of serial and parallel manipulators under external/internal loading can be split in the following sub-problems: (i) stability analysis of serial chain configuration that includes computing of the loaded equilibrium configuration, and (ii) stability of the end-okatform location of serial and parallel manipulators.

5.3 Stability of kinematic chain configuration under loading

Usually external and internal loadings have affects both end-point location and configuration of serial chain. Therefore, in order to address to the stability of the kinematic chain configuration; firstly; it is required to compute the loaded equilibrium configuration.

5.3.1 Static equilibrium

The static equilibrium equations for the manipulators with internal and external loadings (that are applied to both end-effector and intermediate nodes) differ from those used for the end-point loaded manipulator. Using the principle of virtual work it has been proved that the desired static equilibrium equations can be presented as

$$\begin{aligned} \mathbf{J}_{\theta}^{(G)T}\cdot\mathbf{G}+\mathbf{J}_{\theta}^{(F)T}\cdot\mathbf{F} &= \mathbf{K}_{\theta}\cdot\left(\boldsymbol{\theta}-\boldsymbol{\theta}^{0}\right) \\ \mathbf{J}_{q}^{(G)T}\cdot\mathbf{G}+\mathbf{J}_{q}^{(F)T}\cdot\mathbf{F} &= \mathbf{0} \end{aligned} \tag{5.3}$$

where

$$\mathbf{J}_{\theta}^{(\mathrm{F})}=\mathbf{J}_{\theta}^{(n)};\quad \mathbf{J}_{\mathrm{q}}^{(F)}=\mathbf{J}_{\mathrm{q}}^{(n)};\quad \mathbf{J}_{\theta}^{(\mathrm{G})}=\left[\mathbf{J}_{\theta}^{(1)\mathrm{T}}\ldots\mathbf{J}_{\theta}^{(n)\mathrm{T}}\right]^{\mathrm{T}};$$
$$\mathbf{J}_{\mathrm{q}}^{(\mathrm{G})}=\left[\mathbf{J}_{\mathrm{q}}^{(1)\mathrm{T}}\ldots\mathbf{J}_{\mathrm{q}}^{(n)\mathrm{T}}\right]^{\mathrm{T}};\qquad \mathbf{G}=\left[\mathbf{G}_1{}^{\mathrm{T}}\ldots\mathbf{G}_n{}^{\mathrm{T}}\right]^{\mathrm{T}} \tag{5.4}$$

and Jacobians with respect to the virtual and passive joint coordinates respectively can be computed as

$$\mathbf{J}_{\theta}^{(j)}=\frac{\partial}{\partial\boldsymbol{\theta}}\mathbf{g}_j\left(\mathbf{q},\boldsymbol{\theta}\right);\qquad \mathbf{J}_{\mathrm{q}}^{(j)}=\frac{\partial}{\partial\mathbf{q}}\mathbf{g}_j\left(\mathbf{q},\boldsymbol{\theta}\right) \tag{5.5}$$

To obtain a relation between the external loading $\mathbf{F}$ and internal coordinates of the kinematic chain $(\mathbf{q},\boldsymbol{\theta})$ corresponding to the static equilibrium, Eq. (5.3) should be solved either for given values of $\mathbf{F}$ or for different given values of $\mathbf{t}$. In [13] these problems were referred to as the original and the dual ones respectively, but the dual problem was discovered to be the most convenient from computational point of view. Hence, let us solve static equilibrium equations with respect to manipulator configuration $(\mathbf{q},\boldsymbol{\theta})$ and external loading $\mathbf{F}$ for given end-effector position $\mathbf{t}=\mathbf{g}(\mathbf{q},\boldsymbol{\theta})$ and function of auxiliary-loadings $\mathbf{G}(\mathbf{q},\boldsymbol{\theta})$

Since usually this system has no analytical solution, iterative numerical technique can be applied. For this purpose, the kinematic equations may be linearized in the neighborhood of the current configuration $(\mathbf{q}_i,\boldsymbol{\theta}_i)$

$$\mathbf{t}_{i+1}=\mathbf{g}\left(\mathbf{q}_i,\boldsymbol{\theta}_i\right)+\mathbf{J}_{\theta}^{(\mathrm{F})}\left(\mathbf{q}_i,\boldsymbol{\theta}_i\right)\cdot\left(\boldsymbol{\theta}_{i+1}-\boldsymbol{\theta}_i\right)+\mathbf{J}_{\mathrm{q}}^{(\mathrm{F})}\left(\mathbf{q}_i,\boldsymbol{\theta}_i\right)\cdot\left(\mathbf{q}_{i+1}-\mathbf{q}_i\right); \tag{5.6}$$

where the subscript "*i*" denotes the iteration number and the changes in Jacobians $\mathbf{J}_{\theta}^{(\mathrm{G})}$, $\mathbf{J}_{\theta}^{(\mathrm{F})}$, $\mathbf{J}_{\mathrm{q}}^{(\mathrm{G})}$, $\mathbf{J}_{\mathrm{q}}^{(\mathrm{F})}$ and variation of the auxiliary loadings $\mathbf{G}(\mathbf{q},\boldsymbol{\theta})$ from iteration to iteration are assumed to be negligible. Correspondingly, the static equilibrium equations in the neighborhood of $(\mathbf{q}_i,\boldsymbol{\theta}_i)$ may be rewritten as

$$\begin{aligned}&\mathbf{J}_{\theta}^{(\mathrm{G})\mathrm{T}}\cdot\mathbf{G}+\mathbf{J}_{\theta}^{(\mathrm{F})\mathrm{T}}\cdot\mathbf{F}_{i+1}=\mathbf{K}_{\theta}\cdot\left(\boldsymbol{\theta}_{i+1}-\boldsymbol{\theta}^0\right)\\&\mathbf{J}_{\mathrm{q}}^{(\mathrm{G})\mathrm{T}}\cdot\mathbf{G}+\mathbf{J}_{\mathrm{q}}^{(\mathrm{F})\mathrm{T}}\cdot\mathbf{F}_{i+1}=\mathbf{0}\end{aligned}. \tag{5.7}$$

Thus, combining Eq. (4.13) and (4.14), the iterative algorithm for computing the static equilibrium configuration for given end-effector location can be presented as

$$\begin{bmatrix}\mathbf{F}_{i+1}\\ \mathbf{q}_{i+1}\\ \boldsymbol{\theta}_{i+1}\end{bmatrix}=\begin{bmatrix}\mathbf{0} & \mathbf{J}_{\mathrm{q}}^{(\mathrm{F})} & \mathbf{J}_{\theta}^{(\mathrm{F})}\\ \mathbf{J}_{\mathrm{q}}^{(\mathrm{F})\mathrm{T}} & \mathbf{0} & \mathbf{0}\\ \mathbf{J}_{\theta}^{(\mathrm{F})\mathrm{T}} & \mathbf{0} & -\mathbf{K}_{\theta}\end{bmatrix}^{-1}\cdot\begin{bmatrix}\mathbf{t}_{i+1}-\mathbf{g}\left(\mathbf{q}_i,\boldsymbol{\theta}_i\right)+\mathbf{J}_{\theta}^{(\mathrm{F})}\cdot\boldsymbol{\theta}_i+\mathbf{J}_{\mathrm{q}}^{(\mathrm{F})}\cdot\mathbf{q}_i\\ -\mathbf{J}_{\mathrm{q}}^{(\mathrm{G})\mathrm{T}}\cdot\mathbf{G}_i\\ -\mathbf{J}_{\theta}^{(\mathrm{G})\mathrm{T}}\cdot\mathbf{G}_i-\mathbf{K}_{\theta}\cdot\boldsymbol{\theta}^0\end{bmatrix} \tag{5.8}$$

where $\mathbf{G}_{i+1}=\mathbf{G}(\mathbf{q}_{i+1},\boldsymbol{\theta}_{i+1})$.

The proposed algorithm allows us to compute the static equilibrium configuration for the serial chains with passive joints and all types of loadings (internal preloading, external loadings applied to any point of the manipulator and loading from the technological process). The convergence properties of this algorithm are similar to one presented in [13]. Also, it can be modified to solve the problem of computing the equilibrium configuration corresponding to given external loading.

5.3.2 Stability criterion

To evaluate stability of the static equilibrium configuration $(\mathbf{q}, \boldsymbol{\theta})$ of a separate kinematic chain, let us assume that the end-point is fixed at the point $\mathbf{t} = (\mathbf{p}, \boldsymbol{\varphi})^{\mathrm{T}}$ corresponding to the external load $\mathbf{F}$, but the joint coordinates are given small virtual displacements $\delta\mathbf{q}$, $\delta\boldsymbol{\theta}$ satisfying the geometrical constraint (4.3), i.e.

$$\mathbf{t} = \mathbf{g}(\mathbf{q}, \boldsymbol{\theta}); \qquad \mathbf{t} = \mathbf{g}(\mathbf{q} + \delta\mathbf{q}, \boldsymbol{\theta} + \delta\boldsymbol{\theta}) \tag{5.9}$$

For these assumptions, let us compute the total virtual work in the joints that must be positive for a stable equilibrium and negative for an unstable one. To achieve the virtual configuration $(\mathbf{q} + \delta\mathbf{q}, \boldsymbol{\theta} + \delta\boldsymbol{\theta})$ and restore the equilibrium conditions, each joint must include a virtual spring that generates the generalized forces/torques $\delta\boldsymbol{\tau}_{\mathrm{q}}$, $\delta\boldsymbol{\tau}_{\theta}$ which satisfies the equations:

$$\mathbf{J}_{\theta}^{\mathrm{T}} \cdot \mathbf{F} = \mathbf{K}_{\theta} \cdot (\boldsymbol{\theta} - \boldsymbol{\theta}_0); \qquad \mathbf{J}_{\mathrm{q}}^{\mathrm{T}} \cdot \mathbf{F} = 0 \tag{5.10}$$

$$\begin{aligned} (\mathbf{J}_{\theta} + \delta\mathbf{J}_{\theta})^{\mathrm{T}} \cdot \mathbf{F} &= \mathbf{K}_{\theta} \cdot (\boldsymbol{\theta} - \boldsymbol{\theta}_0 + \delta\boldsymbol{\theta}) + \delta\boldsymbol{\tau}_{\theta} \\ (\mathbf{J}_{\mathrm{q}} + \delta\mathbf{J}_{\mathrm{q}})^{\mathrm{T}} \cdot \mathbf{F} &= \delta\boldsymbol{\tau}_{q} \end{aligned} \tag{5.11}$$

After relevant transformations, the virtual torques may be expressed as

$$\delta\boldsymbol{\tau}_{\theta} = \delta(\mathbf{J}_{\theta}^{\mathrm{T}} \cdot \mathbf{F}) - \mathbf{K}_{\theta} \cdot \delta\boldsymbol{\theta}; \qquad \delta\boldsymbol{\tau}_{\mathrm{q}} = \delta(\mathbf{J}_{\mathrm{q}}^{\mathrm{T}} \cdot \mathbf{F}) \tag{5.12}$$

where $\delta(\ldots)$ denotes the differential with respect to $\delta\mathbf{q}$, $\delta\boldsymbol{\theta}$ that may be expanded via Hessians of the scalar function $\Psi = \mathbf{g}(\mathbf{q}, \boldsymbol{\theta})^{\mathrm{T}} \cdot \mathbf{F}$:

$$\begin{aligned} \delta(\mathbf{J}_{\theta}^{\mathrm{T}} \cdot \mathbf{F}) &= \mathbf{H}_{\theta\mathrm{q}}^{\mathrm{F}} \cdot \delta\mathbf{q} + \mathbf{H}_{\theta\theta}^{\mathrm{F}} \cdot \delta\boldsymbol{\theta} \\ \delta(\mathbf{J}_{\mathrm{q}}^{\mathrm{T}} \cdot \mathbf{F}) &= \mathbf{H}_{\mathrm{qq}}^{\mathrm{F}} \cdot \delta\mathbf{q} + \mathbf{H}_{\mathrm{q}\theta}^{\mathrm{F}} \cdot \delta\boldsymbol{\theta} \end{aligned} \tag{5.13}$$

provided that

$$\begin{aligned} \mathbf{H}_{\mathrm{qq}}^{\mathrm{F}} &= \partial^2\Psi / \partial\mathbf{q}^2; \qquad \mathbf{H}_{\theta\theta}^{\mathrm{F}} = \partial^2\Psi / \partial\boldsymbol{\theta}^2; \\ \mathbf{H}_{\mathrm{q}\theta}^{\mathrm{F}} &= \mathbf{H}_{\theta\mathrm{q}}^{\mathrm{F}\,\mathrm{T}} = \partial^2\Psi / \partial\mathbf{q}\,\partial\boldsymbol{\theta} \end{aligned} \tag{5.14}$$

Further, taking into account that the virtual displacement from $(\mathbf{q}, \boldsymbol{\theta})$ to $(\mathbf{q} + \delta\mathbf{q}, \boldsymbol{\theta} + \delta\boldsymbol{\theta})$ leads to a gradual change of the torques in the virtual joints from **(0, 0)** to $(\delta\boldsymbol{\tau}_{\mathrm{q}}, \delta\boldsymbol{\tau}_{\theta})$, the virtual work may be computed as a half of the corresponding scalar products

$$\delta W = -\frac{1}{2}\left(\delta\boldsymbol{\tau}_{\theta}^{\mathrm{T}} \cdot \delta\boldsymbol{\theta} + \delta\boldsymbol{\tau}_{\mathrm{q}}^{\mathrm{T}} \cdot \delta\mathbf{q}\right) \tag{5.15}$$

where the minus sign takes into account the adopted conventions for the positive directions of the forces and displacements. Hence, after appropriate substitutions and transformations to the matrix form, the desired stability condition may be written as

$$\delta W = -\frac{1}{2}\begin{bmatrix}\delta\boldsymbol{\theta}^{\mathrm{T}} & \delta\mathbf{q}^{\mathrm{T}}\end{bmatrix} \cdot \begin{bmatrix}\mathbf{H}_{\theta\theta}^{\mathrm{F}} - \mathbf{K}_{\theta} & \mathbf{H}_{\mathrm{q}\theta}^{\mathrm{F}} \\ \mathbf{H}_{\theta\mathrm{q}}^{\mathrm{F}} & \mathbf{H}_{\mathrm{qq}}^{\mathrm{F}}\end{bmatrix} \cdot \begin{bmatrix}\delta\boldsymbol{\theta} \\ \delta\mathbf{q}\end{bmatrix} > 0 \tag{5.16}$$

where $\delta\mathbf{q}$ and $\delta\boldsymbol{\theta}$ must satisfy (5.9).

In order to take into account the relation between $\delta\mathbf{q}$ and $\delta\boldsymbol{\theta}$ that is imposed by (5.9), let us apply the first-order expansion of the function $\mathbf{g}(\boldsymbol{\theta}, \mathbf{q})$ that yields the following linear relation

$$\begin{bmatrix}\mathbf{J}_\theta & \mathbf{J}_q\end{bmatrix}\cdot\begin{bmatrix}\delta\boldsymbol{\theta}\\ \delta\mathbf{q}\end{bmatrix}=\mathbf{0} \tag{5.17}$$

Then, applying the SVD-factorization of $[\mathbf{J}_\theta, \mathbf{J}_q]$

$$\begin{bmatrix}\mathbf{J}_\theta & \mathbf{J}_q\end{bmatrix}=\begin{bmatrix}\mathbf{U}_\theta & \mathbf{U}_q\end{bmatrix}\cdot\begin{bmatrix}\mathbf{S}_r & \\ & \mathbf{0}\end{bmatrix}\cdot\begin{bmatrix}\mathbf{V}_\theta^{\mathrm{T}}\\ \mathbf{V}_q^{\mathrm{T}}\end{bmatrix} \tag{5.18}$$

and extracting from $\mathbf{V}_\theta$, $\mathbf{V}_q$ the sub-matrices $\mathbf{V}_\theta^{\mathrm{o}}$, $\mathbf{V}_q^{\mathrm{o}}$ corresponding to zero singular values, a relevant null-space of the system (5.17) may be presented as

$$\delta\boldsymbol{\theta}=\mathbf{V}_\theta^{\mathrm{o}}\cdot\delta\boldsymbol{\mu};\qquad \delta\mathbf{q}=\mathbf{V}_q^{\mathrm{o}}\cdot\delta\boldsymbol{\mu} \tag{5.19}$$

where $\delta\boldsymbol{\mu}$ is the arbitrary vector of the appropriate dimension (equal to the rank-deficiency of the integrated Jacobian $[\mathbf{J}_\theta, \mathbf{J}_q]$). Hence, changing of the potential energy δW because of variation of the redundant variables $\delta\boldsymbol{\mu}$ (5.16) may be rewritten as

$$\delta W=-\frac{1}{2}\delta\boldsymbol{\mu}^{\mathrm{T}}\cdot\begin{bmatrix}\mathbf{V}_\theta^{\mathrm{o}}\\ \mathbf{V}_q^{\mathrm{o}}\end{bmatrix}^{\mathrm{T}}\cdot\begin{bmatrix}\mathbf{H}_{\theta\theta}^{\mathrm{F}}-\mathbf{K}_\theta & \mathbf{H}_{q\theta}^{\mathrm{F}}\\ \mathbf{H}_{\theta q}^{\mathrm{F}} & \mathbf{H}_{qq}^{\mathrm{F}}\end{bmatrix}\cdot\begin{bmatrix}\mathbf{V}_\theta^{\mathrm{o}}\\ \mathbf{V}_q^{\mathrm{o}}\end{bmatrix}\cdot\delta\boldsymbol{\mu}>0 \tag{5.20}$$

that must be satisfied for all arbitrary non-zero $\delta\boldsymbol{\mu}$. Hence, the considered static equilibrium configuration $(\mathbf{q}, \boldsymbol{\theta})$ is stable if (and only if) the matrix

$$S_c=\begin{bmatrix}\mathbf{V}_\theta^{\mathrm{o}}\\ \mathbf{V}_q^{\mathrm{o}}\end{bmatrix}^{\mathrm{T}}\cdot\begin{bmatrix}\mathbf{H}_{\theta\theta}^{\mathrm{F}}-\mathbf{K}_\theta & \mathbf{H}_{q\theta}^{\mathrm{F}}\\ \mathbf{H}_{\theta q}^{\mathrm{F}} & \mathbf{H}_{qq}^{\mathrm{F}}\end{bmatrix}\cdot\begin{bmatrix}\mathbf{V}_\theta^{\mathrm{o}}\\ \mathbf{V}_q^{\mathrm{o}}\end{bmatrix}<0 \tag{5.21}$$

is negative-definite. It is worth mentioning that the obtained result is in a good agreement with the previous studies [4], where (for the manipulators without passive joints) the stiffness properties were defined by the matrix $\mathbf{K}_\theta-\mathbf{H}_{\theta\theta}^{\mathrm{F}}$ that evidently must be positive-definite for the stable configurations.

Thus, the proposed stability analysis technique for serial chain with the passive joints and related matrix stability criterion for the kinematic chain configuration allow us to estimate the stability of the serial chain configuration under the external loading in the case of single and multiple equilibriums.

5.4 Stability of The end-platform location under external loading

Similar in the structural mechanics stability of the robot end-platform location is defined by the Cartesian stiffness matrix. However, stiffness matrices of serial and parallel manipulators are computed in a different manner (here, to compute stiffness matrix of parallel manipulator it is required to have stiffness matrices of all its serial chains). Let us address them sequentially.

5.4.1 Cartesian stiffness matrix of a serial kinematic chain

Following the virtual work technique and using static equilibrium equations (5.3), force deflection relations for the considered serial chain can be expressed as

$$\begin{bmatrix} \delta\mathbf{t} \\ \mathbf{0} \\ \mathbf{0} \end{bmatrix} = \begin{bmatrix} \mathbf{0} & \mathbf{J}_{\mathrm{q}}^{(\mathrm{F})} & \mathbf{J}_{\theta}^{(\mathrm{F})} \\ \mathbf{J}_{\mathrm{q}}^{(\mathrm{F})\mathrm{T}} & \mathbf{H}_{\mathrm{qq}} & \mathbf{H}_{\mathrm{q}\theta} \\ \mathbf{J}_{\theta}^{(\mathrm{F})\mathrm{T}} & \mathbf{H}_{\theta\mathrm{q}} & -\mathbf{K}_{\theta}+\mathbf{H}_{\theta\theta} \end{bmatrix} \cdot \begin{bmatrix} \delta\mathbf{F} \\ \delta\mathbf{q} \\ \delta\boldsymbol{\theta} \end{bmatrix} \tag{5.22}$$

where Hessians can be computed as

$$\mathbf{H}_{\mathrm{v}_1\mathrm{v}_2} = \mathbf{H}_{\mathrm{v}_1\mathrm{v}_2}^{(\mathrm{F})} + \mathbf{H}_{\mathrm{v}_1\mathrm{v}_2}^{(\mathrm{G})} + \mathbf{J}_{\mathrm{v}_1}^{(\mathrm{G})\mathrm{T}} \cdot \frac{\partial}{\partial \mathbf{v}_2}\mathbf{G}\,, \tag{5.23}$$

where $(\mathbf{v}_1, \mathbf{v}_2) \in \{(\mathbf{q},\mathbf{q}), (\mathbf{q},\boldsymbol{\theta}), (\boldsymbol{\theta},\mathbf{q}), (\boldsymbol{\theta},\boldsymbol{\theta})\}$ and

$$\mathbf{H}_{\mathrm{v}_1\mathrm{v}_2}^{(\mathrm{G})} = \sum_{j=1}^{n} \frac{\partial^2}{\partial \mathbf{v}_1 \partial \mathbf{v}_2}\left(\mathbf{g}_j^{\mathrm{T}} \cdot \mathbf{G}_j\right); \quad \mathbf{H}_{\mathrm{v}_1\mathrm{v}_2}^{(\mathrm{F})} = \sum_{j=1}^{n} \frac{\partial^2}{\partial \mathbf{v}_1 \partial \mathbf{v}_2}\left(\mathbf{g}^{\mathrm{T}} \cdot \mathbf{F}\right);. \tag{5.24}$$

Hence, the desired stiffness matrices can be computed via the matrix inversion

$$\left[\begin{array}{c|c|c} \mathbf{K}_{\mathrm{C}} & * & * \\ \hline * & * & * \\ \hline * & * & * \end{array}\right] = \begin{bmatrix} \mathbf{0} & \mathbf{J}_{\mathrm{q}}^{(\mathrm{F})} & \mathbf{J}_{\theta}^{(\mathrm{F})} \\ \mathbf{J}_{\mathrm{q}}^{(\mathrm{F})\mathrm{T}} & \mathbf{H}_{\mathrm{qq}} & \mathbf{H}_{\mathrm{q}\theta} \\ \mathbf{J}_{\theta}^{(\mathrm{F})\mathrm{T}} & \mathbf{H}_{\theta\mathrm{q}} & -\mathbf{K}_{\theta}+\mathbf{H}_{\theta\theta} \end{bmatrix}^{-1} \tag{5.25}$$

Further, using several analytical transformations and applying the block matrix inversion technique of Frobenius [42], the Cartesian stiffness matrix can be compute as

$$\mathbf{K}_{\mathrm{C}} = \mathbf{K}_{C}^{0(F)} + \mathbf{K}_{C}^{0(F)} \cdot \mathbf{k}_{\mathrm{q}}^{\mathrm{F}} \cdot \mathbf{K}_{C}^{0(F)} \tag{5.26}$$

where the first term $\mathbf{K}_{C}^{0(F)} = (\mathbf{J}_{\theta} \cdot \mathbf{k}_{\theta}^{\mathrm{F}} \cdot \mathbf{J}_{\theta}^{\mathrm{T}})^{-1}$ exactly corresponds to the classical formula defining stiffness of the kinematic chain without passive joints in the loaded mode, [5], and the second term take into account influence of passive joints via matrix $\mathbf{k}_{\mathrm{q}}^{\mathrm{F}}$

$$\mathbf{k}_{\mathrm{q}}^{\mathrm{F}} = \mathbf{J}_{\mathrm{q}}^{\mathrm{F}} \cdot \left(\mathbf{H}_{\mathrm{qq}} + \mathbf{H}_{\mathrm{q}\theta} \cdot \mathbf{k}_{\theta}^{\mathrm{F}} \cdot \mathbf{H}_{\theta\mathrm{q}} - \mathbf{J}_{\mathrm{q}}^{\mathrm{F}T} \cdot \mathbf{K}_{C}^{0(F)} \cdot \mathbf{J}_{\mathrm{q}}^{\mathrm{F}}\right)^{-1} \cdot \mathbf{J}_{\mathrm{q}}^{\mathrm{F}T} \tag{5.27}$$

here $\mathbf{k}_{\theta}^{\mathrm{F}}$ denotes the modified joint compliance matrix $\mathbf{k}_{\theta}^{\mathrm{F}} = (\mathbf{K}_{\theta} - \mathbf{H}_{\theta\theta})^{-1}$ and matrix $\mathbf{J}_{\mathrm{q}}^{\mathrm{F}}$ denotes the modified Jacobian with respect to passive joints $\mathbf{J}_{\mathrm{q}}^{\mathrm{F}} = \left(\mathbf{J}_{\mathrm{q}} + \mathbf{J}_{\theta} \cdot \mathbf{k}_{\theta}^{\mathrm{F}} \cdot \mathbf{H}_{\theta\mathrm{q}}\right)$.

Thus, the Cartesian stiffness matrix obtained using Eq. (4.28) allows us to analyze the stability of the serial manipulator (or kinematic chain) end-point location under external/internal loadings. If this stiffness matrix is positive definite the end-point location is stable, and if it is rank-deficient (negative definite) it is possible to move end-point location without additional efforts.

5.4.2 Cartesian stiffness matrix of parallel manipulator

Let us assume that a parallel manipulator may be presented as a strictly parallel system of the actuated serial legs connecting the base and the end-platform [45]. Using the methodology described in previous

sections and applying it to each leg, there can be computed a set of *m* Cartesian stiffness matrices $\mathbf{K}_{\mathrm{C}}^{(i)}$ expressed with respect to the same coordinate system but corresponding to different platform points (Figure 5.4). If initially the chain stiffness matrices were computed in local coordinate systems, their transformation is performed in a standard way [46].

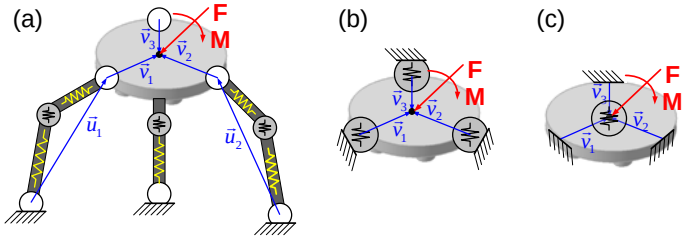

Figure 5.4 Typical parallel manipulator (a) and transformation of its VJM models (b, c)

After such extension, an equivalent stiffness matrix of the leg may be expressed using relevant expression for a usual serial chain, i.e. as $\mathbf{J}_{\mathrm{v}}^{(i)-\mathrm{T}}\cdot\mathbf{K}_{\mathrm{C}}^{(i)}\cdot\mathbf{J}_{\mathrm{v}}^{(i)-1}$, where the Jacobian $\mathbf{J}_{\mathrm{v}}^{(i)}$ defines differential relation between the coordinates of the *i*-th virtual spring and the reference frame of the end-platform. Hence, the final expression for the stiffness matrix of the considered parallel manipulator can be written as

$$\mathbf{K}_{\mathrm{C}}^{(m)} = \sum_{i=1}^{m}\left(\mathbf{J}_{\mathrm{v}}^{(i)^{-\mathrm{T}}}\cdot\mathbf{K}_{\mathrm{C}}^{(i)}\cdot\mathbf{J}_{\mathrm{v}}^{(i)^{-1}}\right) \tag{5.28}$$

where *m* is the number of serial kinematic chains in the manipulator architecture.

As a result, Eq. (5.28) allows us to compute the Cartesian stiffness matrix for the parallel manipulator based on the stiffness matrices for serial chains and transformation Jacobians $\mathbf{J}_{\mathrm{v}}^{(i)}$, which define geometrical mapping between the end-points of serial chains and the reference point frame (the end-effector). Hence, the axes of all virtual springs are parallel to the axes *x*, *y*, *z* of this system. This allows us to evaluate Jacobians $\mathbf{J}_{\mathrm{v}}^{(i)}$ and their inverses from the geometry of end-platform analytically

$$\mathbf{J}_{\mathrm{v}}^{(i)} = \begin{bmatrix}\mathbf{I}_3 & (\mathbf{v}_i\times)\\ \mathbf{0} & \mathbf{I}_3\end{bmatrix}_{6\times6}, \qquad \mathbf{J}_{\mathrm{v}}^{(i)-1} = \begin{bmatrix}\mathbf{I}_3 & -(\mathbf{v}_i\times)\\ \mathbf{0} & \mathbf{I}_3\end{bmatrix}_{6\times6} \tag{5.29}$$

where $\mathbf{I}_3$ is 3×3 identity matrix, and $(\mathbf{v}\times)$ is a skew-symmetric matrix corresponding to the vector $\mathbf{v}$, that defines the end-platform location with respect to the end-point of kinematic chain.

It should be mentioned that the proposed approach is also able to take into account geometry of end-platform and it connection with kinematic chains in an explicit form. Finally, using results of Eq. (5.28) it is possible to analyze the stability of the end-effector location of the parallel manipulator under external loading.

5.5 *Application examples*

5.5.1 Stiffness analysis for serial chain with 1D-springs

Let us illustrate the efficiency of the developed techniques on the example of 3-link kinematic chain with rigid links and two virtual springs between them. It is assumed that both ends of the chain are fixed with rotational passive joints, all link length are equal to l and the stiffness coefficient of both springs are equal to K_θ. The end-point location of considered serial chain can be expressed using geometrical model as

$$\begin{aligned} x &= l\cdot\cos(q)+l\cdot\sin(q+\theta_1)+l\cdot\cos(q+\theta_1+\theta_2) \\ y &= l\cdot\sin(q)+l\cdot\sin(q+\theta_1)+l\cdot\sin(q+\theta_1+\theta_2) \end{aligned} \qquad (5.30)$$

where coordinates x, y define end-point location and angle φ defines its orientation, q and θ_1, θ_2 are passive and virtual joint coordinates respectively that define serial chain configuration. It is assumed that external loading is applied along x-direction only and manipulator end-point can move along x-axis only. So external loading $\mathbf{F}$ can be presented as $\mathbf{F}=\begin{bmatrix} F & 0 \end{bmatrix}^T$ where F is applied external loading along x-axis.

Assuming that the initial values of the actuating coordinates (i.e. before the loading) are denoted as θ_1^0, θ_2^0, the potential energy stored in the virtual springs may be expressed as the following function of the redundant variable

$$E(q)=\frac{1}{2}K_\theta\cdot\left(\theta_1(q)-\theta_1^0\right)^2+\frac{1}{2}K_\theta\cdot\left(\theta_2(q)-\theta_2^0\right)^2 \qquad (5.31)$$

where K_θ is the stiffness coefficient, and θ_1, θ_2 are computed via the inverse kinematics. Using these equations, the desired equilibriums may be computed from the extremum of $E(q)$. In particular, stable equilibriums correspond to minima of this function, and unstable ones correspond to maxima.

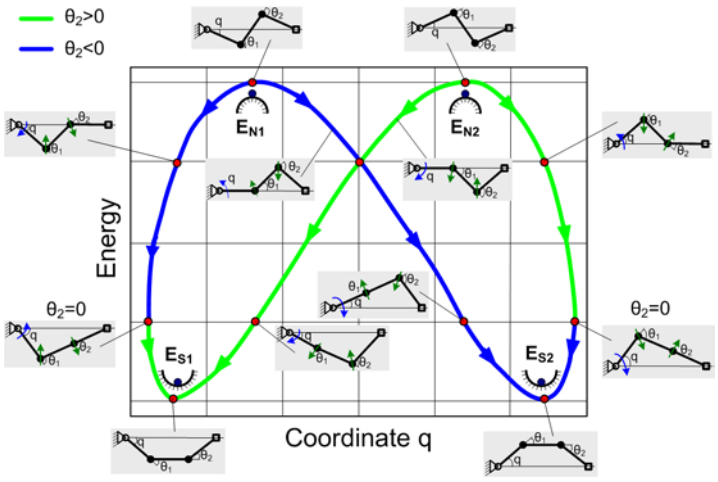

Figure 5.5 Energy diagram for 3-link serial chain

To illustrate this approach, Figure 5.5 presents a case study for the initial S-configuration ($q^0=0^\circ$, $\boldsymbol{\theta}_1^0=0^\circ$ and $\boldsymbol{\theta}_1^0=0^\circ$). It allows comparing 12 different shapes of the deformated chain and selecting the best /worst cases with respect to the energy. As it follows from these results, here there are two symmetrical maximum and two minimum, i.e. two stable and two unstable equilibriums. Besides, the stable equilibriums

correspond to Π-shaped deformated postures, and the unstable ones correspond to Z-shaped postures, as it is shown in Figure 5.6

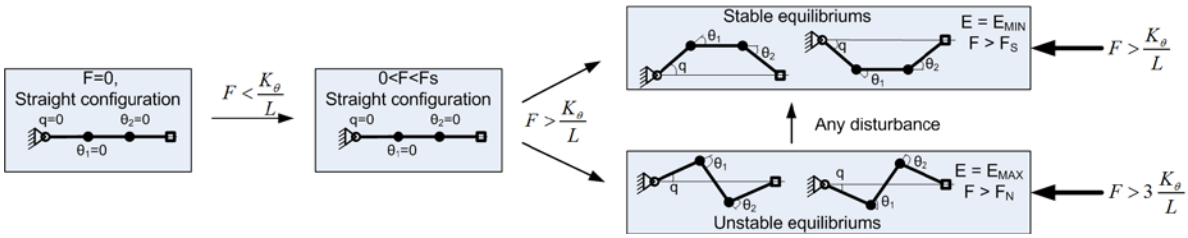

Figure 5.6 Evolution of the S-configuration under loading

If the assumption concerning small values of δ is released, analytical solutions for the non-trivial equilibriums may be still derived. In particular, for the stable equilibrium, one can get

$$F_S(\Delta) = \frac{K_\theta}{L} \cdot \frac{\varphi}{\sin\varphi} \tag{5.32}$$

where $\varphi = \pm\arccos(1-\Delta/2)$. For the unstable equilibrium similar equation may be written as

$$F_N(\Delta) = \frac{K_\theta}{L} \cdot \frac{\cos(q+\theta)+2\cdot\cos q}{\sin\theta} \cdot \theta \tag{5.33}$$

where

$$q = \pm\arccos\left(\frac{12-6\Delta+\Delta^2}{12-4\Delta}\right);\ \theta = \mp\arccos\left(1-\frac{3\Delta}{2}+\frac{\Delta^2}{4}\right) \tag{5.34}$$

Corresponding plots with the bifurcation are presented in Figure 5.7. The interpretation of this plot is similar to the axial compression of a straight column, which is a classical example in the strength of materials. It should be noted, that the developed numerical algorithm exactly produces the curve corresponding to the stable equilibrium.

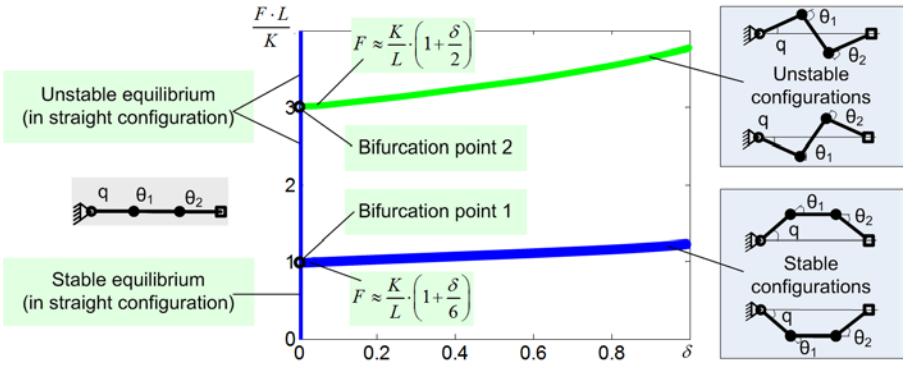

Figure 5.7 Force-deflection relations for S-configuration

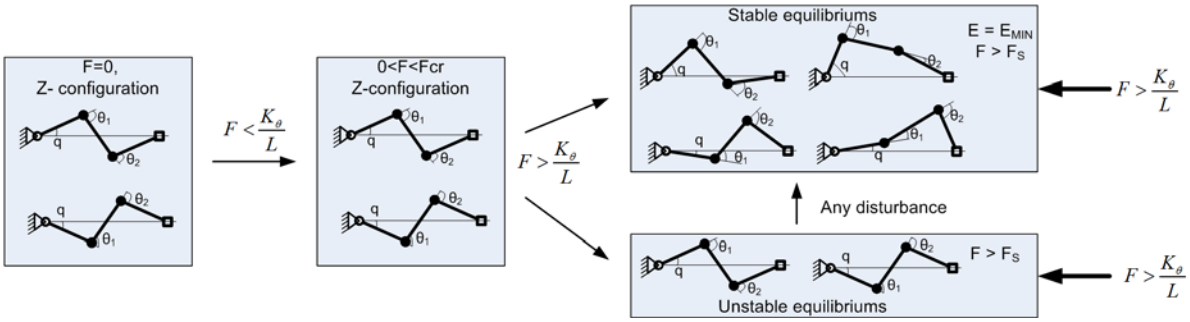

Figure 5.8 Evolution of the Z-configuration under loading

However, for Z-configuration that corresponds to the unloaded zig-zag shape, the stiffness behavior demonstrates the buckling that leads to sudden transformation from a symmetrical to a non-symmetrical posture as shown in Figure 5.8. Here, there exist two stable equilibriums that differ in the values of the potential energy,

In order to analyze stability of different configurations let us define Jacobians and Hessian matrices. For the considered serial chain Jacobinas can be expressed as

$$\mathbf{J}_\theta = l\cdot\begin{bmatrix} -\sin(q+\theta_1)-\sin(q+\theta_1+\theta_2) & -\sin(q+\theta_1+\theta_2) \\ \cos(q+\theta_1)+\cos(q+\theta_1+\theta_2) & \cos(q+\theta_1+\theta_2) \end{bmatrix} \tag{5.35}$$

and

$$\mathbf{J}_q = l\cdot\begin{bmatrix} -\sin(q)-\sin(q+\theta_1)-\sin(q+\theta_1+\theta_2) \\ \cos(q)+\cos(q+\theta_1)+\cos(q+\theta_1+\theta_2) \end{bmatrix} \tag{5.36}$$

and Hessians as

$$\mathbf{H}_{\theta\theta} = -F\cdot l\begin{bmatrix} \cos(q+\theta_1)+\cos(q+\theta_1+\theta_2) & \cos(q+\theta_1+\theta_2) \\ \cos(q+\theta_1+\theta_2) & \cos(q+\theta_1+\theta_2) \end{bmatrix} \tag{5.37}$$

$$\mathbf{H}_{\theta q} = -F\cdot l\cdot\begin{bmatrix} \cos(q+\theta_1)+\cos(q+\theta_1+\theta_2) \\ \cos(q+\theta_1+\theta_2) \end{bmatrix} \tag{5.38}$$

$$\mathbf{H}_{q\theta} = -F\cdot l\cdot\begin{bmatrix} \cos(q+\theta_1)+\cos(q+\theta_1+\theta_2) \\ \cos(q+\theta_1+\theta_2) \end{bmatrix}^T \tag{5.39}$$

$$\mathbf{H}_{qq} = -F\cdot l\cdot\left[\cos(q)+\cos(q+\theta_1)+\cos(q+\theta_1+\theta_2)\right] \tag{5.40}$$

The eigenvectors for the matrix $\mathbf{V}$ that is required in (5.21) can be obtained from the matrix $\mathbf{J}^T\cdot\mathbf{J}$, where $\mathbf{J} = [\mathbf{J}_\theta, \mathbf{J}_q]$, which for the considered serial chain can be computed from

$$\mathbf{J}^T\cdot\mathbf{J} = -F_x^2\cdot l^2\cdot\begin{bmatrix} 3 & 2+\cos(\theta_2) & 2+\cos(\theta_2) \\ 2+\cos(\theta_2) & 2 & 1+\cos(\theta_2) \\ 2+\cos(\theta_2) & 1+\cos(\theta_2) & 1 \end{bmatrix} \tag{5.41}$$

In order to obtain eigenvalues of (5.41), it is required to solve the third order equation

$$\lambda^3 - 6\lambda^2 - \lambda\cdot(6\cos(\theta_2) - 2) - 3\cos^3(\theta_2) - 4\cos^2(\theta_2) + \\ + 2\cos(\theta_2) + 1 = 0 \qquad (5.42)$$

with respect to λ.

Using the above equations, let us investigate stability of 3-link serial chain using the developed matrix criterion in the S- and Z- configurations (these shapes of the chain correspond to the unloaded configurations). For the Z-configuration the unloaded configuration is defined by the angles $q^0 = 9.90^\circ$, $\boldsymbol{\theta}_1^0 = -30^\circ$ and $\boldsymbol{\theta}_1^0 = 30^\circ$ that correspond to the end point location $x = 2.91l$; $y = 0$. Modeling results are presented in Table 5.1. This table includes the external loadings F that are normalized with respect to K_θ / L, the Cartesian stiffnesses K_C that are also normalized with respect to K_θ / L, and the stability of serial chain configuration S_c (as it was mentioned negative value corresponds to stable configuration and positive to unstable configuration) as well as the shapes of the chains. The results have been obtained for the cases of $\Delta = 0$ and $\Delta = 0.2$, here Δ is the normalized the end-point deflection $\Delta = \delta / l$, and δ is the absolute displacement.

Table 5.1 Stability of 3-link serial chain under loading

	S-configuration		Z-configuration	
	stable	unstable	stable	unstable
		$\Delta = 0$		
Shape	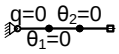	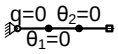	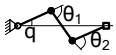	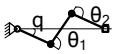
F	0.5	2	0	-3.05
K_C	Inf	Inf	16.93	0.53
S_c	-0.60	0.30	-0.67	1.33
		$\Delta = 0.2$		
Shape	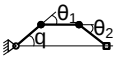	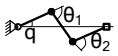	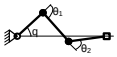	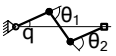
F	-1.03	-3.11	-1.05	-3.03
K_C	0.18	0.57	0.21	0.81
S_c	-0.63	1.34	-0.35	1.26

The results show that for the stable configurations the value of S_c is always negative and for the unstable configurations it is positive. Hence, numerical results that have been obtained using the stability criterion (5.21) are in a good agreement with analytical ones. Moreover, it is shown that for the unstable configuration the stiffness coefficient K_C is positive and, consequently, it cannot be used for the stability analysis of kinematic chain configuration.

5.5.2 Stability of serial chain under auxiliary loading

Let us now focus on the stability analysis of a serial chain under auxiliary loadings applied to an intermediate node. It is assumes that the considered chain consists of two rigid links separated by a flexible joint and two passive joints at both ends. It is assumed that the left passive joint is fixed with a physical constraint, while the right one is balanced by external loading F_x and can be moved along *x* direction (Figure 4.2). Besides, here both rigid links have the same length L and the actuator stiffness is K_θ.

Let us assume that the initial configuration (i.e. for $M_\theta = 0$) of the manipulator corresponds to $\theta_0 = -\pi/6$, where $\theta = -2\cdot\alpha$ is the coordinate of the actuated joint, α is the angle between the first link and x-direction. It is also assumed that the external loading G is applied to the intermediate nod (Figure 4.2) and it is required to apply the external loading (F_x, F_y) at the end-point to compensate the auxiliary loading G. Since this example is quite simple, it is possible to obtain the force-deflection relation and the stiffness coefficient analytically. The force-displacement relation and the stiffness can be expressed in a parametric form as

$$F_x = -\frac{G}{2}\cdot\frac{\cos\alpha}{\sin\alpha} - 2\cdot\frac{K_\theta}{L}\cdot\frac{\alpha-\alpha_0}{\sin\alpha}; \qquad F_y = -\frac{G}{2} \tag{5.43}$$

$$K_x = -\frac{G}{4L}\cdot\frac{1}{\sin^3\alpha} - \frac{K_\theta}{L^2}\cdot\frac{(\alpha-\alpha_0)\cdot\cos\alpha - \sin\alpha}{\sin^3\alpha} \tag{5.44}$$

where $\alpha \in (-\pi/2;\ \pi/2)$ is treated as a parameter, $K_y = 0$.

As it follows from expression (4.32), the stiffness coefficient K_x essentially depends on the auxiliary loading G, coefficient K_x can be both positive and negative or even equal to zero when the auxiliary loading is equal to its critical value $G^* = 4K_\theta / L\cdot\sin\alpha_0$. It is evident that the case $G > G^*$ is very dangerous from practical point of view, since the chain configuration is unstable.

The force-deflection relations and values of translational stiffness K_x are presented in Figure 4.3. They show that the auxiliary loading G significantly reduces the stiffness of the serial chain. Further increasing of the auxiliary loading up to $G = 1.5\cdot G^*$ leads to the unstable configuration with negative stiffness $-7.46\cdot K_\theta / L^2$.

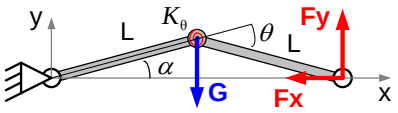

Figure 5.9 Kinematic chain with compliant actuator between two links and its static forces

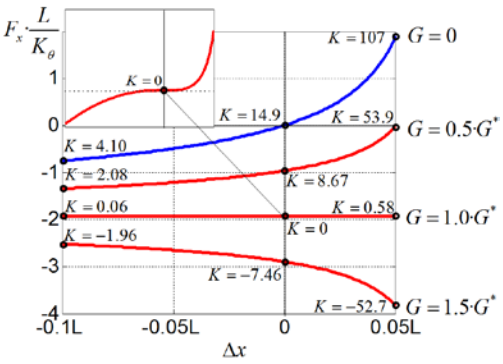

Figure 5.10 Force-deflections relations for different values of auxiliary loading G
($G^* = 4K_\theta / L\cdot\sin\alpha_0$, $K_x = K\cdot K_\theta / L^2$)

Table 5.2 Translational stiffness $K = K_x\cdot L^2 / K_\theta$ and stability coefficients S_c for different values of auxiliary loading G and different displacements Δx ($G^* = 4K_\theta / L\cdot\sin\alpha_0$)

G	Performance measures	$\Delta x = -0.05L$	$\Delta x = 0$	$\Delta x = 0.05L$
0	K	6.69	14.9	107
	S_c	-0.50	-0.66	-1.29
$0.5 \cdot G^*$	K	3.36	8.67	53.9
	S_c	-0.28	-0.35	-0.66
$1.0 \cdot G^*$	K	0.03	0	0.58
	S_c	-0.06	-0.04	-0.03
$1.5 \cdot G^*$	K	–3.31	–7.46	–52.7
	S_c	0.16	0.26	0.60

To investigate the stability of serial chain configuration and the stability of the end-point location additional, analysis have been performed. Simulation results are summarized in Table 5.2 that contains both translational stiffness $K = K_x \cdot L^2 / K_\theta$ and stability coefficients δW for different values of auxiliary loading G and displacements Δx. The results confirm that when auxiliary loading G overcomes it critical value G^* both configuration and the end-point location of serial chain become unstable. Hence, the presented case study demonstrates rather interesting features of stiffness behavior for kinematic chains under auxiliary loading that where not studied before (negative stiffness, non-monotonic force-deflection curves, etc.).

5.5.3 Kinetostatic singularity in the neighborhood of the flat configuration

Let us consider now an example that deals with the stability analysis of Orthoglide manipulator (Figure 5.11a). Detailed specification of this manipulator can be found in [19], some results on the stiffness analysis have been presented in [8][13]. In this case study let us address the stiffness analysis (which includes stability analysis of end-point location under external loading) of Orthoglide manipulator in the neighborhood of a flat configuration. Simulation results for this posture are presented in Figure 5.11b and Table 5.3 where d_0 denotes the initial distance from the flat singularity, K_0 is the translational stiffness for the unloaded mode, $(\Delta_{cr}^+, F_{cr}^+)$ and $(\Delta_{cr}^-, F_{cr}^-)$ are respectively the critical deflection and the critical force for the opposite directions of the displacement. As it follows from these results, in the neighborhood of the flat singularity the stiffness properties are essentially non-symmetrical with respect to the force direction. In particular, for the inside-direction of the loading, the force increases non-linearly but monotonically while the deflection augments. However, for the outside-direction, initially the manipulator reacts to the external loading in the same way: increasing of the deflection leads to increasing of the resisting elastic force. But after achieving the critical value, the reacting force begins decrease, the configuration becomes unstable and the manipulator abruptly changes its posture to the symmetrical ones. After that, the manipulator demonstrates stable behavior with respect to the loading.

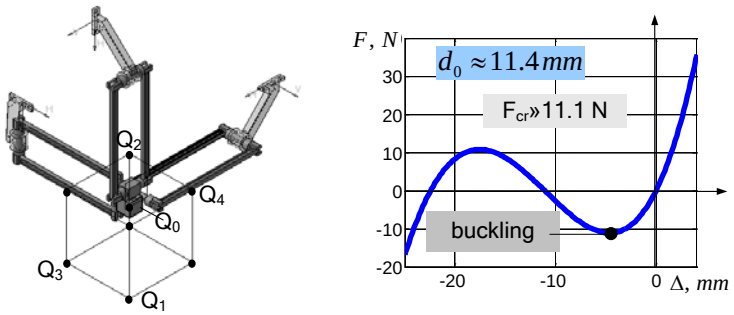

(a) Orthoglide manipulator (b) force-deflection relation

Figure 5.11 Force-displacement relations for Orthoglide manipulators (distance to the singularity is 11.4 mm)

Table 5.3 Summary of stiffness analysis in the neighborhood of the flat singularity

Configuration	d_0, [mm]	F_{cr}^-, [kN]	Δ_{cr}^-, [mm]	F_{cr}^+, [kN]	Δ_{cr}^+, [mm]
Point Q_2	91.7	-2.06	-5.7	2.20	4.9
Point Q_2^a	46.0	-0.70	-17.1	1.45	11
Point Q_2^b	11.4	-0.01	-4.6	0.92	24
Q_2 = (-76.35, -76.35, -76.35); Q_2^a = (-100, -100, -100); Q_2^b = (-120, -120, -120)					

The simplest model that explains the above described phenomenon is presented in Figure 5.12. It is derived via generalization of the "toggle-frame" construction, with relevant modifications motivated by the Orthoglide architecture and relative stiffness properties of its elements. Here, the elasticity is concentrated at the basis of the manipulator legs and it is presented by linear springs with the parameter K_θ. It is assumed that initial distance between the end-point and the singularity-plane is $d_0 = L\sin\varphi_0$, where φ_0 is corresponding angle between the leg and the plane. The derived expressions

$$F = 3K_\theta L_0\left(1-\cos\varphi_0/\cos\varphi\right)\sin\varphi;$$
$$\Delta d = L_0\left(\sin\varphi_0-\sin\varphi\right) \qquad (5.45)$$

perfectly describe the shape of the force-deflection curves obtained from the complete stiffness models.

Besides, more detailed analysis shows extremely fast reduction of the stiffness while approaching this singularity. Corresponding expressions derived for small value of φ_0 yield a linear relation for the critical deflection $\Delta_{cr} \approx 0.42 d_0$ and cubic relation for the critical force $F_{cr} \approx K_\theta / \sqrt{3}L^2 \cdot d_0^3$. Hence, this simplified model is in good agreement with the simulation results and justifies conventional kinematic design objectives (velocity transmission factors, condition number, etc.) that preserve the manipulator from approaching the flat posture.

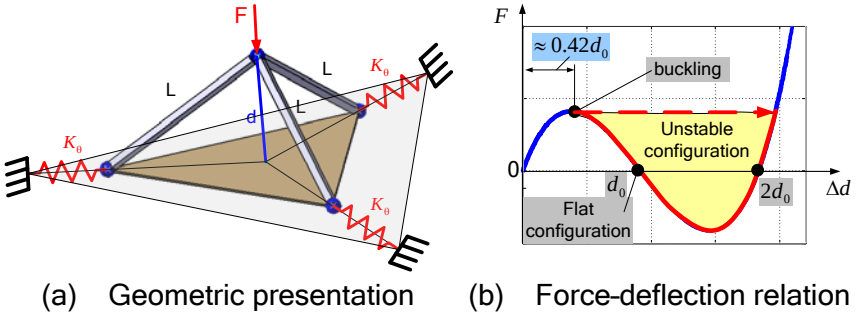

(a) Geometric presentation (b) Force-deflection relation

Figure 5.12 Simplified stiffness model of Orthoglide-type manipulators for near-flat configuration

Hence, the considered example illustrates the ability of proposed technique to obtain the full-scale force-deflection relation for the parallel manipulators that is suitable for the stability analysis of end-point location under the external loading. It proves that the common notion of the "distance-to-singularity" that is used in kinematics must be revised in elastostatics taking into account that loading essentially reduces the margin of the manipulator structural stability.

5.6 Conclusions

The Chapter presents new approach for the stability analysis of parallel manipulators under internal and external loadings applied to different points. In contrast to other works, it is proposed to address both stability of the end-effector location and stability of kinematic chain configuration. This approach is based on the non-linear stiffness analysis that includes computing the static equilibrium configuration corresponding to the given loadings as well as computing the Cartesian stiffness matrices for serial chains and parallel manipulators. The advantages of the proposed approach are illustrated by several examples

5.7 References

[1] Corradini C., Fauroux J.C., Krut S., Company O., 2004, "Evaluation of a 4 degree of freedom parallel manipulator stiffness," Proceedings of the 11th World Cong. in Mechanism & Machine Science (IFTOMM'2004), pp. 1857-1861.

[2] Deblaise, D., Hernot, X., Maurine, P., 2006, "A systematic analytical method for PKM stiffness matrix calculation," Proceedings of ICRA conference, pp. 4213-4219,.

[3] Salisbury, J., 1980, "Active Stiffness Control of a Manipulator in Cartesian Coordinates," 19*th IEEE CDC conference*, pp. 87–97.

[4] Chen, Sh.-F., Kao, I.,, 2002, "Geometrical Approach to The Conservative Congruence Transformation (CCT) for Robotic Stiffness Control," Proceedings of ICRA, pp 544-549.

[5] Alici. G., Shirinzadeh, B., 2005, "Enhanced stiffness modeling, identification and characterization for robot manipulators," Proceedings of IEEE Transactions on Robotics 21(4) 554–564.

[6] Gosselin, C., 1990, "Stiffness mapping for parallel manipulators," IEEE Transactions on Robotics and Automation 6(3) 377–382,.

[7] Dumas, C., Caro, S., Cherif, M., Garnier, S, Fure,t B., 2010, "A Methodology for Joint Stiffness Identification of Serial Robots," Intelligent Robots and Systems (IROS), pp. 464 - 469

[8] Pashkevich A., Chablat D. & Wenger P., 2010. "Stiffness analysis of overconstrained parallel manipulators," Mechanism and Machine Theory, 44 pp. 966-982.

[9] Tyapin, I., Hovland, G., 2009, "Kinematic and elastostatic design optimization of the 3-DOF Gantry-Tau parallel kinamatic manipulator," Modelling, Identification and Control, 30(2) pp. 39-56

[10] Pashkevich, A., Klimchik, A., Chablat, D., 2011, "Enhanced stiffness modeling of manipulators with passive joints", Mechanism and Machine Theory, 46(5), pp. 662-679.

[11] Wei, W., Simaan, N., 2010, "Design of planar parallel robots with preloaded flexures for guaranteed backlash prevention, Journal of Mechanisms and Robotics 2(1) 10 pages.

[12] Yi, B.-J., Freeman, R.A., 1993, "Geometric analysis antagonistic stiffness redundantly actuated parallel mechanism," Journal of Robotic Systems 10(5) pp. 581-603.

[13] Quennouelle, C. & Gosselin, C.M., 2008, "Stiffness Matrix of Compliant Parallel Mechanisms," In Springer Advances in Robot Kinematics: Analysis and Design, pp. 331-341.

[14] Xi, F., Zhang, D., Mechefske, Ch.M., Lang, Sh.Y.T., 2004, "Global kinetostatic modelling of tripod-based parallel kinematic machine," Mechanism and Machine Theory 39 pp. 357–377.

[15] Chakarov, D., 2004, "Study of antagonistic stiffness of parallel manipulators with actuation redundancy," Mechanism and Machine Theory 39, pp. 583–601.

[16] Kövecses, J., Angeles, J., 2007, "The stiffness matrix in elastically articulated rigid-body systems," Multibody System Dynamics pp. 169–184.

[17] Gantmacher, F., 1959, "Theory of matrices," AMS Chelsea

[18] Merlet, J.-P., 2008, "Parallel Robots," *2nd Edition*, Springe.

[19] Angeles, J., 2007, "Fundamentals of Robotic Mechanical Systems: Theory, Methods, and Algorithms," Springer, New York.

[20] Chablat, D., Wenger, P., 2003, "Architecture Optimization of a 3-DOF Parallel Mechanism for Machining Applications, the Orthoglide," IEEE Transactions On Robotics and Automation 19(3) pp. 403-410.

6 STIFFNESS MODELING OF NON-PERFECT PARALLEL MANIPULATORS

6.1 Introduction

IN modern industrial robotics, stiffness becomes one of the most important performance measures that defines potential accuracy of the manipulator. This problem has been in the focus of numerous works [1-5], where different solutions for serial and parallel manipulators have been proposed assuming that the manipulator geometry perfectly corresponds to the nominal one. However in practice, parallel manipulators usually composed of non-perfect serial chains, whose geometrical parameters differ from the nominal values. It is evident that these manufacturing errors may generate essential internal forces and have affect on the manipulator stiffness behavior. However, this problem has attracted very limited attention in robotics.

In general, there exist several stiffness modeling methods, which were analyzed in details in our previous works [6-8]. For the industrial applications, the most popular technique is based on the Virtual Joint Modeling (VJM) approach that was firstly introduced in robotics by Salisbury and Gosselin [10-11] and has been further developed by a number of authors [7-9]. It extends the conventional rigid-body model of the robotic manipulator by adding virtual springs that take into account elastostatic properties of links and joints. In the first works, it was explicitly assumed that the main sources of elasticity are concentrated in actuated joints. Correspondingly, the links were assumed to be rigid and the VJM model included one-dimensional springs only. Recent modifications of this approach describes elastostatic properties of links using 6×6 non-diagonal stiffness matrices [11] that are computed taking into account real shape of complex links [12]. Using this approach it is possible to obtain a rather general non-linear stiffness model for a serial chain [7] and to compute the Cartesian stiffness matrix even for singular configurations.

For parallel robots, the VJM technique can be applied either in a straightforward way (by considering the static equilibrium equations for all chains simultaneously [13-14] or by decomposing the manipulator into a set of separate serial chains, obtaining the stiffness models for all of them and further aggregation of these models in a united one corresponding to the parallel manipulator. It is obvious that the first approach, which incorporates solution of high order non-linear matrix equations [13, 15], is rather tedious to be applied to real life industrial problems. In contrast, the second approach relies on relatively simple techniques that are well developed for serial manipulators. The latter was partially implemented in [6, 16], where the manipulator structure was assumed to be strictly parallel (i.e. without internal loops) and the kinematic chains where assembled in the same end-point. Under this assumption, the stiffness matrix of the parallel manipulator can be computed via simple summation of the chain stiffness matrices. However, in more general (and practically important) cases where the kinematic chains are connected to different points of the end-platform, this technique cannot be applied directly.

Another limitation of existing results in this area is related to the assumption that the assembling does not produce any internal forces/torques. But in practice, numerous errors are accumulated in serial chains [17] and they cause non-negligible internal forces in manipulator joints (even if the external force applied to the end-effector is equal to zero). Furthermore, the kinematic chains of the robotic manipulators may include some additional elastic elements in the actuated or/and passive joints that are intended to increase the robot positioning accuracy or to improve the stiffness properties in certain workspace areas. For example, to eliminate the backlash, the gear trains may include spring-loaded scissor elements that generate the internal

forces, which must be also integrated in the stiffness model [18]. Similar forces may also arise in the parallel manipulators with antagonistic actuating [14]. Other examples include parallel manipulators with springs interposed in the passive joints in order to improve stiffness in the singularity neighborhood.

As follows from relevant studies performed by the authors, the internal forces may essentially influence on the manipulator behavior (modify the stiffness matrix, change the end-effector location, etc.) and should be obviously taken into account in the stiffness model. However, most of existing works ignore this issue.

Thus, this Chapter focus on the stiffness modeling of parallel manipulators with non-perfect serial chains. To address this problem the remainder of the Chapter is organized as follows: Section II proposes stiffness modeling background, Section III deals with aggregation of stiffness models without loading, Section IV extends aggregation technique for the case of loaded mode, Section V illustrates developed technique by the example of Orthoglide manipulator and, finally, Section VI summarizes the main contributions.

6.2 Stiffness modeling background

The stiffness modeling technique developing in this work is based on our previous results [6-7], that deal with perfect manipulators. Let us present them briefly.

For the considered manipulators, if the external loading is equal to zero, all kinematic chains can be aligned and matched in the same target point $\mathbf{t}_0$. In the neighborhood of this point, for each *i*th kinematic chain the desired stiffness model is defined by the non-linear force-deflection relation

$$\mathbf{F}_i = f_i(\mathbf{t} \mid \mathbf{t}_0) \tag{6.1}$$

where $\mathbf{t}$ denotes the end-effector location and $\mathbf{F}_i$ is the corresponding external loading applied to the chain end-point. To obtain the function $f_i(.)$, it can be used the following iterative procedure

$$\begin{bmatrix} \mathbf{F}_i' \\ \mathbf{q}_i' \\ \boldsymbol{\theta}_i' \end{bmatrix} = \begin{bmatrix} \mathbf{0} & \mathbf{J}_{\mathrm{qi}} & \mathbf{J}_{\theta \mathrm{i}} \\ \mathbf{J}_{\mathrm{qi}}^{\mathrm{T}} & \mathbf{0} & \mathbf{0} \\ \mathbf{J}_{\theta \mathrm{i}}^{\mathrm{T}} & \mathbf{0} & -\mathbf{K}_{\theta \mathrm{i}} \end{bmatrix}^{-1} \begin{bmatrix} \mathbf{t} - \mathbf{g}_i + \mathbf{J}_{\mathrm{qi}}\, \mathbf{q}_i + \mathbf{J}_{\theta \mathrm{i}}\, \boldsymbol{\theta}_i \\ \mathbf{0} \\ -\mathbf{K}_{\theta \mathrm{i}}\, \boldsymbol{\theta}_{0\mathrm{i}} \end{bmatrix} \tag{6.2}$$

where the subscript "*i*" denotes the serial chain number, the prime corresponds to the next iteration, $(\mathbf{q}_i, \boldsymbol{\theta}_i)$ defines the chain configuration that depends on the passive and virtual joint coordinates $\mathbf{q}_i$ and $\boldsymbol{\theta}_i$ respectively, $\mathbf{J}_{\mathrm{q}}(\mathbf{q}, \boldsymbol{\theta})$ and $\mathbf{J}_{\theta}(\mathbf{q}, \boldsymbol{\theta})$ are corresponding Jacobian matrices computed for current configuration, $\boldsymbol{\theta}_0$ is preloading in the virtual joints, matrix $\mathbf{K}_{\theta}$ describes the joints stiffness properties, function $\mathbf{t} = \mathbf{g}_i(\mathbf{q}_i, \boldsymbol{\theta}_i)$ defines the chain geometry,

After linearization, for each given $\mathbf{t}$, the Cartesian stiffness matrices $\mathbf{K}_{\mathrm{C}}^{(i)}$ of all kinematic chains can be computed as

$$\mathbf{K}_{\mathrm{C}} = \mathbf{K}_C^{0(F)} - \mathbf{K}_C^{0(F)} \cdot \left(\mathbf{J}_{\mathrm{q}} + \mathbf{J}_{\theta} \cdot \mathbf{k}_{\theta}^{\mathrm{F}} \cdot \mathbf{H}_{\theta \mathrm{q}}^{\mathrm{F}} \right) \cdot \mathbf{K}_{\mathrm{Cq}} \tag{6.3}$$

where the first term $\mathbf{K}_C^{0(F)} = (\mathbf{J}_{\theta}\, \mathbf{k}_{\theta}^{\mathrm{F}}\, \mathbf{J}_{\theta}^{\mathrm{T}})^{-1}$ corresponds to the classical formula defining stiffness of the kinematic chain without passive joints in the loaded mode [19] and the second term takes into account influence of the passive joints. Besides, the stiffness matrix $\mathbf{K}_{\mathrm{Cq}}$ (defining a linear mapping of the end-point displacement $\delta\mathbf{t}$ to the deflections in the passive joints $\delta\mathbf{q}$) can be computed as

$$\mathbf{K}_{Cq} = -\left(\mathbf{H}_{qq}^{F} + \mathbf{H}_{q\theta}^{F}\,\mathbf{k}_{\theta}^{F}\,\mathbf{H}_{\theta q}^{F} - \left(\mathbf{J}_{q}^{T} + \mathbf{H}_{q\theta}^{F}\,\mathbf{k}_{\theta}^{F}\,\mathbf{J}_{\theta}^{T}\right)\mathbf{K}_{C}^{0(F)}\left(\mathbf{J}_{q} + \mathbf{J}_{\theta}\,\mathbf{k}_{\theta}^{F}\,\mathbf{H}_{\theta q}^{F}\right)\right)^{-1}\left(\mathbf{J}_{q}^{T} + \mathbf{H}_{q\theta}^{F}\,\mathbf{k}_{\theta}^{F}\,\mathbf{J}_{\theta}^{T}\right)\mathbf{K}_{C}^{0(F)} \tag{6.4}$$

Here $\mathbf{k}_{\theta}^{F} = (\mathbf{K}_{\theta} - \mathbf{H}_{\theta\theta}^{F})^{-1}$ and $\mathbf{H}_{v_1 v_2}^{F} = \partial^2\left(\mathbf{g}^{T}\,\mathbf{F}\right)/\partial\mathbf{v}_1\partial\mathbf{v}_2$ are the Hessian matrices with respect to combination of the passive and virtual joint coordinates $(\mathbf{q},\mathbf{q})$, $(\mathbf{q},\boldsymbol{\theta})$, $(\boldsymbol{\theta},\mathbf{q})$, $(\boldsymbol{\theta},\boldsymbol{\theta})$.

In addition, linearization provides the matrix $\mathbf{K}_{C\theta}$ that defines linear mappings of the end-point displacement $\delta\mathbf{t}$ to the virtual joint coordinates $\delta\boldsymbol{\theta}$

$$\mathbf{K}_{C\theta} = \mathbf{k}_{\theta}^{F}\,\mathbf{J}_{\theta}^{T}\,\mathbf{K}_{C} + \mathbf{k}_{\theta}^{F}\,\mathbf{H}_{\theta q}^{F}\,\mathbf{K}_{Cq} \tag{6.5}$$

that is computed using the same intermediate variables

This approach allows us to obtain the non-linear force-deflection relation for each serial chain as well as to compute the Cartesian stiffness matrices for any given target point $\mathbf{t}_0$ and given the end-point location $\mathbf{t}$. However, it cannot be applied directly for parallel manipulators with non-perfect serial chains because it is implicitly assumed here that assembling in the point $\mathbf{t}_0$ does not require any forces applied to the chain end-point, i.e. $f_i(\mathbf{t}_0 \mid \mathbf{t}_0) = \mathbf{0}$. Thus a dedicated technique, which is considered in this Chapter, is required.

6.3 Stiffness models aggregation for small loading

In this section it is assumed that the external loading applied to the mobile platform of the parallel manipulator is small enough and a linearization-based approach is reasonable. It proposes the stiffness model aggregation technique for both perfect and non-perfect serial chains.

6.3.1 Stiffness model aggregation for perfect chains

In this case, it is assumed that all the chains can be assembled in the target point $\mathbf{t}_0$ without any external loading that may be expressed as $f_i(\mathbf{t}_0 \mid \mathbf{t}_0) = \mathbf{0}$. So, for the parallel manipulator, the desired force-deflection relation can be written as

$$\mathbf{F} = \mathbf{K}_{C}\cdot(\mathbf{t} - \mathbf{t}_0) \tag{6.6}$$

where the total Cartesian stiffness matrix $\mathbf{K}_{C}$ is computed using the chain aggregation formula

$$\mathbf{K}_{C} = \sum_{i=1}^{m} \mathbf{J}_{v}^{(i)^{-T}}\,\mathbf{K}_{C}^{(i)}\,\mathbf{J}_{v}^{(i)^{-1}} \tag{6.7}$$

which integrates the Cartesian stiffness matrices $\mathbf{K}_{C}^{(i)}$ of all *m* chains taking into account the difference between the reference point of the end-platform and the end-points of the chains (where the chains are connected to the mobile platform, Figure 6.1). The latter is expressed via the Jacobians $\mathbf{J}_{v}^{(i)}$ that are described in details in [8].

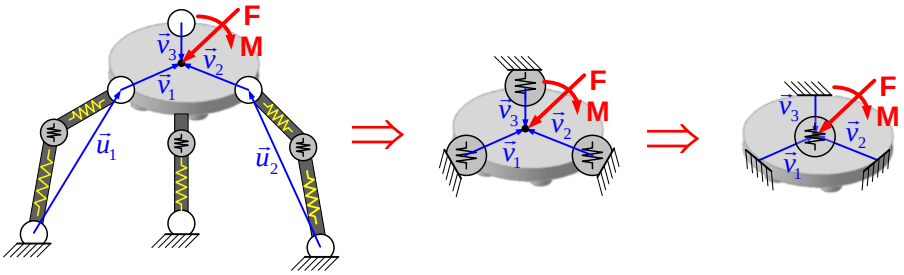

Figure 6.1 Transformation of VJM models of typical parallel manipulator

Further, linear relations between the end-platform displacement $\mathbf{t}-\mathbf{t}_0$ and variations $\delta\mathbf{q}_i, \delta\boldsymbol{\theta}_i$ in the joint coordinates of the chains may be presented as

$$\delta\mathbf{q}_i = \mathbf{K}_{\mathrm{Cq}}^{(i)} \cdot \mathbf{J}_v^{(i)^{-1}} \cdot (\mathbf{t}-\mathbf{t}_0); \qquad \delta\boldsymbol{\theta}_i = \mathbf{K}_{\mathrm{C}\theta}^{(i)} \cdot \mathbf{J}_v^{(i)^{-1}} \cdot (\mathbf{t}-\mathbf{t}_0) \tag{6.8}$$

where, the joint sensitivity matrices $\mathbf{K}_{\mathrm{Cq}}^{(i)}, \mathbf{K}_{\mathrm{C}\theta}^{(i)}$ are computed from (6.4) and (4.30) assuming that $\mathbf{F}=\mathbf{0}$ and by neglecting all Hessians (here, the matrices $\mathbf{K}_{\mathrm{Cq}}^{(i)}, \mathbf{K}_{\mathrm{C}\theta}^{(i)}$ are expressed with respect to the chain end-points).

6.3.2 Stiffness model aggregation for non-perfect chains

If the kinematic chains are non-perfect, the corresponding force-deflection relation (6.1) is shifted with respect to the point $\mathbf{t}_0$, i.e. $f_i(\mathbf{t}_0 \mid \mathbf{t}_0) \neq \mathbf{0}$. So, the manipulator assembling in this point requires application of some non-zero forces $\mathbf{F}_i$ that generally do not compensate each other. Correspondingly, the end-platform location differs from $\mathbf{t}_0$ if the external force applied to the end-platform is equal to zero. Let us denote this difference as $\Delta\mathbf{t}$ and revise the above matrix equations (6.6)-(6.8) assuming that, without the external loading, the chain end-point is shifted by $\boldsymbol{\varepsilon}_i$ with respect to $\mathbf{t}_0$ (it can be also expressed as $f_i(\mathbf{t}_0+\boldsymbol{\varepsilon}_i \mid \mathbf{t}_0)=\mathbf{0}$).

Using these notations, the desired stiffness model can be described by the following expressions

$$\mathbf{F} = \mathbf{K}_{\mathrm{C}} \cdot (\mathbf{t}-\mathbf{t}_0+\Delta\mathbf{t}) \tag{6.9}$$

and

$$\begin{aligned} \delta\mathbf{q}_i &= \mathbf{K}_{\mathrm{Cq}}^{(i)} \cdot \mathbf{J}_v^{(i)^{-1}} \cdot (\mathbf{t}-\mathbf{t}_0+\Delta\mathbf{t}_i); \\ \delta\boldsymbol{\theta}_i &= \mathbf{K}_{\mathrm{C}\theta}^{(i)} \cdot \mathbf{J}_v^{(i)^{-1}} \cdot (\mathbf{t}-\mathbf{t}_0+\Delta\mathbf{t}_i) \end{aligned} \tag{6.10}$$

where the vectors $\Delta\mathbf{t}$, $\Delta\mathbf{t}_i$ should be computed using the assumptions presented above. To find these additional parameters of the stiffness model, let us apply the energy based approach.

To compute the end-platform deflection $\Delta\mathbf{t}$, let us assume that the geometrical errors are small enough. So, the stiffness matrices of the serial chains $\mathbf{K}_{\mathrm{C}}^{(i)}$ are the same at the points O, B_i' and O'' (Figure 6.2) and computed for the nominal configurations $\mathbf{q}_i, \boldsymbol{\theta}_i$ using the above presented technique. This allows us to apply the energy based approach and to express the potential energy of the parallel manipulator with geometrical errors in kinematic chains as

$$E = \frac{1}{2}\sum_{i=1}^{m}\left((\boldsymbol{\varepsilon}_i-\Delta\mathbf{t})^{\mathrm{T}} \cdot \mathbf{K}_{\mathrm{C}}^{(i)} \cdot (\boldsymbol{\varepsilon}_i-\Delta\mathbf{t})\right) \tag{6.11}$$

where $\Delta\mathbf{t} = (\Delta\mathbf{p}, \Delta\boldsymbol{\varphi})$ is displacement (position and orientation) of the reference point.

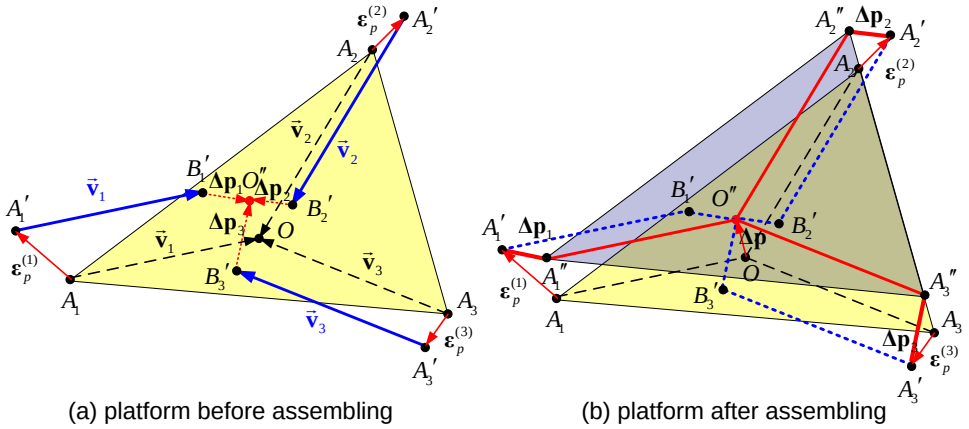

Figure 6.2 Transformation of characteristic points of serial chains in assembling of non-perfect parallel manipulator; (A_i, A_i' - end-point locations of serial chain before assembling for perfect and non-perfect manipulators respectively, A_i'' - end-point location of serial chain after assembling for non-perfect manipulator)

To compute the end-platform deflection $\Delta\mathbf{t}$, let us assume that the geometrical errors are small enough. So, the stiffness matrices of the serial chains $\mathbf{K}_{\mathrm{C}}^{(i)}$ are the same at the points O, B_i' and O'' (Figure 6.2) and computed for the nominal configurations $\mathbf{q}_i, \boldsymbol{\theta}_i$ using the above presented technique. This allows us to apply the energy based approach and to express the potential energy of the parallel manipulator with geometrical errors in kinematic chains as

$$E = \frac{1}{2}\sum_{i=1}^{m}\left(\left(\boldsymbol{\varepsilon}_i - \Delta\mathbf{t}\right)^{\mathrm{T}} \cdot \mathbf{K}_{\mathrm{C}}^{(i)} \cdot \left(\boldsymbol{\varepsilon}_i - \Delta\mathbf{t}\right)\right) \tag{6.12}$$

where $\Delta\mathbf{t} = (\Delta\mathbf{p}, \Delta\boldsymbol{\varphi})$ is displacement (position and orientation) of the reference point.

It is obvious that after assembling, the considered mechanical system will occupy the most advantageous configuration with respect to the potential energy, i.e. $E \to \min_{\Delta\mathbf{t}}$. It means that the desired vector $\Delta\mathbf{t}$ can be found from the expression

$$\frac{\partial E}{\partial \Delta\mathbf{t}} = \sum_{i=1}^{m}\left(\mathbf{K}_{\mathrm{C}}^{(i)} \cdot \left(\Delta\mathbf{t} - \boldsymbol{\varepsilon}_i\right)\right) = 0 \tag{6.13}$$

that yields the following linear equation

$$\sum_{i=1}^{m}\mathbf{K}_{\mathrm{C}}^{(i)} \cdot \Delta\mathbf{t} = \sum_{i=1}^{m}\left(\mathbf{K}_{\mathrm{C}}^{(i)} \cdot \boldsymbol{\varepsilon}_i\right) \tag{6.14}$$

which allows us to evaluate the end-platform deflection

$$\Delta\mathbf{t} = \left(\sum_{i=1}^{m}\mathbf{K}_{\mathrm{C}}^{(i)}\right)^{-1} \cdot \sum_{i=1}^{m}\left(\mathbf{K}_{\mathrm{C}}^{(i)} \cdot \boldsymbol{\varepsilon}_i\right) \tag{6.15}$$

and the end-platform location after assembling

$$\mathbf{t}' = \mathbf{t}^0 + \Delta\mathbf{t} \tag{6.16}$$

For each separate kinematic chain, the end-frame deflections due to assembling can be expressed as

$$\Delta\mathbf{t}_i = \Delta\mathbf{t} - \boldsymbol{\varepsilon}_i = \left(\sum_{i=1}^{m}\mathbf{K}_{\mathrm{C}}^{(i)}\right)^{-1}\cdot\sum_{i=1}^{m}\left(\mathbf{K}_{\mathrm{C}}^{(i)}\cdot\boldsymbol{\varepsilon}_i\right) - \boldsymbol{\varepsilon}_i \tag{6.17}$$

This allows us to compute the loading for each kinematic chain applied to the end-point (due to interaction with other non-perfect chains)

$$\mathbf{F}_i = \mathbf{K}_{\mathrm{C}}^{(i)}\cdot\Delta\mathbf{t}_i \tag{6.18}$$

and corresponding loadings in the virtual joints $\boldsymbol{\tau}_\theta^{(i)}$

$$\boldsymbol{\tau}_\theta^{(i)} = \mathbf{J}_\theta^{(i)\mathrm{T}}\cdot\mathbf{F}_i = \mathbf{J}_\theta^{(i)\mathrm{T}}\cdot\mathbf{K}_{\mathrm{C}}^{(i)}\cdot\Delta\mathbf{t}_i \tag{6.19}$$

It is worth mentioning that here $\sum_{i=1}^{m}\mathbf{F}_i = \mathbf{0}$, since there is no external loading applied to the platform reference point after the assembling. Besides, it is possible to compute relevant deflections of the virtual and passive joint coordinates of the chains

$$\boldsymbol{\theta}_i = \mathbf{K}_{\mathrm{C}\theta}^{(i)}\cdot\Delta\mathbf{t}_i; \qquad \Delta\mathbf{q}_i = \mathbf{K}_{\mathrm{Cq}}^{(i)}\cdot\Delta\mathbf{t}_i \tag{6.20}$$

caused by the assembling.

Thus, the above expressions allow us to evaluate the end-platform deflection and internal forces/torques caused by assembling of kinematic chains with geometrical errors. However, the total manipulator Cartesian stiffness matrix $\mathbf{K}_{\mathrm{C}}$ is assumed to be the same as in Section III.A, since the geometrical errors are assumed to be small enough.

6.4 Stiffness models aggregation for high loading

In this section it is assumed that the external loading can be high enough to cause non-linear effect in the manipulator stiffness behavior. It proposes numerical algorithms for computing both direct and inverse force-deflection relations that are referred below to as non-linear stiffness and compliance models respectively.

6.4.1 Stiffness model of parallel manipulator

Let us focus on the aggregation of stiffness models of separate serial chains into the stiffness model of the whole parallel manipulator in the loaded mode. To solve this problem, it is necessary to obtain the non-linear force-deflection relation, which takes into account elastostatic properties of all kinematic chains, and to compute corresponding Cartesian stiffness matrix.

Let us assume that the end-points of all kinematic chains are aligned and matched in the same target point $\mathbf{t}_0$, which corresponds to the desired end-platform location. This point is assumed to be known and allows us to compute, from the inverse kinematic model, the actuator and passive joint coordinates defining nominal configurations of the chains $(\mathbf{q}_{0i}, \boldsymbol{\theta}_{0i})$. It is also assumed that the stiffness models of all kinematic

chains have been already obtained using techniques proposed in Sections II and are presented in the form of partial non-linear force-deflection relations $\mathbf{F}_i = f_i(\mathbf{t} \mid \mathbf{t}_0)$ corresponding to the target point $\mathbf{t}_0$.

It is evident that the external loading $\mathbf{F}$ changes the end-platform location $\mathbf{t}_0$, hence it is reasonable to consider the set of locations $\mathbf{t}$ in the neighborhood of target one. Under the above assumptions, for any given point $\mathbf{t}$ from neighborhood of $\mathbf{t}_0$ it is possible to compute both the partial forces $\mathbf{F}_i$ and corresponding equilibrium configurations $(\mathbf{q}_i, \boldsymbol{\theta}_i)$. Then, in accordance with the superposition principle, the desired non-linear force-deflection relation for the whole parallel manipulator can be found by straightforward summation of all partial forces $\mathbf{F}_i$, i.e.

$$\mathbf{F} = \sum_{i=1}^{m} f_i(\mathbf{t} \mid \mathbf{t}_0) \tag{6.21}$$

where $\mathbf{F}$ denotes the total external loading applied to the end-platform. Corresponding curves can be obtained by multiple repetition of the above described procedures for different values of the end-platform location $\mathbf{t}$.

Furthermore, for each given $\mathbf{t}$, the stiffness matrices $\mathbf{K}_{\mathrm{C}}^{(i)}$ of all kinematic chains can be computed using expression (4.28) This allows us to compute the Cartesian stiffness matrix $\mathbf{K}_{\mathrm{C}}$ of the whole parallel manipulator as a sum

$$\mathbf{K}_{\mathrm{C}} = \sum_{i=1}^{m} \mathbf{K}_{\mathrm{C}}^{(i)} \tag{6.22}$$

However, the matrices $\mathbf{K}_{\mathrm{Cq}}^{(i)}$ and $\mathbf{K}_{\mathrm{C}\theta}^{(i)}$ defining the "sensitivity" of the chain joint coordinates $(\mathbf{q}_i, \boldsymbol{\theta}_i)$ to the end-platform displacement cannot be aggregated in this way, they should be used separately to evaluate stresses in joints/links and resistance of the chain configurations with respect to external loading $\mathbf{F}$

$$\begin{aligned} &\boldsymbol{\tau}_{\theta}^{(i)} = \mathbf{J}_{\theta}^{(i)\mathrm{T}} \cdot \mathbf{K}_{\mathrm{C}}^{(i)} \cdot (\mathbf{t} - \mathbf{t}_0); \\ &\delta\mathbf{q}_i = \mathbf{K}_{\mathrm{Cq}}^{(i)} \cdot (\mathbf{t} - \mathbf{t}_0); \; \delta\boldsymbol{\theta}_i = \mathbf{K}_{\mathrm{C}\theta}^{(i)} \cdot (\mathbf{t} - \mathbf{t}_0) \end{aligned} \tag{6.23}$$

where $\mathbf{J}_{\theta}^{(i)}$ is Jacobian matrix of *i*-th kinematic chain with respect to virtual joint coordinates.

It is worth mentioning that above it was implicitly assumed that the manipulator assembling is equivalent to the aligning and matching of the chain end-frames. To deal with more general case, when the chains are connected to the different points of the platform, it is necessary to slightly modify the chain geometrical models and to re-compute the forces/torques and the stiffness matrices by adding a virtual rigid link connecting the end-point of the chain and the reference point of the platform. After the relevant transformations that are described before, the above presented technique can be applied straightforwardly.

Besides, in contrast to Section III, here there are no evident differences in stiffness models aggregation of perfect and non-perfect kinematic chains. However, here the chain geometrical errors are implicitly included in the functions $\mathbf{g}_i^{\varepsilon}(\mathbf{q}_i, \boldsymbol{\theta}_i)$. In particular for non-perfect chains, it is assumed that the nominal values of the joint coordinates $(\mathbf{q}_{0i}, \boldsymbol{\theta}_{0i})$ produce the end-point location vector which differs from $\mathbf{t}_0$:

$$\mathbf{g}_i^{\varepsilon}(\mathbf{q}_{0i}, \boldsymbol{\theta}_{0i}) = \mathbf{t}_0 + \boldsymbol{\varepsilon}_i \tag{6.24}$$

where $\boldsymbol{\varepsilon}_i$ accumulates influences of all geometrical errors on the end-point location of *i*-th chain. As a result, the end-platform cannot be located in the target point $\mathbf{t}_0$ without external loading, i.e.

$$\sum_{i=1}^{m} f_i(\mathbf{t}\,|\,\mathbf{t}_0)\Big|_{\mathbf{t}=\mathbf{t}_0} \neq \mathbf{0} \tag{6.25}$$

Moreover, without external loading, the end-platform location $\mathbf{t}_\varepsilon$ is different from the target one $\mathbf{t}_0$. The vector $\mathbf{t}_\varepsilon$ can be computed from the equation

$$\sum_{i=1}^{m} f_i(\mathbf{t}_\varepsilon\,|\,\mathbf{t}_0) = \mathbf{0} \tag{6.26}$$

which will be considered in Section IV.B. Corresponding internal forces $\mathbf{F}_i^\varepsilon$ defining the chain loadings due to the geometrical errors in the chains can be computed by simple substitution $\mathbf{t}_\varepsilon$ to the partial force deflection relations

$$\mathbf{F}_i^\varepsilon = f_i(\mathbf{t}\,|\,\mathbf{t}_0)\Big|_{\mathbf{t}=\mathbf{t}_\varepsilon} \tag{6.27}$$

It is obvious that the sum of the $\mathbf{F}_i^\varepsilon$ is equal to zero but they produce stresses in the links and joints if the parallel manipulator is over-constrained.

Hence, the developed aggregation technique allows us to obtain the non-linear force-deflection relation for a parallel manipulator in the loaded mode as well as to compute Cartesian stiffness matrices for any given target point $\mathbf{t}_0$ and given set of the end-point locations $\{\mathbf{t}\}$. This technique is summarized in Figure 6.3.

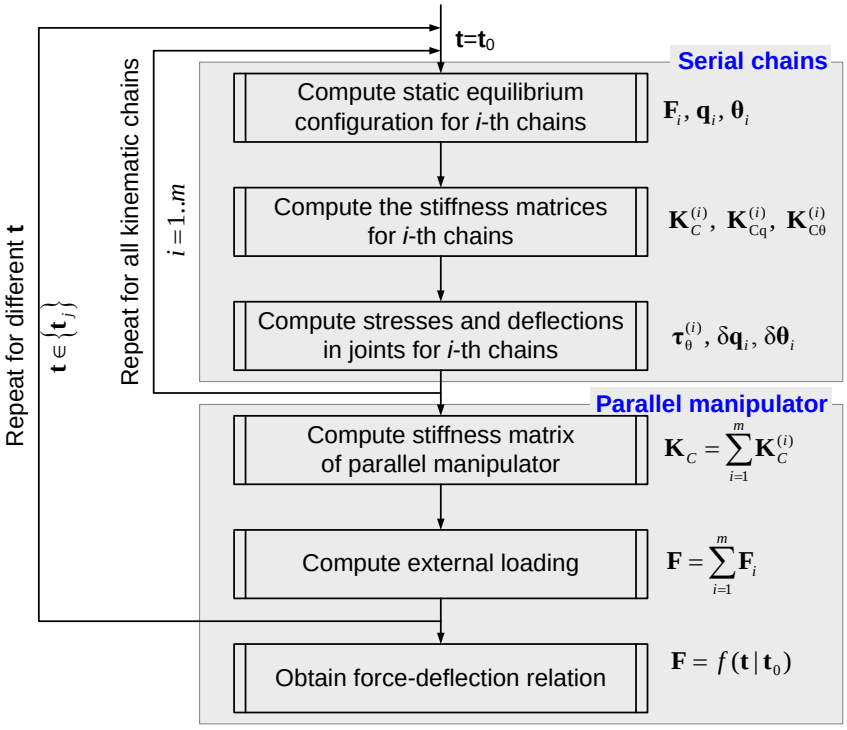

Figure 6.3 Aggregation of serial chains stiffness models technique

6.4.2 Compliance model of parallel manipulator

The non-linear force-deflection relation (6.21) allows us to evaluate the external force/torque $\mathbf{F}$ required to locate the manipulator in the target point $\mathbf{t}$ (assuming that the actuated coordinates are computed for the end-platform location $\mathbf{t}_0$ corresponding to the unloaded configuration). However in practice, it is often necessary to determine the end platform resistance to the external loading, i.e. to compute the deflection caused by the force $\mathbf{F}$ applied to the end-platform. The desired value can be found from the non-linear compliance model that in general case is expressed as

$$\mathbf{t} = f^{-1}(\mathbf{F} \,|\, \mathbf{t}_0) \tag{6.28}$$

and is defined by the inverse $f^{-1}(...)$ which for parallel manipulators usually exists (due to over-constrained structure). In contrast, for serial chains with passive joints, the function $f^{-1}(...)$ cannot be computed since the corresponding Cartesian stiffness matrix $\mathbf{K}_{\mathrm{C}}^{(i)}$ is singular.

It is obvious that in a general case, the function $f^{-1}(...)$ cannot be expressed analytically. Hence, it is required that a dedicated iterative procedure, which is able to solve the non-linear equation (6.28) for $\mathbf{t}$ (assuming that $\mathbf{F}$ is given). It is proposed here to apply a modification of Newton-Raphson technique which iteratively updates the desired value $\mathbf{t}$ in accordance with the expression

$$\mathbf{t}' = \mathbf{t} + \mathbf{K}_{\mathrm{C}}^{-1}(\mathbf{t} \,|\, \mathbf{t}_0) \cdot \left(\mathbf{F} - f(\mathbf{t} \,|\, \mathbf{t}_0)\right) \tag{6.29}$$

where $\mathbf{t}'$ corresponds to the next iteration, $\mathbf{K}_{\mathrm{C}}(\mathbf{t} \,|\, \mathbf{t}_0)$ is the Cartesian stiffness matrix computed in the point $\mathbf{t}$, and $\mathbf{t}_0$ denotes the unloaded location of the end-platform. For this iterative scheme, $\mathbf{t}_0$ can be also used as the initial value of $\mathbf{t}$. Similar to Section IV.A, within each iterative loop, corresponding configurations $(\mathbf{q}_i, \boldsymbol{\theta}_i)$, the loadings $\mathbf{F}_i$ and stiffness matrices $\mathbf{K}_{\mathrm{C}}^{(i)}$ for each kinematic chain are computed using equations (6.2), and (4.28) respectively,

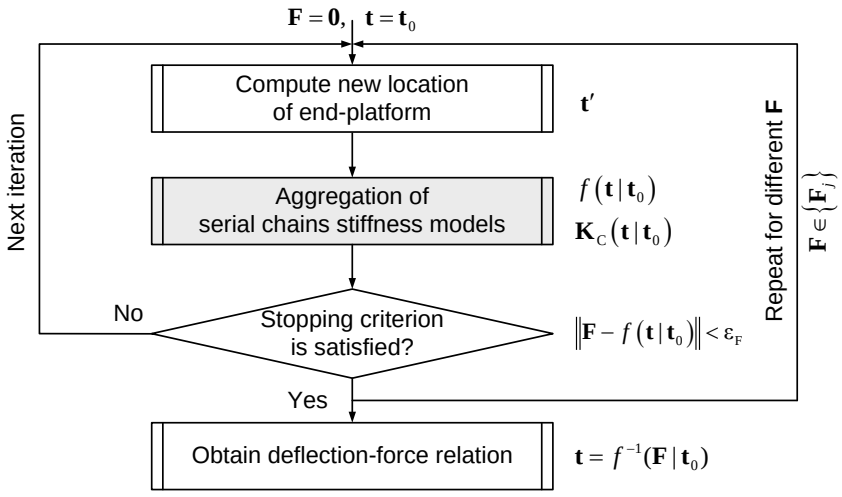

Figure 6.4 Procedure for obtaining deflection-force relation for loaded parallel manipulator

As it follows from the relevant study, convergence of this iterative procedure is good enough if the function $f(...)$ is smooth and non-singular in the neighborhood of $\mathbf{t}_0$. If it is required to improve convergence, it is possible to modify force $\mathbf{F}$ from iteration to iteration in accordance with the expression $\mathbf{F}' = \alpha \cdot \mathbf{F}$, where a

scalar variable α is monotonically increasing from 0 up to 1. The stopping criterion can be expressed in a straightforward way as

$$\left\| \mathbf{F} - f\left(\mathbf{t} \mid \mathbf{t}_0\right) \right\| < \varepsilon_F \tag{6.30}$$

where ε_F is the desired accuracy. More details presentation of the developed iterative routines is given in Figure 6.4 .

6.5 Application examples

6.5.1 Aggregation non-perfect serial chains without loading

Let us illustrate the developed stiffness model aggregation technique by examples that deal with assembling of Orthoglide parallel translational manipulator with geometrical errors in kinematic chains (Fig. 6.5) [20]. Let us assume that the manipulators have geometrical errors in the kinematic chains, which have effects on the end-point location and provoke internal loadings in the joints.

Taking into account the shape of the dexterous workspace, let us focus on the stiffness analysis of these manipulators in five characteristic points: isotropic point Q_0, two limit points Q_1 and Q_2. with symmetrical configuration and two limit points Q_3 and Q_4. with non-symmetrical configuration [5-7]. Let us estimate the end-effector location and internal deflections/loadings caused by the geometrical errors in the chains. The stiffness matrices of the chains in the points Q_0...Q_4 have been computed using the technique proposed in Section 6.3.1.

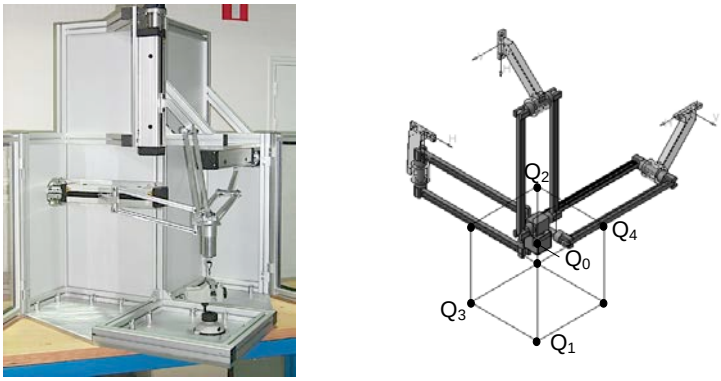

(a) Photo (b) CAD-model

Figure 6.5 CAD models of 3-PUU and Orthoglide manipulators

For illustration purposes, let us investigate two types of geometrical errors

Case A: Each actuator of the manipulator has a *position error* 1 mm in actuator location;

Case B: Each actuator of the manipulator has an *angular error* 1° in actuator location.

In case A, as it follows from the chains geometry, the deflections of the chain end-points before assembling $\boldsymbol{\varepsilon}_i = \boldsymbol{\varepsilon}_i^0$. In case B, the values $\boldsymbol{\varepsilon}_i$ should be computed using the geometrical model $\mathbf{g}_i(\mathbf{q}_i, \boldsymbol{\theta}_i)$:

Table 6.1 Assembling of Orthoglide manipulator with non-perfect chains: loadings and displacements for the Case A ($\Delta\mathbf{t}=[\delta_1,\,\delta_2,\,\delta_3,\,0,\,0,\,0]^T$, $\mathbf{F}_1=\mathbf{0}$, $\mathbf{F}_2=\mathbf{0}$, $\mathbf{F}_3=\mathbf{0}$)

Point	Displacement of end-point $\Delta\mathbf{t}$	Deflections and loadings in joints and links
Q_0	$\delta_1=\delta_2=\delta_3=1\,\text{mm};$	$\Delta q^{\max}=0.18^\circ$
Q_1	$\delta_1=\delta_2=\delta_3=0.50\,\text{mm}$	$\Delta q^{\max}=0.14^\circ$
Q_2	$\delta_1=\delta_2=\delta_3=2.02\,\text{mm};$	$\Delta q^{\max}=0.42^\circ$
Q_3	$\delta_1=\delta_2=0.73\,\text{mm};$ $\delta_3=0.27\,\text{mm}$	$\Delta q^{\max}=0.20^\circ$
Q_4	$\delta_1=\delta_2=0.56\,\text{mm};$ $\delta_3=1.28\,\text{mm}$	$\Delta q^{\max}=0.26^\circ$
$\theta_{\text{p}}^{\max}=0;\quad \theta_{\varphi}^{\max}=0;\quad \tau_{\text{p}}^{\max}=0;\quad \tau_{\varphi}^{\max}=0$		

Table 6.2 Assembling of Orthoglide manipulator with non-perfect chains: loadings and displacements for the case B ($\Delta\mathbf{t}=[\delta_1,\,\delta_2,\,\delta_3,\,\varphi_1,\,\varphi_2,\,\varphi_3]^T$, $\mathbf{F}_1\neq\mathbf{0}$, $\mathbf{F}_2\neq\mathbf{0}$, $\mathbf{F}_3\neq\mathbf{0}$)

Point	Displacement of end-point $\Delta\mathbf{t}$	Deflections and loadings in joints and links
Q_0	$\delta_1=\delta_2=\delta_3=0\,\text{mm};$ $\varphi_1=\varphi_2=\varphi_3=0.03^\circ;$	$M^{\max}=2.09\,\text{N}\cdot\text{m};\Delta q^{\max}=0.31^\circ$ $\theta_{\text{p}}^{\max}=0.05\,\text{mm};\ \theta_{\varphi}^{\max}=0.94^\circ$ $\tau_{\text{p}}^{\max}=0;\ \tau_{\varphi}^{\max}=2.09\,\text{N}\cdot\text{m}$
Q_1	$\delta_1=\delta_2=\delta_3=0.41\,\text{mm};$ $\varphi_1=\varphi_2=\varphi_3=-0.62^\circ;$	$M^{\max}=8.91\,\text{N}\cdot\text{m};\Delta q^{\max}=0.63^\circ$ $\theta_{\text{p}}^{\max}=0.54\,\text{mm};\quad \theta_{\varphi}^{\max}=1.74^\circ$ $\tau_{\text{p}}^{\max}=0;\ \tau_{\varphi}^{\max}=11.96\,\text{N}\cdot\text{m}$
Q_2	$\delta_1=\delta_2=\delta_3=-0.96\,\text{mm};$ $\varphi_1=\varphi_2=\varphi_3=0.21^\circ;$	$M^{\max}=1.48\,\text{N}\cdot\text{m};\Delta q^{\max}=0.52^\circ$ $\theta_{\text{p}}^{\max}=0.14\,\text{mm};\quad \theta_{\varphi}^{\max}=0.80^\circ$ $\tau_{\text{p}}^{\max}=0;\ \tau_{\varphi}^{\max}=1.75\,\text{N}\cdot\text{m}$
Q_3	$\delta_1=-0.91\,\text{mm};\ \varphi_1=-0.19^\circ$ $\delta_2=1.31\,\text{mm};\ \varphi_2=-0.49^\circ$ $\delta_3=0.58\,\text{mm};\ \varphi_3=0.44^\circ$	$M^{\max}=4.33\,\text{N}\cdot\text{m};\ \Delta q^{\max}=0.67^\circ$ $\theta_{\text{p}}^{\max}=0.99\,\text{mm};\ \theta_{\varphi}^{\max}=1.49^\circ$ $\tau_{\text{p}}^{\max}=0;\ \tau_{\varphi}^{\max}=4.84\,\text{N}\cdot\text{m}$
Q_4	$\delta_1=0.93\,\text{mm};\ \varphi_1=0.33^\circ$ $\delta_2=-0.10\,\text{mm};\ \varphi_2=0.22^\circ$ $\delta_3=-0.25\,\text{mm};\ \varphi_3=-0.31^\circ$	$M^{\max}=2.98\,\text{N}\cdot\text{m};\Delta q^{\max}=0.59^\circ$ $\theta_{\text{p}}^{\max}=0.62\,\text{mm};\quad \theta_{\varphi}^{\max}=1.30^\circ$ $\tau_{\text{p}}^{\max}=0;\quad \tau_{\varphi}^{\max}=4.0\,\text{N}\cdot\text{m}$

Further, substituting deflections $\boldsymbol{\varepsilon}_i$ and corresponding chain stiffness matrices $\mathbf{K}_{\text{C}}^{(i)}$ into formulas (6.15) - (6.20), we can compute the desired assembling-induced values of the end-platform displacement, the internal forces/torques and the relevant displacements in virtual and passive joints. Main results of this study are summarized in Tables 6.1–6.2, where $\Delta q^{\max}$ is the maximum rotational displacement of passive joints, $\theta_{\text{p}}^{\max},\theta_{\varphi}^{\max}$ are maximum displacement of translational and rotational virtual springs respectively, $\tau_{\text{p}}^{\max}$, $\tau_{\varphi}^{\max}$ are maximum torques in translational and rotational virtual joints respectively, $M^{\max}$ is the maximum moment in the chains, caused by assembling of a parallel manipulator with the non-perfect kinematic chains.

These results show that in the Case A (Table 6.1), the geometrical errors in the kinematic chains do not cause any internal loading. However, they provoke the shift of the end-platform location up to 2.02 mm (point Q_2). Corresponding changes in passive joint coordinates are about 0.42 (point Q_2).

In contrast, in the Case B, the geometrical errors in the kinematic chains of Orthoglide (Table 6.2) cause essential internal loadings. For instance, in point Q_1 the torque applied to the end-point of the chain can reach up to $8.91\,\mathrm{N\cdot m}$. This loading induces displacements up to $0.41\,\mathrm{mm}$ and 0.62° for translational and rotational virtual springs respectively. It should be noted that here the loadings for rotational virtual springs are up to $11.96\,\mathrm{N\cdot m}$, but for translational virtual springs they are equal to zero (in spite of non-zero deflections in them). Nevertheless, this result is reasonable due to the non-diagonal structure of the matrices $\mathbf{K}_{\mathrm{C}}^{(i)}$ representing couplings between rotational and translational deflections. Variations in the passive joint coordinates can reach up to 0.67° (Point Q_3). For the end-platform, this case study gives the positional deflection up to 1.31 mm (Point Q_3) and the rotational deflection up to 0.62° (Point Q_1). It is obvious that the total sum of all internal loadings is equal to zero.

6.5.2 Aggregation non-perfect serial chains under loading

Now let us consider aggregation of Orthoglide manipulator under external loading caused by groove milling.. According to [21], such technological process causes forces $F_r = 215\,N$; $F_t = -10\,N$; $F_z = -25\,N$. The tool length $h = 100\,mm$ leads to torques on the manipulator end-effector $M_x, = 1\,N\cdot m$ and $M_y, = 21.5\,N\cdot m$. It is assumed that the manipulator has two sources of inaccuracy

(i) the assembling errors in the kinematic chains causing internal forces and relevant deflections in joints and links due to manipulator over-constrained structure;

(ii) the external loading $\|\mathbf{F}\| = 217\,N$ caused by the cutting forces, which generates essential compliance deflections causing non-desirable end-platform displacement.

Similar to previous example, it is assumed that firs source of inaccuracy can be caused by translational (Case A) and rotational (Case B) errors in the actuator locations.

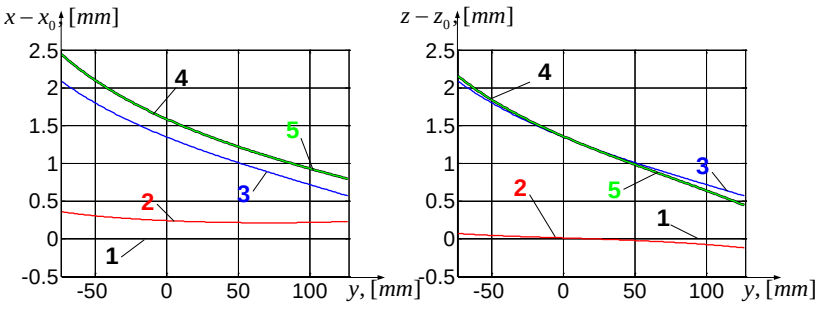

(a) Errors in x-direction (a) Errors in z-direction

Figure 6.6 Displacements caused different sources of inaccuracy during milling as the crow flies from point Q2 to Q4 using Orthoglide manipulator (Case A): (1) target trajectory, (2) displacements caused by cutting forces, (3) displacements caused by non-perfect geometry, (4) total compliance error, (5) displacements obtained using superposition principle.

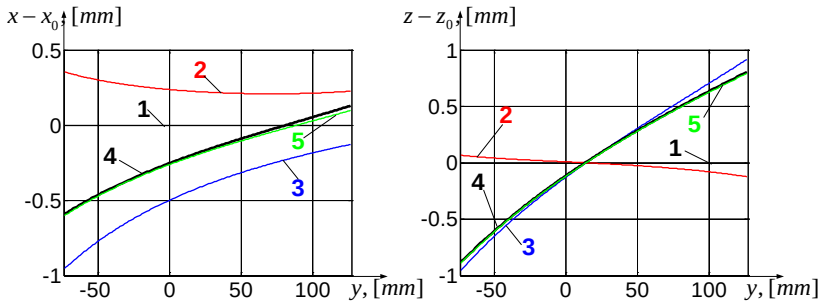

(a) Errors in x-direction (a) Errors in z-direction

Figure 6.7 Displacements caused different sources of inaccuracy during milling as the crow flies from point Q2 to Q4 using Orthoglide manipulator (Case B): (1) target trajectory, (2) displacements caused by cutting forces, (3) displacements caused by non-perfect geometry, (4) total compliance error, (5) displacements obtained using superposition principle.

Let us illustrate aggregation technique when Orthoglide perform milling from the point Q_2 to Q_5(-73.65, 126.35, -73.65) following the straight line. Simulation results for two error sources for the Case A and Case B are presented in Figure 6.6 and Figure 6.7 respectively. They include target trajectories (1), displacements caused by cutting forces (2) and non-perfect geometry (3) as well as total compliance error (4) and displacement obtained using superposition principle (5). The results presented for displacements in x- and z-directions.

The results show changing of different error sources and compliance error while the trajectory that define by non-linear functions. It should be mentioned, that in Case B superposition of two error sources cannot is differ from total compliance error, however in Case B both curves are closed enough. The main factor that causes difference between the trajectories is the changes in the stiffness matrix because of changing of the end-point location (the order of errors is not important, in both cases when we take into account the second error it should be computed in the neighborhood of current configuration, however for the results that have been obtained using superposition principle both errors have been computed for the original (target) end-point location).

The obtained results illustrate developed aggregation technique, show its advantages are suitable both for further error compensation and for the optimization workpiece location in the manipulator workspace.

6.6 *Conclusion*

This Chapter presents non-liner stiffness modeling technique for parallel manipulators composed of non-perfect serial chains, whose geometry differ from the nominal one and where essential internal forces/torques are generated. This technique is based on the developed aggregation procedure that combines the chain stiffness models and produces the relevant force-deflection relation, the aggregated Cartesian stiffness matrix and also allows us to evaluate changes in the reference point location caused by inaccuracy in kinematic chains. In addition, expressions for computing of the internal deflections and forces/torques in joints are proposed. The developed technique can be applied to both over-constrained and under-constrained manipulators, it is suitable for the cases of both small and large deflections.

The advantages of the developed technique are illustrated by an example that deals with over-constrained parallel manipulator of the Orthoglide architecture. It demonstrates the technique ability to evaluate the end-effector deflections caused by conventional sources (cutting forces/torques applied to the end-effector that arise while workpiece processing) and also induced by inaccuracy in serial chains of the parallel manipulator. Relevant plots that illustrate influence of different error sources on the manipulator position accuracy are presented.

In future, the proposed technique will be integrated in a software toolbox that can be used for parallel manipulators of complex architecture and applied to the industrial problem of the compliance error compensation in robotic machining cells.

6.7 References

[1] O. Company, S. Krut, F. Pierrot, Modelling and preliminary design issues of a 4-axis parallel machine for heavy parts handling, Journal of Multibody Dynamics 216 (2002) 1–11.

[2] J. Kövecses, J. Angeles, The stiffness matrix in elastically articulated rigid-body systems, Multibody System Dynamics 18(2) (2007) 169–184.

[3] T. Bonnemains, H. Chanel, C. Bouzgarrou and P. Ray, Definition of a new static model of parallel kinematic machines: highlighting of overconstraint influence, in: Proceedings of IEEE Int. Conference on Intelligent Robots and Systems (IROS), 2008, pp. 2416–2421.

[4] D. Deblaise, X. Hernot, P.Maurine, A systematic analytical method for PKM stiffness matrix calculation, In: Proceedings of the IEEE International Conference on Robotics and Automation (ICRA), Orlando, Florida, 2006, pp. 4213-4219.

[5] Y. Li, Q. Xu, Stiffness analysis for a 3-PUU parallel kinematic machine, Mechanism and Machine Theory 43(2) (2008) 186-200.

[6] A. Pashkevich, D. Chablat, P. Wenger, Stiffness analysis of overconstrained parallel manipulators, Mechanism and Machine Theory 44 (2009) 966-982.

[7] A. Pashkevich, A. Klimchik, D. Chablat, "Enhanced stiffness modeling of manipulators with passive joints", Mechanism and Machine Theory, vol. 46(5), pp. 662-679, 2011.

[8] A. Pashkevich, A. Klimchik, S. Caro, D. Chablat, Cartesian stiffness matrix of manipulators with passive joints: analytical approach, In: IEEE/RSJ International Conference on Intelligent Robots and Systems (IROS 2011), September 25-30, 2011, USA, San Francisco, California, pp. 4034-4041.

[9] J. Salisbury, Active Stiffness Control of a Manipulator in Cartesian Coordinates, in: 19th IEEE Conference on Decision and Control, 1980, pp. 87–97.

[10] Gosselin, C., 1990, "Stiffness mapping for parallel manipulators," IEEE Transactions on Robotics and Automation 6(3) 377–382

[11] I. Tyapin, G. Hovland, Kinematic and elastostatic design optimization of the 3-DOF Gantry-Tau parallel kinamatic manipulator,Modelling, Identification and Control, 30(2) (2009) 39-56

[12] A. Pashkevich, A. Klimchik, D. Chablat, Ph. Wenger, Accuracy Improvement for Stiffness Modeling of Parallel Manipulators, In: Proceedings of 42nd CIRP Conference on Manufacturing Systems, Grenoble, France, 2009.

[13] C. Quennouelle, C. M. Gosselin, Stiffness Matrix of Compliant Parallel Mechanisms, In: Springer Advances in Robot Kinematics: Analysis and Design, 2008, pp. 331-341.

[14] D. Chakarov, "Study of antagonistic stiffness of parallel manipulators with actuation redundancy," Mechanism and Machine Theory. Vol. 39(6), pp. 583–601, 2004.

[15] Yi, B.-J., Freeman, R.A., 1993, "Geometric analysis antagonistic stiffness redundantly actuated parallel mechanism," Journal of Robotic Systems 10(5) pp. 581-603.

[16] F. Xi, D. Zhang, Ch. M. Mechefske, Sh. Y. T. Lang, "Global kinetostatic modelling of tripod-based parallel kinematic machine," Mechanism and Machine Theory 39 (4), pp. 357–377, 2004.

[17] R. Rizk, N. Andreff, J.C. Fauroux, J.M. Lavest and G. Gogu, Precision Study of a Decoupled Four Degrees of Freedom Parallel Robot Including Manufacturing and Assembling Errors, Advances in Integrated Design and Manufacturing in Mechanical, S. Tichkiewitch et al. (eds.), Springer 2007, Engineering II, 111–127.

[18] W. Wei, N. Simaan, "Design of planar parallel robots with preloaded flexures for guaranteed backlash prevention," ASME Journal of Mechanisms and Robotics, Vol. 2(1) , 10 pages, 2010

[19] G. Alici, B. Shirinzadeh, Enhanced stiffness modeling, identification and characterization for robot manipulators, Proceedings of IEEE Transactions on Robotics 21(4) (2005) 554–564.

[20] D. Chablat, P. Wenger, Architecture Optimization of a 3-DOF Parallel Mechanism for Machining Applications, the Orthoglide, IEEE Transactions On Robotics and Automation 19(3) (2003) 403-410.

[21] F. Majou, C. Gosselin, P. Wenger, D. Chablat, Parametric stiffness analysis of the Orthoglide, Mechanism and Machine Theory 42 (2007) 296-311.

7 COMPLIANCE ERROR COMPENSATION TECHNIQUE FOR PARALLEL ROBOTS COMPOSED OF NON-PERFECT SERIAL CHAINS

7.1 Introduction

In machining applications, robot accuracy depends on a numbers of factors [1]. The most essential of them are related to manufacturing tolerances leading to geometrical parameters deviation with respect to their nominal values (geometrical errors) as well as to the end-effector deflections caused by the cutting forces and torques (compliance errors). Usually, in applications where the external forces/torques applied to the end-effector are relatively small, the prime source of manipulator inaccuracy are the *geometrical errors* [2, 3]. These errors are associated with differences between nominal and actual values of the link/joint parameters. Typical examples of them are the differences between the nominal and the actual lengths of links, differences between zero values of actuator coordinates in real robot and mathematical model embedded in controller (joint offsets); they can also be induced by non-perfect assembling of different elements and arise in shifting and/or rotation of the frames associated with different components, which normally are assumed to be matched and aligned. It is clear that the geometrical errors do not depend on the manipulator configuration, while their effect on the position accuracy depends on it. At present, there exists a number of sophisticated calibration techniques that are able to identify differences between actual and nominal geometrical parameters [4-9]. Consequently, this type of errors can be efficiently compensated for either by adjusting the controller input (i.e. the target point coordinates) or by straightforward modification of geometrical model parameters used in the robot controller.

In some other cases, the geometrical errors may be dominated by *non-geometrical* ones that are caused by influence of a number of factors [10-12]. For instance, the forces/torques associated with the tool-workpiece interaction in the technological process may cause essential deformations of the manipulator components (compliance errors) [13]. Also, the environmental conditions (temperature, atmospheric pressure and others) may affect physical properties of manipulator components and lead to undesirable changes in link dimensions. It is worth mentioning that, in the regular service conditions, the *compliance errors* are the most significant ones. Generally, they depend on two main factors: (i) the stiffness of the robotic manipulator and (ii) loading applied to it. Similar to the geometrical ones, the compliance errors highly depend on the manipulator configuration and essentially differ throughout the workspace. Their influence is particularly important for heavy robots and for manipulators with low stiffness. For example, the cutting forces/torques from the technological process may induce significant deformations, which are not negligible in the precise machining. In this case, influence of the compliance errors on the robot position accuracy can be even higher than the geometrical ones. This issue is very important for the designers of parallel manipulators, who often are looking for a compromise between the manipulator stiffness and its dynamic capabilities [14].

Thus, this Chapter focuses on the compliance error compensation that is able to take into account both conventional error sources (compliance errors caused by external and internal forces/torques) and errors caused by assembling of non-perfect over-constrained parallel mechanisms. To address these problems, the remainder of the chapter Chapter is organized as follows: Section 8.2 presents review on the compliance error compensation methods, Section 8.3 provides required background for the stiffness modeling, Section 8.4 proposes the non-linear compliance errors compensation technique, in Section 8.5 the efficiency of the

developed technique is illustrated by the groove milling using Orthoglide manipulator, and, finally, Section 8.6 summarizes the main results of the chapter Chapter.

7.2 Problem of compliance error compensation

In many robotic applications such as machining, grinding, trimming etc., the interaction between the workpiece and the end-effector causes essential deflections that significantly decrease the processing accuracy and quality of the final product. To overcome this difficulty, it is possible to modify either control algorithm or the prescribed trajectory, which is used as the reference input for a control system [15]. This Chapter focuses on the second approach that is considered to be more realistic in the practice. In contrast to the previous works, the proposed compliance error compensation technique is based on the non-linear stiffness model of the manipulator that is able to take into account significant external loading [16].

Usually, the problem of the robot error compensation can be solved in two ways that differ in degree of modification of the robot control software:

(a) by *modification of the manipulator model* (Figure 7.1a) which better suits to the real manipulator and is used by the robot controller (in simple case, it can be limited by tuning of the nominal manipulator model, but may also involve essential model enhancement by introducing additional parameters, if it is allowed by a robot manufacturer);

(b) by *modification of the robot control program* (Figure 7.1b) that defines the prescribed trajectory in Cartesian space (here, using relevant error model, the input trajectory is generated in such way that under the loading the output trajectory coincides with the desired one).

It is clear that the first approach can be implemented in on-line mode, while the second one requires preliminary off-line computations. It is worth mentioning that the stiffness models being used in this work are suitable for both of these approaches. But in practice it is rather unrealistic to include the stiffness model in a commercial industrial controller where all transformations between the joint and Cartesian coordinates are based on the manipulator geometrical model. In contrast, the off-line error compensation, based on the second approach, is attractive for industrial applications.

For the *geometrical errors*, relevant compensation techniques are already well developed. Comprehensive review of related works is given in [2, 9, 17]. Here, if the main error sources are concentrated in the link length or in the joint offsets, the compensation is reduced to straightforward modification of the manipulator parameters in the robot controller. Otherwise, if there are any geometrical error sources that are not presented in the nominal inverse/direct kinematics, relevant modification of the controller input is required. In this case, it is possible to use (in off-line mode) either extended geometrical model with additional parameters or simply a non-linear function that describes the error distribution throughout the workspace. Examples of such a function are given in [18, 19] where the neural network technique is employed. In the frame of this work, it is assumed that the geometrical errors are less essential compared to the non-geometrical ones caused by the interaction between the machining tool and workpiece. So, the main attention will be paid to the *compliance errors* and their compensation techniques.

For the *compliance errors*, the compensation technique must rely on two components. The first of them describes distribution of the stiffness properties throughout the workspace and is defined by the stiffness

matrix as a function of the joint coordinates or the Cartesian location [16]. The second component describes the forces/torques acting on the end-effector while the manipulator is performing its manufacturing task (manipulator *loading*). In this work, it is assumed that the second component is given and can be obtained either from the dedicated technological process model or by direct measurements using the force/torque sensor integrated into the end-effector. However it is necessary to take into account that the force sensors introduce additional undesirable compliance which has direct affect on the position accuracy [20, 21].

The *stiffness matrix* required for the compliance errors compensation highly depends on the robot configuration and essentially varies throughout the workspace. Hypothetically, it can be also approximated by a neural network, similar to the geometrical error compensation mentioned above. However, this approach is not practically attractive, so it is more convenient to compute the stiffness matrix using specially developed expressions and algorithms.

From general point of view, full-scale compensation of the compliance errors requires essential revision of the manipulator model embedded in the robot controller. In fact, instead of conventional geometrical model that provides inverse/direct coordinate transformations from the joint to Cartesian spaces and vice versa, here it is necessary to employ the so-called *kinetostatic model* [22]. The later defines the mapping between the joint and Cartesian spaces taking into account deflections caused by external forces/torques applied to the manipulator end-effector. It is essentially more complicated than the geometrical model and requires rather intensive computations that are presented in Section 8.3.

If the compliance errors are relatively small, composition of conventional geometrical model and the stiffness matrix give rather accurate approximation of the modified mapping from the joint to Cartesian space. In this case, for the first compensation scheme (see Figure 7.1a), the kinetostatic model can be easily implemented online if there is access to the control software modification. Otherwise, the second scheme (see Figure 7.1b) can be easily applied. Moreover, with regard to the robot-based machining, there is a solution that does not require force/torque measurements or computations [15, 23, 24]. Its basic idea is presented in Figure 7.2, where at the first stage it is performed, the machining experiment gives a trajectory corrupted by the compliance errors. Then, the difference between the desired and the obtained trajectories is evaluated via appropriate measurements, which give the compliance errors along the path. Using this data and assuming that the stiffness model is linear, the target trajectory for the robot controller is modified by applying the "mirror" technique (where corresponding points of the corrupted and target trajectories are symmetrical with respect to the relevant points of the desired trajectory). In order to improve accuracy in [25] it was proposed to perform the machining experiments several times. Starting from the second experiment the target trajectory for the robot controller has been modified by applying the "mirror" technique for the measurements obtained during previous experiments. An evident advantage of this technique is its applicability to the compensation of all types of the robot errors, including geometrical and compliance ones. However, this approach is only suitable for the large-scale production where the manufacturing task and the workpiece location remains the same. Eastwood and Webb [26] proposed polar compensation methodology for gravitational deflection compensation for hybrid parallel kinematic machines. In some other works [26, 27] the problems of geometrical and compliance errors compensation have been considered simultaneously but these techniques cannot be applied to robot-based machining directly.

(a) Modification of the manipulator model

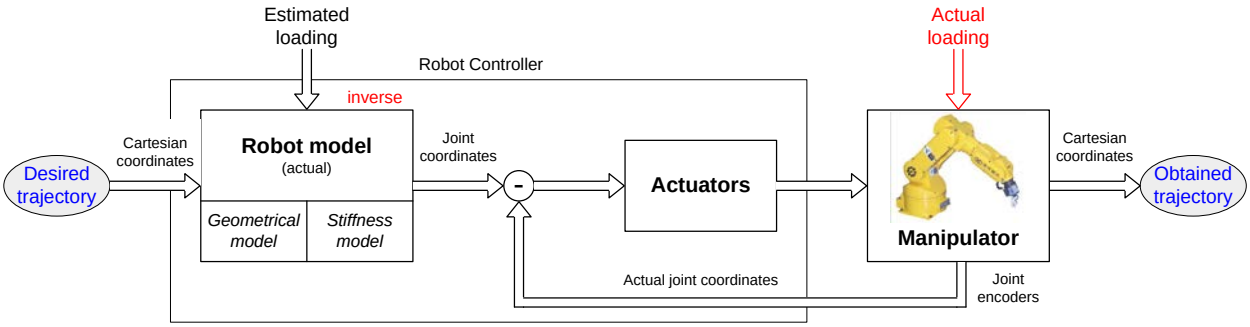

(b) Modification of the target trajectory

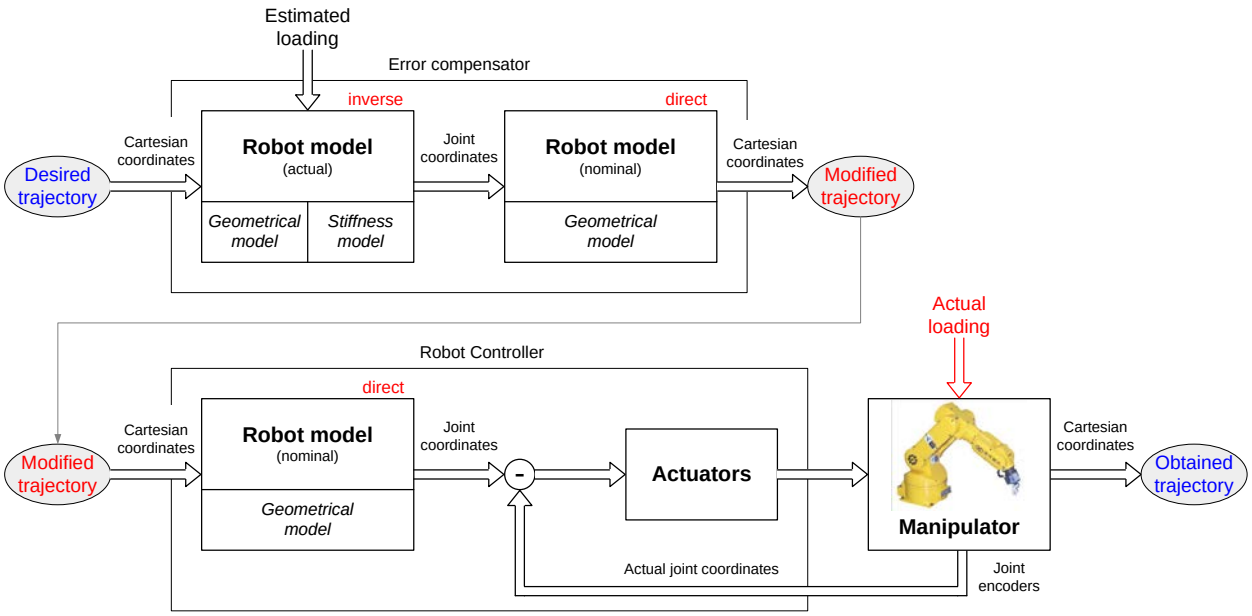

Figure 7.1 Robot error compensation methods

Hence, to be applied to the robotic-based machining, the existing compliance errors compensation techniques should be essentially revised to take into account essential forces and torques as well as some other important error sources (inaccuracy in serial chains, for instance). This problem is in the scope of this work.

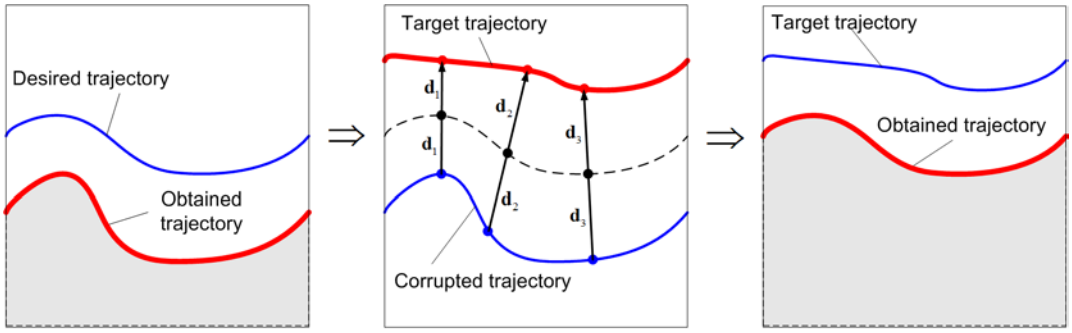

Figure 7.2 Method of symmetrical trajectory for compensation of the compliance errors

7.3 Stiffness modeling background

The compliance error compensation technique developing in this work is based on our previous results [16], which provide a nonlinear stiffness modeling technique for the manipulators with passive joints. This approach is based on the Virtual Joint Modeling (VJM) method, which extended the conventional rigid-body model of the robotic manipulator by adding virtual springs that take into account elastostatic properties of links and joints. The method proposed by Salisbury in 1980 [29] has found numerous modifications [29-33] and at present it is the most popular stiffness analysis method in robotics. Let us summarise here the main expressions that will be used in the nonlinear compliance error compensation technique.

It is assumed that the end-points of all kinematic chains are aligned and matched in the same target point $\mathbf{t}_0$, which corresponds to the desired end-platform location. This point is assumed to be known and allows us to compute, from the inverse kinematic model, the actuator and passive joint coordinates defining nominal configurations of the chains $(\mathbf{q}_{0i},\boldsymbol{\theta}_{0i})$. Static equilibrium for serial chain that corresponds to applied loading can be computed using the following iterative procedure

$$\begin{bmatrix}\mathbf{F}_i'\\ \mathbf{q}_i'\\ \boldsymbol{\theta}_i'\end{bmatrix}=\begin{bmatrix}\mathbf{0} & \mathbf{J}_{\mathrm{qi}}(\mathbf{q}_i,\boldsymbol{\theta}_i) & \mathbf{J}_{\mathrm{\theta i}}(\mathbf{q}_i,\boldsymbol{\theta}_i)\\ \mathbf{J}_{\mathrm{qi}}^{\mathrm{T}}(\mathbf{q}_i,\boldsymbol{\theta}_i) & \mathbf{0} & \mathbf{0}\\ \mathbf{J}_{\mathrm{\theta i}}^{\mathrm{T}}(\mathbf{q}_i,\boldsymbol{\theta}_i) & \mathbf{0} & -\mathbf{K}_{\mathrm{\theta i}}\end{bmatrix}^{-1}\cdot\begin{bmatrix}\mathbf{t}-\mathbf{g}_i\left(\mathbf{q}_i,\boldsymbol{\theta}_i\right)+\mathbf{J}_{\mathrm{qi}}(\mathbf{q}_i,\boldsymbol{\theta}_i)\cdot\mathbf{q}_i+\mathbf{J}_{\mathrm{\theta i}}(\mathbf{q}_i,\boldsymbol{\theta}_i)\cdot\boldsymbol{\theta}_i\\ \mathbf{0}\\ -\mathbf{K}_{\mathrm{\theta i}}\cdot\boldsymbol{\theta}_{0\mathrm{i}}\end{bmatrix} \tag{7.1}$$

where the subscript "(*i*)" denotes the serial chain number, the prime define new static equilibrium configuration that should be used in the next iteration as a current one, $\mathbf{F}$ is external loading applied to the end-point of kinematic chain, joint coordinates $(\mathbf{q},\boldsymbol{\theta})$ define serial chain configuration that corresponds the applied loading $\mathbf{F}$, $\mathbf{J}_{\mathrm{q}}(\mathbf{q},\boldsymbol{\theta})$ and $\mathbf{J}_{\theta}(\mathbf{q},\boldsymbol{\theta})$ are Jacobian matrices with respect to passive $\mathbf{q}$ and virtual $\boldsymbol{\theta}$ joint coordinates respectively computed for current serial chain configuration, matrix $\mathbf{K}_{\theta}$ is stiffness matrix of serial chain in the joint coordinates, vector $\mathbf{t}$ defines end-effector location under the loading. Function $\mathbf{g}(\mathbf{q},\boldsymbol{\theta})$ defines geometry of serial chain, $\boldsymbol{\theta}_0$ is preloading in virtual joints. So, partial non-linear force-deflection relations corresponding to the target point $\mathbf{t}_0$ can be presented in the form

$$\mathbf{F}_i = f_i(\mathbf{t}\,|\,\mathbf{t}_0) \tag{7.2}$$

Then, in accordance with the superposition principle, the non-linear force-deflection relation for the whole parallel manipulator can be found by straightforward summation of all partial forces $\mathbf{F}_i$, i.e.

$$\mathbf{F} = \sum_{i=1}^{m} f_i\left(\mathbf{t} \mid \mathbf{t}_0\right) \tag{7.3}$$

where $\mathbf{F}$ denotes the total external loading applied to the end-platform. As a result, corresponding curves can be obtained by multiple repetition of the above described procedures for different values of the end-platform location $\mathbf{t}$.

Furthermore, for each given $\mathbf{t}$, the Cartesian stiffness matrices $\mathbf{K}_{\mathrm{C}}^{(i)}$ of all kinematic chains, that correspond to the loading configuration can be computed using the following expression

$$\mathbf{K}_{\mathrm{C}}^{(i)} = \mathbf{K}_{C}^{0(F)} - \mathbf{K}_{C}^{q(F)} \tag{7.4}$$

where the first term $\mathbf{K}_{C}^{0(F)} = (\mathbf{J}_{\theta} \cdot \mathbf{k}_{\theta}^{\mathrm{F}} \cdot \mathbf{J}_{\theta}^{\mathrm{T}})^{-1}$ exactly corresponds to the classical formula defining stiffness of the kinematic chain without passive joints in the loaded mode [34, 35] and the second term $\mathbf{K}_{C}^{q(F)}$ takes into account influence of passive joints and can be computed as

$$\mathbf{K}_{C}^{q(F)} = -\mathbf{K}_{C}^{0(F)} \cdot \mathbf{J}_{\mathrm{q}}^{(F)} \cdot \left(\mathbf{H}_{\mathrm{qq}}^{\mathrm{F}} + \mathbf{H}_{\mathrm{q}\theta}^{\mathrm{F}} \cdot \mathbf{k}_{\theta}^{\mathrm{F}} \cdot \mathbf{H}_{\theta\mathrm{q}}^{\mathrm{F}} - \mathbf{J}_{\mathrm{q}}^{(F)T} \cdot \mathbf{K}_{C}^{0(F)} \cdot \mathbf{J}_{\mathrm{q}}^{(F)}\right)^{-1} \cdot \mathbf{J}_{\mathrm{q}}^{(F)T} \cdot \mathbf{K}_{C}^{0(F)} \tag{7.5}$$

where $\mathbf{J}_{\mathrm{q}}^{(F)} = \mathbf{J}_{\mathrm{q}} + \mathbf{J}_{\theta} \cdot \mathbf{k}_{\theta}^{\mathrm{F}} \cdot \mathbf{H}_{\theta\mathrm{q}}^{\mathrm{F}}$.

Finally, this allows us to compute the Cartesian stiffness matrix $\mathbf{K}_{\mathrm{C}}$ of the whole parallel robot as a sum

$$\mathbf{K}_{\mathrm{C}} = \sum_{i=1}^{m} \mathbf{K}_{\mathrm{C}}^{(i)} \tag{7.6}$$

This approach allows us to obtain the non-linear force-deflection relation for a parallel manipulator in the loaded mode as well as to compute Cartesian stiffness matrices for any given target point $\mathbf{t}_0$ and given the end-point location $\mathbf{t}$. However, it cannot be applied for the compliance errors compensation straightforwardly. Thus a dedicated technique, that is considered in this Chapter, is required.

7.4 Nonlinear technique for compliance error compensation

In industrial robotic controllers, the manipulator motions are usually generated using the inverse kinematic model that allows us to compute the input signals for actuators $\boldsymbol{\rho}_0$ corresponding to the desired end-effector location $\mathbf{t}_0$, which is assigned assuming that the compliance errors are negligible. However, if the external loading is essential, the kinematic control becomes non-applicable because of changes in the end-platform location. It can be computed from the non-linear compliance model as

$$\mathbf{t}_{\mathrm{F}} = f^{-1}\left(\mathbf{F} \mid \mathbf{t}_0\right) \tag{7.7}$$

where the subscript 'F' refers to the loaded mode.

To compensate this undeterred end-platform displacement from $\mathbf{t}_0$ to $\mathbf{t}_{\mathrm{F}}$, the target point should be modified in such a way that, under the loading $\mathbf{F}$, the end-platform is located in the desired point $\mathbf{t}_0$. This requirement can be expressed using the stiffness model in the following way

$$\mathbf{F} = f\left(\mathbf{t}_0 \mid \mathbf{t}_0^{(\mathrm{F})}\right) \tag{7.8}$$

where $\mathbf{t}_0^{(\mathrm{F})}$ denotes the modified target location. Hence, the problem is reduced to the solution of the nonlinear equation (7.8) for $\mathbf{t}_0^{(\mathrm{F})}$, while $\mathbf{F}$ and $\mathbf{t}_0$ are assumed to be given. It is worth mentioning that this

equation completely differs from the equation $\mathbf{F} = f(\mathbf{t} \mid \mathbf{t}_0)$, where the unknown variable is $\mathbf{t}$. It means that here the compliance model does not allow us to compute the modified target point $\mathbf{t}_0^{(\mathrm{F})}$ straightforwardly, while the linear compensation technique directly operates with Cartesian compliance matrix [10, 23].

To solve equation (7.8) for $\mathbf{t}_0^{(\mathrm{F})}$, the Newton-Raphson technique can be applied. It yields the following iterative scheme

$$\mathbf{t}_0^{(\mathrm{F})\prime} = \mathbf{t}_0^{(\mathrm{F})} + \mathbf{K}_{\mathrm{t.p.}}^{-1}(\mathbf{t}_0 \mid \mathbf{t}_0^{(\mathrm{F})}) \cdot \left(\mathbf{F} - f(\mathbf{t}_0 \mid \mathbf{t}_0^{(\mathrm{F})})\right) \tag{7.9}$$

where the prime corresponds to the next iteration and $\mathbf{K}_{\mathrm{t.p.}}(\mathbf{t}_0 \mid \mathbf{t}_0^{(\mathrm{F})})$ is Cartesian stiffness matrix computed with respect to the second argument of the stiffness model $\mathbf{F} = f(\mathbf{t} \mid \mathbf{t}_0)$

$$\mathbf{K}_{\mathrm{t.p.}}(\mathbf{t} \mid \mathbf{t}_0) = \frac{\partial f(\mathbf{t} \mid \mathbf{t}_0)}{\partial \mathbf{t}_0} \tag{7.10}$$

This argument $\mathbf{t}_0$ can be interpreted as the target point. Here, the location $\mathbf{t}_0$ can also be used as the initial value of $\mathbf{t}_0^{(\mathrm{F})}$. The stopping criterion can be expressed as

$$\left\| \mathbf{F} - f\left(\mathbf{t}_0 \mid \mathbf{t}_0^{(\mathrm{F})}\right) \right\| < \varepsilon_{\mathrm{F}} \tag{7.11}$$

where ε_{F} is the desired accuracy.

To overcome computational difficulties related to the evaluation of the matrix $\mathbf{K}_{\mathrm{t.p.}}(\mathbf{t}_0 \mid \mathbf{t}_0^{(\mathrm{F})})$, it is possible to use its simple approximation that does not change from iteration to iteration. In particular, assuming that $\mathbf{t}$ and $\mathbf{t}_0$ are close enough and the stiffness properties do not vary substantially in their neighborhood, the stiffness model can be approximated by a linear expression $\mathbf{F} = \mathbf{K}_{\mathrm{C}}(\mathbf{t} - \mathbf{t}_0)$, which gives $\mathbf{K}_{\mathrm{t.p.}} = -\mathbf{K}_{\mathrm{C}}$. Hence, the iterative scheme (7.9) can be modified as

$$\mathbf{t}_0^{(\mathrm{F})\prime} = \mathbf{t}_0^{(\mathrm{F})} - \alpha \cdot \mathbf{K}_{\mathrm{C}}^{-1}(\mathbf{t}_0 \mid \mathbf{t}_0^{(\mathrm{F})}) \cdot \left(\mathbf{F} - f(\mathbf{t}_0 \mid \mathbf{t}_0^{(\mathrm{F})})\right) \tag{7.12}$$

where $\alpha \in (0,1)$ is the scalar parameter ensuring the convergence. Using the non-linear compliance model (7.7), this idea can also be implemented in an iterative algorithm

$$\mathbf{t}_0^{(\mathrm{F})\prime} = \mathbf{t}_0^{(\mathrm{F})} + \alpha \cdot \left(\mathbf{t}_0 - f^{-1}(\mathbf{F} \mid \mathbf{t}_0^{(\mathrm{F})})\right) \tag{7.13}$$

which does not include stiffness matrices $\mathbf{K}_{\mathrm{C}}$ or $\mathbf{K}_{\mathrm{t.p.}}$. Obviously, this is the most computationally convenient solution and it will be used in the next section.

It should be mentioned that the considered case deals with a perfect parallel manipulator where end-points of all kinematic chains are aligned and matched. However, in practice, kinematic chains may include some errors that do not allow us to assemble them with the same end-platform location. In this case it is required to compensate two types of errors (caused by the external loading $\mathbf{F}$ and inaccuracy in the serial chains). The second source of errors can be taken into account by changing of target location $\Delta\mathbf{t}_{0i}$ for each kinematic chain

$$\Delta\mathbf{t}_{0i} = \Delta\mathbf{t}_0 + \Delta\mathbf{t}_\varepsilon - \boldsymbol{\varepsilon}_i \tag{7.14}$$

where $\Delta\mathbf{t}_\varepsilon$ is the end-platform deflections due to assembling of non-perfect kinematic chains and $\boldsymbol{\varepsilon}_i$ is shifting of the end-point location of i^{th} kinematic chain because of geometrical errors. Using the principle of virtual work it can be proved that $\Delta\mathbf{t}_\varepsilon$ can be computed as

$$\Delta\mathbf{t}_\varepsilon = \left(\sum_{i=1}^{m}\mathbf{K}_{\text{C}}^{(i)}\right)^{-1}\cdot\sum_{i=1}^{m}\left(\mathbf{K}_{\text{C}}^{(i)}\cdot\boldsymbol{\varepsilon}_i\right) \tag{7.15}$$

where $\mathbf{K}_{\text{C}}^{(i)}$ defines the Cartesian stiffness matrix of *i*-th kinematic chain that can be computed using techniques proposed in the previous Section and m is the number of kinematic chains in the parallel manipulator. More detailed presentation of the developed iterative routines is given in Figure 7.3.

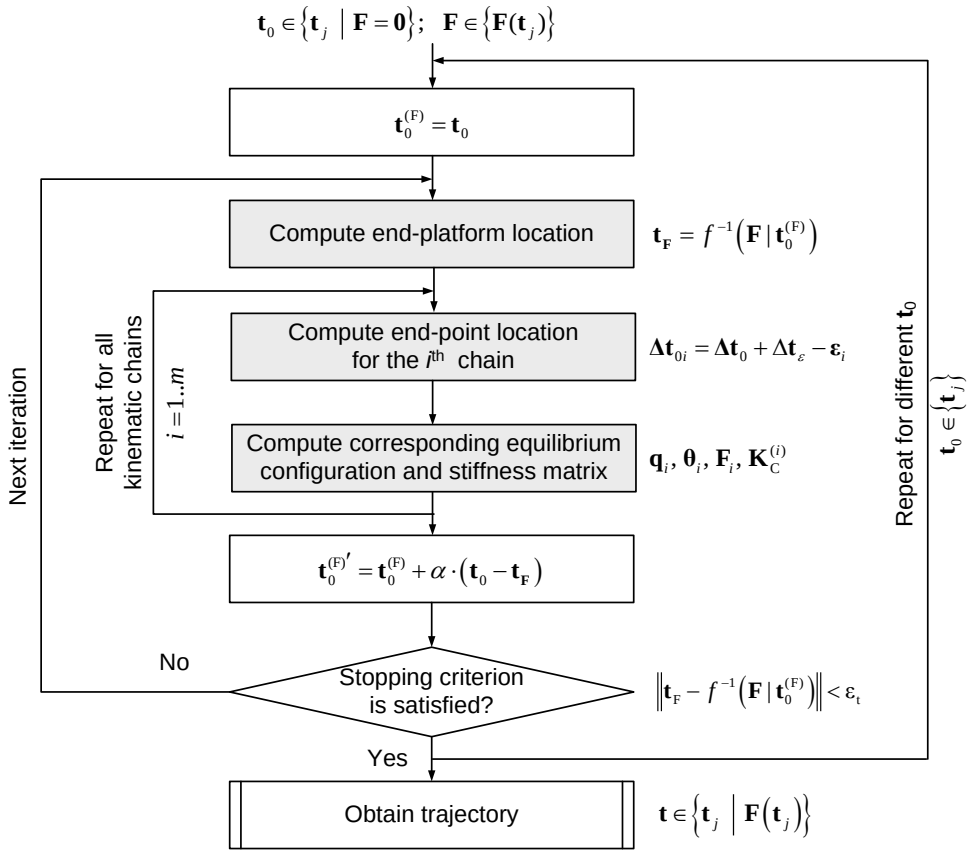

Figure 7.3 Procedure for compensation of compliance errors in parallel manipulator

Hence, using the proposed computational techniques, it is possible to compensate a main part compliance errors by proper adjusting the reference trajectory that is used as an input for robotic controller. In this case, the control is based on the inverse kinetostatic model (instead of kinematic one) that takes into account both the manipulator geometry and elastic properties of its links and joints. Efficiency of this technique is confirmed by an example presented in the next section.

7.5 *Illustrative example: compliance error compensation for milling*

Let us illustrate the developed compliance errors compensation technique by an example of the circle groove milling with the Orthoglide manipulator (Figure 7.4). Detailed specification of this manipulator can be found in [37]. According to [38], such technological process causes the loading $F_r = 215\,N$; $F_t = -10\,N$; $F_z = -25\,N$ that together with angular parameter $\varphi = [0, 360^\circ]$ define the forces F_x, F_y and F_z (Figure 7.4b,c). Here, the tool length h is equal to $100\,mm$. It is assumed that the manipulator has two sources of inaccuracy

(i) the assembling errors in the kinematic chains (assembling errors in actuator angular locations of about 1° around the corresponding actuated axis) causing internal forces and relevant deflections in joints and links due to manipulator over-constrained structure;

(ii) the external loading $\|\mathbf{F}\| = 217\,N$ caused by the cutting forces, which generates essential compliance deflections causing non-desirable end-platform displacement.

It is worth mentioning that the non-linear compliance error compensation technique, which has been developed in previous section, allows us to compensate influence of both the above mentioned factors

(a) Orthoglide manipulator

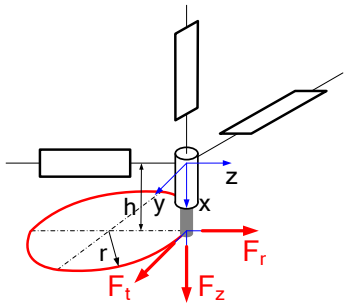

(b) groove milling with Orthoglide

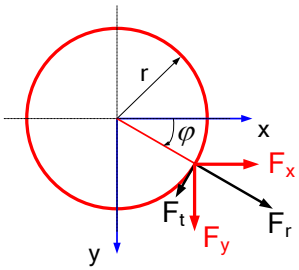

(c) milling forces

Figure 7.4 Milling forces for groove milling using Orthoglide manipulator

Assuming that the milling trajectory is oriented in xy-plane, the loading that corresponds to grove milling can be expressed as

$$\mathbf{F} = (F_x,\ F_y,\ F_z, -F_y \cdot h,\ F_x \cdot h,\ 0) \tag{7.16}$$

where F_x and F_y depend on the machining tool orientation angle φ (Figure 7.4b,c) as

$$F_x = F_r \cos\varphi + F_t \sin\varphi; \qquad F_y = F_r \sin\varphi + F_t \cos\varphi \tag{7.17}$$

In order to illustrate influence of different error sources on the machining trajectory, let us focus on a small radius of the circle that should be machined. In this case, the stiffness matrix is almost the same along the trajectory. Modeling results in the vicinity of the boundary of the Cartesian workspace (neighborhood of point Q_1, - closest point to the parallel singularity. see [16] for details) are presented in Figure 7.5. They show the influence of different error sources on the machining trajectory without compensation and the revised machining trajectory that should be implemented in robot controller in order to follow the target trajectory while machining. Here, path 5 compensates the effects seen in path 4 such that circle 1 is achieved. It can be seen that the centre of path 5 is on the opposite side of circle 1 compared to path 4. It can also be seen that

the main elliptic direction in path 4 becomes the smallest elliptic direction in path 5. It should be mentioned that because of the torque induced by the cutting forces (tool length 100 mm), the target trajectory and shifted trajectory under the cutting forces are intersecting.

Figure 7.6 illustrates the superposition principle for the errors caused by inaccuracy in serial chains and compliance errors caused by cutting forces. The vectors that are used here have been computed for the cases when there is only one source of error (inaccuracy in serial chains or compliance due to cutting forces). The results show that taking into account two error sources simultaneously, the total error is less than the error obtained using superposition principle, but this difference is not high and both trajectories have similar shape and location. The main factor that causes difference between the obtained trajectories is the changes in the stiffness matrix because of changing of the end-point location (the order of errors is not important, in both cases when we take into account the second error it should be computed in the neighborhood of current configuration, however for the results that have been obtained using superposition principle both errors have been computed for the original (target) end-point location).

Figure 7.7 presents result for the milling of the 50 mm circle. In this case, without compensation, the compliance errors can exceed 0.8 mm, which is rather high for the considered application. After compensation, the above mentioned errors are reduced near to zero (it is obvious that in practice, the compensation level is limited by the accuracy of the stiffness model). This compensation is achieved due to the modification of the actuator coordinates $\boldsymbol{\rho}$ along the machining trajectory. Compared to the relevant values computed via the inverse kinematics, the actuator coordinates differ up to 1.7 mm. Corresponding forces in actuators can reach 300 N. Some more results on the compliance errors compensation are presented in Figure 7.7, which includes plots showing modification of the actuator coordinates $\Delta\boldsymbol{\rho}$, values of the compensated end-effector displacement $\Delta\mathbf{t}$ and the torques in actuators τ. Figure 7.7d,e illustrate the impact of different error sources in the inaccuracy while milling with Orthoglide.

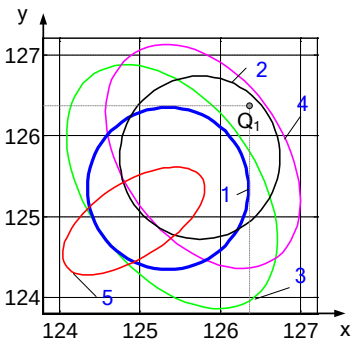

(1) Target trajectory
(2) Shifting of target trajectory caused by errors in serial chains (assembling errors)
(3) Shifting of target trajectory caused by cutting force (compliance errors)
(4) Shifting of target trajectory caused by cutting force and errors in serial chains (assembling errors + compliance errors)
(5) Adjusted trajectory, that insure following the target trajectory while machining

Figure 7.5 Modifications of target trajectory caused by different error sources and adjusted trajectory that insure following the target trajectory while machining

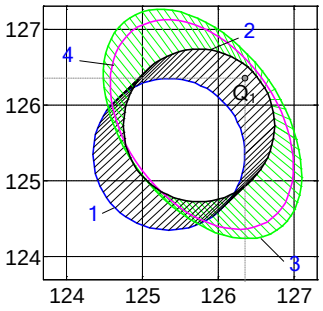

(1) Target trajectory

(2) Shifting of target trajectory caused by errors in serial chains (assembling errors)

(3) Shifting of target trajectory caused by cutting force and errors in serial chains (assembling errors + compliance errors: superposition principle for separate cases)

(4) Shifting of target trajectory caused by cutting force and errors in serial chains (assembling errors + compliance errors: two error sources simultaneously)

Figure 7.6 Superposition of different error sources

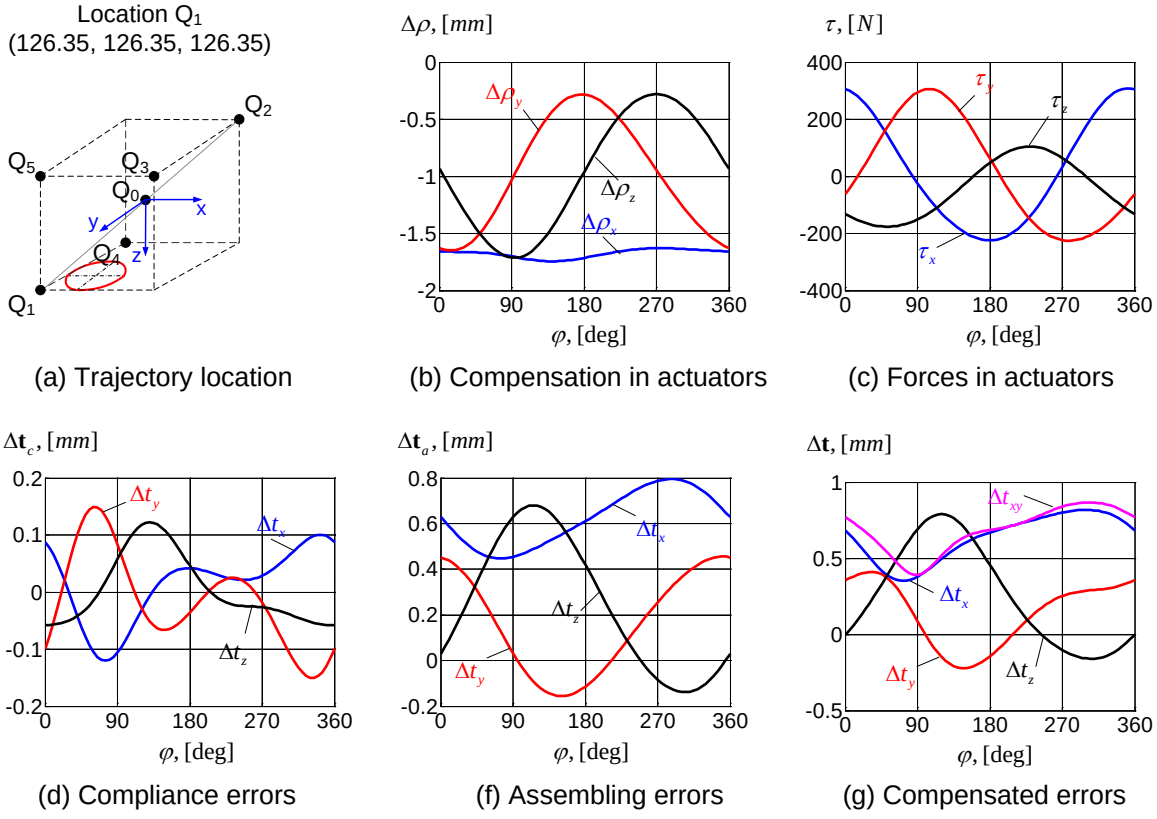

(a) Trajectory location (b) Compensation in actuators (c) Forces in actuators

(d) Compliance errors (f) Assembling errors (g) Compensated errors

Figure 7.7 Compliance error compensation for Orthoglide milling application

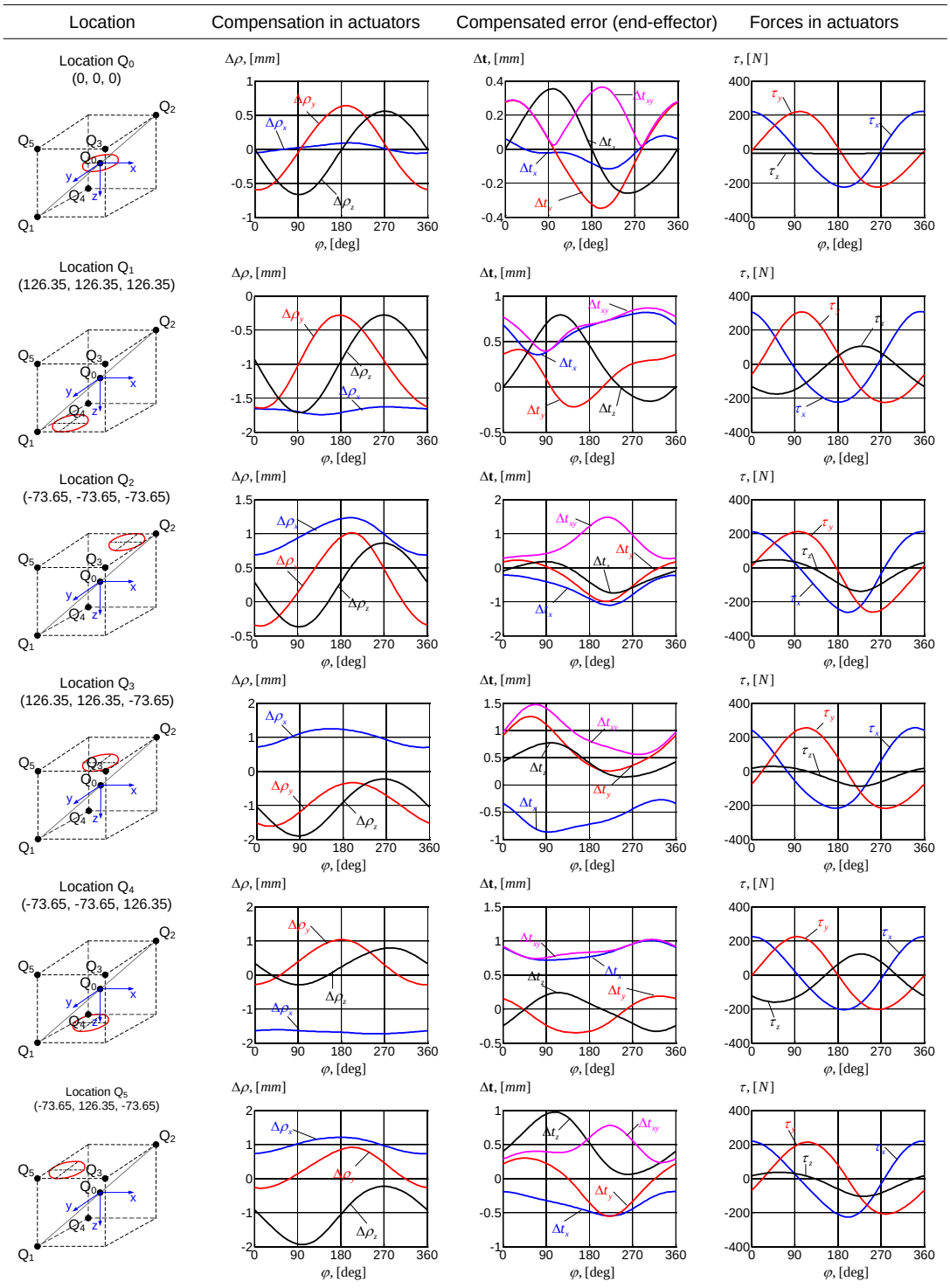

Figure 7.8 Compliance error compensation for Orthoglide milling application with cutting force (215 N, -10 N, -25 N, 1 N·m, 21.5 N·m, 0) for different location of the workpiece

Comparison of results for typical locations of the desired circular trajectory are presented in Figure 7.8. These results include a number of plots showing modification of the actuator coordinates $\Delta\boldsymbol{\rho}$, values of compensated end-effector displacement $\Delta\mathbf{t}$ and the torques in actuators τ. It is shown that for such process parameters, without compensation, the compliance errors can exceed 1.2 mm, which is too high for the considered application. In particular, for the best location Q_0, the cutting forces provoke the end-effector deflection of 0.35 mm. And for the worst location Q_3, the end-effector deflection is about 1.25 mm. Hence, the application of the developed compliance errors compensation technique is reasonable here. Compared to relevant values computed via the inverse kinematics (as in common-used industrial controllers), the actuator coordinates differ up to 0.6 mm for location Q_0, and up to 1.9 mm for location Q_3.

It is worth mentioning, that the shape of the compensation curve $\Delta\boldsymbol{\rho}(\varphi)$ highly depends on the location of the milling trajectory (i.e. the function $\Delta\boldsymbol{\rho}(\varphi)$ cannot be normalized by scaling and shifting) and the compensation procedure requires intensive computing. However, it can be implemented off-line and the robot model motion program can be properly modified.

Hence, the developed algorithm is able to compensate the compliance errors and can be efficient both for off-line trajectory planning and for on-line errors compensation.

7.6 Conclusions

In robotic-based machining, an interaction between the workpiece and technological tool causes essential deflections that significantly decrease the manufacturing accuracy. Relevant compliance errors highly depend on the manipulator configuration and essentially differ throughout the workspace. Their influence is especially important for heavy serial robots and for parallel manipulators, where the compromise between the manipulator stiffness and its dynamic capabilities is quite important. To overcome this difficulty this Chapter presents a new technique for compensation of the compliance errors caused by external/internal loadings in parallel manipulators (including over-constrained ones) composed of non-perfect serial chains. In contrast to previous works, this technique is based on the non-linear stiffness model.

The advantages of the developed technique are illustrated by the example that deals with groove milling with Orthoglide manipulator. It has been shown that the impact of two error sources cannot be taken into account using their superposition principle due to non-linearity of the stiffness model (even for relatively small deflections of the end-effector). Comparison study confirmed that errors to be compensated highly depend on the workpiece location. Besides, in order to compensate the same error for different workpiece locations different modifications in actuated coordinates are required.

In future, the developed compensation technique will be integrated in a software toolbox. This toolbox will also be useful for optimal path planning as well as optimization of the workpiece location. Another problem that should be addressed is an enhancement of the stiffness modeling technique for a more general class of manipulators and other types of loadings (gravity, friction).

7.7 References

[1] V. Robin, L. Sabourin, G. Gogu, Optimization of a robotized cell with redundant architecture, Robotics and Computer-Integrated Manufacturing 27(2011) 13–21

[2] A.Y. Elatta, Li Pei Gen, Fan Liang Zhi, Yu Daoyuan and Luo Fei, An Overview of Robot Calibration, Information Technology Journal 3(2004) 74-78.

[3] L. Rolland, Outils algébriques pour la résolution de problèmes géométriques et l'analyse de trajectoire de robots parallèles prévus pour des applications à haute cadence et grande précision, PhD Thesis, Université Henri Poincaré, 2003.

[4] Z. Roth, B. Mooring, B. Ravani, An overview of robot calibration, IEEE Journal of Robotics and Automation 3(1987) 377-385

[5] D.J. Bennett, J.M. Hollerbach, D. Geiger, Autonomous robot calibration for hand-eye coordination, International Journal of Robotics Research 10 (1991) 550-559.

[6] M. Abtahi, H. Pendar, A. Alasty, G. Vossoughi, Experimental kinematic calibration of parallel manipulators using a relative position error measurement system, Robotics and Computer-Integrated Manufacturing 26(2010) 799–804.

[7] W Khalil, E Dombre, Geometric calibration of robots, Modeling, Identification and Control of Robots, 2004, pp. 257-289

[8] D. Daney, N. Andreff, G. Chabert, Y. Papegay, Interval method for calibration of parallel robots: Vision-based experiments, Mechanism and Machine Theory, Volume 41 (2006) 929-944

[9] J. Hollerbach, W. Khalil, M. Gautier, Springer Handbook of robotics, Springer, 2008, Chap. Model identification, pp. 321-344.

[10] C. Gong, J. Yuan and J. Ni, Nongeometric error identification and compensation for robotic system by inverse calibration, International Journal of Machine Tools & Manufacture 40 (2000) 2119–2137

[11] H. Cui and Z. Zhu, Error Modeling and Accuracy of Parallel Industrial Robots, Source: Industrial-Robotics-Theory-Modelling-Control, ISBN 3-86611-285-8, pp. 964, ARS/plV, Germany, 2006, pp 573-646

[12] I.C. Bogdan, G. Abba: Identification of the servomechanism used for micro-displacement. in: Proceedings of IEEE International Conference on Robotics and Automation (ICRA), 2009, pp. 1986-1991

[13] M A. Meggiolaro, S Dubowsky, C Mavroidis, Geometric and elastic error calibration of a high accuracy patient positioning system, Mechanism and Machine Theory 40 (2005) 415–427

[14] V. V. Cheboxarov, V. F. Filaretov, M. Vukobratoviimage, Raising the stiffness of manipulators with lightweight links, Mechanism and Machine Theory 35 (2000) 1-13

[15] P. Dépincé, J-Y. Hascoët, Active integration of tool deflection effects in end milling. Part 2. Compensation of tool deflection, International Journal of Machine Tools and Manufacture, 46(2006) 945-956

[16] A. Pashkevich, A. Klimchik, D. Chablat, Enhanced stiffness modeling of manipulators with passive joints, Mechanism and Machine Theory 46(2011) 662-679.

[17] R. Bernhardt, S. Albright (Eds.), Robot Calibration, Springer 1994, 328 p.

[18] Xiaolin Zhong, John Lewis, Francis L. N-Nagy, Inverse robot calibration using artificial neural networks, Engineering Applications of Artificial Intelligence 9(1996) 83-93.

[19] Tien-Fu Lu, Grier C. I. Lin, Juan R. He, Neural-network-based 3D force/torque sensor calibration for robot applications, Engineering Applications of Artificial Intelligence 10(1997) 87-97.

[20] E. Budak, Analytical models for high performance milling. Part I: Cutting forces, structural deformations and tolerance integrity, International Journal of Machine Tools and Manufacture 46(2006) 1478-1488.

[21] Springer handbook of mechanical engineering, Ed. K-H Grote and E. Antonsson, Springer, New York 2009

[22] H.-J. Su, J.M. McCartny, A Polynomial Homotopy Formulation of the Inverse Static Analyses of Planar Compliant Mechanisms. Transactions of the ASME 128(2006) 776-786

[23] T.E. Seo, Intégration des effets de déformation d'outil en génération de trajectoires d'usinage, 1998, Thèse de doctorat, IRCCyN - Ecole Centrale de Nantes

[24] S. Gunnarsson, M. Norrlof, G. Hovland, U. Carlsson, T. Brogardh, T. Svensson, S. Moberg, Pathcorrection for an industrial robot. US Patent, No. 7130718, 2000.

[25] C. Dumas Développement de méthodes robotisées pour le parachèvement de pièces métalliques et composites, 2011, Thèse de doctorat, IRCCyN - Université de Nantes

[26] S.J. Eastwood, P.Webb, A gravitational deflection compensation strategy for HPKMs, Robotics and Computer-Integrated Manufacturing 26(2010) 694–702

[27] P. Drouet, S. Dubowsky and C. Mavroidis, Compensation of Geometric and Elastic Deflection Errors in Large Manipulators Based on Experimental Measurements: Application to a High Accuracy Medical Manipulator", submitted to the 6th International Symposium on Advances in Robot Kinematics, 1998,Austria.

[28] M.A. Meggiolaro, C. Mavroidis, S. Dubowsky, Identification and compensation of geometric and elastic errors in large manipulators: application to a high accuracy medical robot, Proceedings of DETC1998: 1998 ASME Design Engineering Technical Conference pp 1-7

[29] J. Salisbury, 1980, Active Stiffness Control of a Manipulator in Cartesian Coordinates, 19*th IEEE Conference on Decision and Control*, pp. 87–97.

[30] I. Tyapin, G. Hovland, Kinematic and elastostatic design optimization of the 3-DOF Gantry-Tau parallel kinamatic manipulator, Modelling, Identification and Control, 30(2009) 39-56

[31] Quennouelle C. & Gosselin C. M.. Stiffness Matrix of Compliant Parallel Mechanisms, In Springer Advances in Robot Kinematics: Analysis and Design, (2008) 331-341.

[32] J.-P. Merlet, C. Gosselin, Parallel mechanisms and robots, In B. Siciliano, O. Khatib, (Eds.), Handbook of robotics, Springer, Berlin, 2008, pp. 269-285.

[33] J. Kövecses, J. Angeles, The stiffness matrix in elastically articulated rigid-body systems, Multibody System Dynamics 18(2007) 169–184.

[34] O. Company, F. Pierrot, J.-C. Fauroux, A Method for Modeling Analytical Stiffness of a Lower Mobility Parallel Manipulator, in: Proceedings of IEEE International Conference on Robotics and Automation (ICRA), 2005, pp. 3232 - 3237

[35] S. Chen and I. Kao, Conservative Congruence Transformation for Joint and Cartesian Stiffness Matrices of Robotic Hands and Fingers, The International Journal of Robotics Research, 19(2000) 835–847

[36] G. Alici, B. Shirinzadeh, Enhanced stiffness modeling, identification and characterization for robot manipulators, Proceedings of IEEE Transactions on Robotics 21(2005) 554–564.

[37] D. Chablat, P. Wenger, Architecture Optimization of a 3-DOF Parallel Mechanism for Machining Applications, the Orthoglide, IEEE Transactions On Robotics and Automation 19(2003) 403-410.

[38] F. Majou, C. Gosselin, P. Wenger, D. Chablat, Parametric stiffness analysis of the Orthoglide, Mechanism and Machine Theory 42(2007) 296-311.

8 CONCLUSIONS

This report is devoted to the enhancement of stiffness modeling technique for serial and parallel manipulators in order to increase the accuracy and efficiency of robotic-based machining of high performance materials by means of compensation of the compliance errors (in on-line and/or off-line mode). To achieve this goal, four main problems were considered.

Chapter 3 deals with the stiffness modeling of serial and parallel manipulators in the unloaded mode (i.e. under assumption of small deformations). The main contributions are in the area of the VJM modeling approach that was enhanced for serial and parallel manipulators with arbitrary location of passive joints. In contrast to other works, the developed technique starts from stiffness modeling of all kinematic chains *separately* and then *aggregates* them in a unique model. Besides, for each kinematic chain, this technique is able to obtain *both non-singular and singular stiffness matrices* that take into account passive joints or the kinematic singularities. Relevant assembling procedure allowed us to compute the *aggregated Cartesian stiffness matrix* of the parallel manipulator and also to evaluate the *internal forces/torques* and *end-platform deflections* caused by geometrical errors in the kinematic chains of over-constrained mechanisms. The developed method combines advantages of the FEA and the VJM modeling approaches (accuracy and computational efficiency respectively) and allows us to obtain the stiffness matrices either in numerical or in analytical form. More precisely, the results and contributions of Chapter 4 include:

- Enhanced VJM-based stiffness modeling technique for serial kinematic chains with arbitrary location of passive joints, which allows us to take into account passive joints in an explicit form and to compute the stiffness matrix for any configuration (even for singular ones). Also, it evaluates internal deflections (and corresponding forces/torques) for kinematic chains with arbitrary number of passive and actuated joints. In contrast to previous results, the developed technique is more computationally efficient, includes low-order matrix inversion, and it is able to obtain even rank-deficient stiffness matrices caused by the presence of passive joints or singular configuration of the kinematic chain.

- Analytical expression for stiffness matrix modification induced by passive joints, which extends the classical stiffness mapping notion for serial manipulators, and related recursive procedure for stiffness matrix elements computing, which allows us to include passive joints sequentially (one-by-one). For typical industrial architectures, which include trivial passive joints (where axes are collinear with Cartesian ones), simple and practically convenient rules for stiffness matrix modification have been proposed. These results significantly simplify computation of the desired stiffness matrix and reduce them to elementary algebraic transformations.

- Stiffness model assembling technique that allows us to aggregate elastostatic models of separate kinematic chains in the stiffness model of the parallel manipulator. It also allows us to evaluate internal deflections and forces/torques in joints, as well as deflections of the reference frame, caused by geometrical errors in kinematic chains. This issue has never been studied in robotic applications before and has essential practical significance for evaluating desired tolerances in links/joints geometry and corresponding internal stresses in over-constrained mechanisms.

Chapters 4-7 deal with the non-linear stiffness modeling of serial and parallel manipulators in the loaded mode (i.e. under assumption of large deformations). The main contributions are in the area of the VJM modeling approach that was generalized for the case of large deflections caused by internal and external loadings applied to the end-point and/or to the intermediate nodes of the kinematic chains. In contrast to other works, the developed technique includes computing of the static equilibrium configuration corresponding to the given loading. In addition, it allows us to check the "internal stability" of relevant chain configuration. Similar to Chapter 3, the stiffness modeling of parallel manipulators starts from kinematic chains, but it yields a non-linear function describing force-deflection relation. Besides, for each kinematic chain, this technique is also able to obtain *both non-singular and singular stiffness matrices*. Relevant aggregation procedure allows us to obtain a non-linear force-deflection (or deflection-force) relation for the parallel manipulator and to compute the *aggregated Cartesian stiffness matrix*, as well as to evaluate the *internal forces/torques* and *end-platform deflections* caused by loadings and geometrical errors in the kinematic chains. Also, this model was used for the compensation of the compliance errors caused by the internal and external loadings. Similar to the previous chapter, the developed method combines advantages of the FEA and the VJM modeling approaches (accuracy and computational efficiency respectively). In more details, the results and contributions of Chapter 4 include

- Non-linear stiffness modeling technique for serial kinematic chains under external and internal loadings (applied to end-point, to the intermediate nodes, preloading in the joints) which includes: computing the static equilibrium configuration in the loaded mode, obtaining full-scale force-deflections relation and computing of the stiffness matrix for the loaded mode
- Stability analysis technique and related matrix stability criterion for kinematic chain configuration under loading in the case of single and multiple equilibriums, which takes into account the second derivatives of the kinematic chain potential energy.
- Enhanced stiffness model aggregation technique for over-constrained parallel manipulators under internal and external loadings, which takes into account shifting of the equilibrium due to loadings and allows to evaluate internal deflections and forces/torques in joints, as well as deflections of the reference point, caused by geometrical errors in kinematic chains.
- Numerical technique for on-line and off-line compensation of the compliance errors caused by external loadings in parallel manipulators (including over-constrained ones) with perfect and non-perfect serial kinematic chains. In contrast to previous works this technique is based on a non-linear stiffness model that gives essential advantages for robotic-based machining, where elastic deflections can be essential.

In general, the obtained results contribute to the area of non-linear stiffness modeling of serial and parallel manipulators and give a robotic designer a useful tool allowing to estimate reasonable limits in minimization of link geometry (cross-section, in particular) in order to avoid potentially dangerous phenomena in the manipulator stiffness behavior under external and internal loadings.